Deriving glacier surface velocities from repeat optical images

Torborg Heid

Department of Geosciences
Faculty of Mathematics and Natural Sciences
University of Oslo

A thesis submitted for the degree of
Philosophiae Doctor (PhD)
Oslo, 2011

Series of dissertations submitted to the
Faculty of Mathematics and Natural Sciences, University of Oslo
No. 1156

ISSN 1501-7710

Cover: Inger Sandved Anfinsen.
Printed in Norway: AIT Oslo AS.

Produced in co-operation with Unipub.
The thesis is produced by Unipub merely in connection with the
thesis defence. Kindly direct all inquiries regarding the thesis to the copyright
holder or the unit which grants the doctorate.

Abstract

The velocity of glaciers is important for many aspects in glaciology. Mass accumulated in the accumulation area is transported down to the ablation area by deformation and sliding due to the gravitational force, and hence glacier velocity is connected to the mass balance of glaciers. It also contributes directly to the mass balance of calving glaciers because it is an important control of the ice discharge rate for such glaciers. Changing glacier velocities is an indicator of instable glaciers, and monitoring velocity over time can make people aware of possible hazards that may arise from instable glaciers. The movement of glaciers is also important for transporting material and for eroding the landscape.

The focus of this thesis is to further develop image matching within glaciology. In image matching, images from two different times are compared using correlation techniques to derive glacier displacement over the time period. Most studies have concentrated on *using* image matching to derive glacier velocities instead of *developing* this method further. To be able to derive the densest possible velocity grids for all glaciers in the world, image matching methods over glacier surfaces have to be explored further.

So far all images that have been used to derive velocity in glaciology have been high or medium spatial resolution images. Low resolution images cover large sections in one image, and this makes them suited for investigating the velocity of large areas such as Antarctic ice shelves. We derive velocities for Antarctic ice shelves using MODIS images with a spatial resolution of 250 m to test whether these images are suited for deriving ice shelf velocity. Because the accuracy is about one fourth of a pixel, and it is possible to use images

acquired several years apart due to the low surface transformation, MODIS images are well suited for deriving velocity of Antarctic ice shelves and also to monitor their changes over time.

We found when comparing different image matching methods over different glacier surfaces that the most commonly used method, normalized cross-correlation, generally performs worse compared to orientation correlation and the matching part of the program COSI-Corr. The only situation where normalized cross-correlation outperforms the two other methods are on narrow glaciers where small window sizes are needed. COSI-Corr performs best overall, but orientation correlation performs almost as well. In addition orientation correlation is the only method that manages to match striped Landsat images after the failure of the Scan Line Corrector. Both orientation correlation and COSI-Corr are considered to be methods well suited for global glacier velocity mapping. Normalized cross-correlation can supplement these two methods on narrow glaciers.

The effort that has been put into developing image matching in glaciology since the start of this study, both in this study and in other studies, makes it possible to derive glacier velocities over large regions, and only computer processing time hinders automatic matching of glacier velocities worldwide. Global glacier velocities can give valuable insights. We show in this thesis that it can give information about how glaciers respond to climate change. Glacier velocity of five regions of the world with negative mass balance is derived, and in all regions the general glacier speed is decreasing over the last decades. In addition global glacier velocities can be used to understand glacier dynamics, and predict glacier hazards. It can be tested against glacier inventory parameters, and it can be used to estimate erosion rates and transport times.

Acknowledgements

First of all I have to thank my supervisor Andreas Kääb for all his help with this thesis. In addition to supervising my work with great enthusiasm, he has passed on a number of good scientific ideas to me which this thesis is based on. Andreas, Bernd Etzelmüller and the project "Monitoring Earth surface changes from space" by Keck Institute for Space Studies have sent me off to attend conferences and courses in numerous places of the world and this has made these three years very memorable. Cecilie Rolstad Denby has been my co-supervisor during this period. She was also my primary supervisor during the work with my master thesis, and she has taught me many things that this PhD thesis has benefited from.

This thesis is a part of the "Precise analysis of mass movements through correlation of repeat images" (CORRIA) project which is funded through the Research Council of Norway. In addition to Andreas Kääb also Misganu Debella-Gilo and Jonas Karstensen have been part of this research group. I am very grateful to them for interesting discussions and constructive feedback on my work. The study has also been supported by the ESA Glaciers_CCI project, International Center for Geohazards, the ESA GlobGlacier project and the NRF IPY Glaciodyn project.

USGS and NSIDC have provided the images used in this study. These two institutions provide access to processed satellite images at no charge, which I highly appreciate. Without their processing, the outcomes of this thesis would have taken much longer to obtain, and without their open access attitude it would have been much more expensive. Glacier outlines have been downloaded from the GLIMS database, and also the free access to this

database is much appreciated.

Finally, a big thank you to all the people who support me and make my life a fun experience. This includes colleagues at the Department of Geosciences, friends everywhere, parents in Hemsedal and my husband Stian. With all of you in my life it is so easy to rest my head and forget about science for a while.

Contents

[1]last name changed to Heid

1

Introduction

The mass transport of snow and ice is a key characteristic for glaciers. The mass surplus accumulated in the accumulation area of glaciers is transported down to the ablation area due to the gravitational force. Glacier velocities are therefore strongly connected with the mass balance of glaciers, and the mass flux through a cross section of a glacier equals the mass balance upglacier when the glacier is in balance (Paterson, 1994). The kinematic boundary condition for glaciers can be expressed as

$$b = \frac{\partial z^s}{\partial t} + v_x^s \frac{\partial z^s}{\partial x} + v_y^s \frac{\partial z^s}{\partial y} - v_z^s \tag{1.1}$$

where b is the mass balance of the surface, z^s is the surface elevation, $\frac{\partial z^s}{\partial t}$ is the change in surface elevation with time, v_x^s and v_y^s are the two horizontal velocity components in the x and y direction, $\frac{\partial z^s}{\partial x}$ and $\frac{\partial z^s}{\partial y}$ are the two components of the surface slope, and v_z^s is the vertical velocity at the surface.

Glaciers move by deformation of ice, sliding at the base and/or deformation of underlying till. The vertical velocity gradient within the glacier due to ice deformation is given by

$$\frac{\partial U}{\partial z} = 2A(\rho g h \, tan \, \alpha)^n \tag{1.2}$$

where U is the velocity, z is the vertical axis, A is a constant that depends on temperature, crystal fabric and impurity content, g is the acceleration due to gravity, h is the vertical position within the glacier, α is the slope of the

glacier surface and n is a constant normally set to 3 in glaciological studies. Eq. 1.2 is given using sine instead of tangent in earlier versions. This is true for parallel sided ice when h is measured perpendicular to the surface and bed slope, whereas the new version allows for any glacier bed geometry (Hooke, 2005; van der Veen and Payne, 2004; Benn and Evans, 2010). By measuring the surface velocity and calculating the velocity gradient based on the above equation it is possible to calculate the mass flux through a cross section for glaciers where all the movement is caused by deformation. This can then be compared to mass balance measurements to determine whether the glacier is in balance or not (Hagen et al., 2006).

Glacier velocity is also an important control of the ice discharge rate for calving glaciers. Rignot and Kanagaratnam (2006) showed that the ice discharge on Greenland doubled from 1996 to 2005 because of glacier acceleration. They also stated that the acceleration in the east was probably due to climate warming. Zwally et al. (2002) suggested that water from surface melting on the Greenland Ice Sheet quickly reaches the glacier bed and lubricates it so that glaciers accelerate. They also argued that ice sheets can respond rapidly to climate change because of this effect. However, Murray et al. (2010) argued that the acceleration of southeastern Greenland glaciers during early 2000s was due to changed ocean currents and not increased surface melting. Reduced instead of increased glacier runoff allowed warm water currents to enter the fjords.

Glacier velocities can also give valuable insight in the stability of glaciers. Seven ice shelves on the Antarctic Peninsula have retreated dramatically or completely disintegrated over the last decades (Cook and Vaughan, 2010). Several of the ice shelves that disintegrated accelerated before they collapsed. Both Larsen A (Bindschadler et al., 1994; Rack et al., 1999) and Larsen B (Skvarca et al., 1999; Rott et al., 2002; Skvarca et al., 2004; Vieli et al., 2006) increased their velocity by approximately 10–15 % in the years prior to their disintegration. Therefore, monitoring changes in ice shelf dynamics can give an early warning of instabilities.

The movement of glaciers can in some cases be a threat to humans. Rivers being dammed by surging or advancing glaciers is one example of such haz-

ards (Hewitt, 1969; Espizua and Bengochea, 1990). Monitoring glacier flow can detect areas with instabilities and focus more research to such areas. By monitoring instable areas it could be possible to predict catastrophes and evacuate people before they take place.

Glacier velocities can be measured using both *in situ* and remote sensing techniques. The velocities of a glacier at any surface point consists of different components that are expressed through the kinematic boundary condition (Eq. 1.1). The different terms are shown in Fig. 1.1. When using *in situ* techniques, stakes are drilled down into the ice, and using either a total station or static GPS, all components of Equation 1.1 can be measured. Using remote sensing techniques, it is not possible to measure v_z^s.

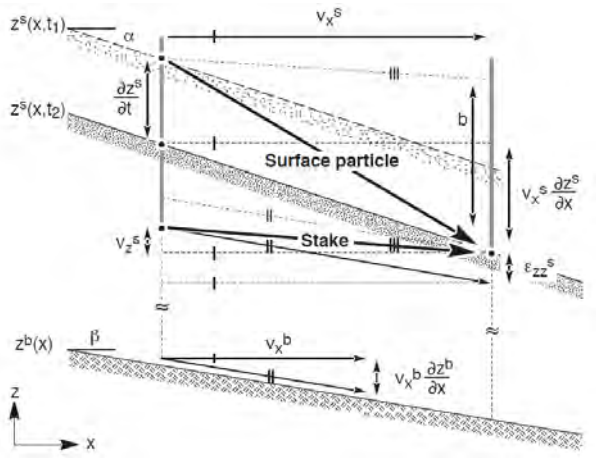

Figure 1.1: The different terms in the kinematic boundary condition. From: Kääb (2005).

Even though it is not possible to measure v_z^s using remote sensing, such techniques are well suited for measuring the other terms, both due to the size and the remoteness of many glaciers and ice caps. There are two techniques that have been applied for this purpose so far, image matching and differential interferometric synthetic aperture radar (DInSAR). Both methods will be described in Chapter 2. The two methods complement each other because

they work over different time spans in glaciological studies. Image matching works over time spans of weeks to years, whereas DInSAR works over time spans of days to weeks.

Both optical images, radar images and detailed digital elevation models (DEMs) can be used for deriving glacier velocities using image matching. The different images and DEMs can be matched using the same methods, but since they have different characteristics image matching of the three types should be studied separately. In this thesis, the focus is on optical images because of the many sensors producing optical images, the large archive of historical optical images, and because glacier inventories are usually based on optical images.

Developing optical image matching techniques for glaciers has received little attention within the glaciological community. Usually glaciologists have focused on one matching method, and there has been little or no comparison of different matching methods. Glaciologists have also focused on images with medium to high spatial resolution, whereas low resolution images have received little attention in this context, in spite of their good coverage both spatially and temporally. Thus there is a need to further develop optical image matching of glaciers. By automatic image matching and post-processing of the results it is possible to derive global velocity measurements, which may open for new understandings within glacier dynamics.

The objectives of this thesis are summarized as follows:

- Prove that it is possible to use optical images with low spatial resolution in glaciological velocity studies.
- Compare different image matching methods to find the best performing method(s).
- Develop image matching in glaciology towards full automation so that it is possible to derive glacier velocities globally.
- Demonstrate that deriving glacier dynamics globally can give valuable insights about glacier dynamics.

2

Remote sensing of glacier velocity

Glacier velocities can be measured using two different remote sensing techniques, image matching and DInSAR. Because these techniques work on different time scales and have different strengths and shortcomings, they complement each other in glaciological studies. The techniques are described in the following sections.

2.1 Image matching

It is possible to derive glacier displacements using optical images, radar images and also using detailed DEMs treated as images. The methods have different strengths and shortcomings, and which image type to use depends on the situation. In all three cases the purpose is to identify the same features in two images from different times so that velocity can be derived.

Optical images have existed for a long time, both as terrestrial images, aerial images and satellite images. There are many optical satellite sensors, and these have generated and still generate a large number of optical data with various spatial resolution. Hence data access is easy using optical images and many of the images are available at no cost. However, optical satellite images of glaciers can only be used if they are obtained during cloud free daylight conditions, and this is a major limitation when using such images. Especially in maritime areas it can be difficult to obtain cloud free images,

and the polar night limits the method to be used only during summer in polar regions. Images also have to contain visual contrast, and this limits the method to mainly be used in the ablation area. Optical image matching as a tool to derive glacier displacement will be discussed thoroughly in Chapter 3.

Radar images are images from active sensors, and hence these are not dependent on daylight. Radar signals also penetrate clouds, which makes it possible to obtain images also during cloudy conditions. However, they do not extend as far back in time as optical images, and there are not as many sensors providing radar images as there are sensors providing optical images. They also have different spatial resolution in the azimuth and range directions. One image consists of both an amplitude part and a phase part, and image matching of radar images can be done using the complex image, called "speckle tracking", using only the amplitudes, called "intensity tracking", or using the coherence, called "coherence tracking". Matching of the complex image gives a higher accuracy of the measurements. However, in order to match using also the phase there has to be coherence between the images and coherence is easily lost, especially in the shear zone of glaciers. Image matching of radar images has been frequently used to derive glacier displacements (e.g. Michel and Rignot, 1999; Joughin, 2002; Strozzi et al., 2002; Luckman et al., 2003, 2007; de Lange et al., 2007; Quincey et al., 2009a,b; Giles et al., 2009).

For DEMs to be accurate enough to be used to derive glacier displacements, they have to be derived using laser scanning and not traditional photogrammetry. Laser scanning is an active method. Here the time it takes from the light is transmitted until it comes back, reflected by the surface, is measured. The limitation for laser scanning is wet areas and clouds, because the laser beam is absorbed by water. Currently only terrestrial and airborne laser scanners can create the dense and accurate DEMs needed for matching to derive glacier displacements. This method is therefore the least common method used to derive glacier velocities, but it has been used in a few glaciological studies (e.g. Abdalati and Krabill, 1999; Rees and Arnold, 2007; Schwalbe and Maas, 2009).

The time interval between the different images depends on the method. For speckle tracking the radar phase coherence has to be preserved, and therefore the time interval has to be shorter using this method than using the other methods. In the other methods only the glacier features have to be preserved, and these are preserved longer than the radar phase coherence.

2.2 DInSAR

The phase difference between two SAR images acquired from different positions is a function of elevation and displacement in the line of sight direction. It is possible, by differencing SAR interferograms, to be left with only displacement. This differencing can be done in different ways depending on the availability of data. An already existing DEM can be used to create a synthetic interferogram containing only the elevation, and then subtract this from the real interferogram. Alternatively 3 or 4 passes can be combined to two interferograms, and these two can be differenced to contain only the displacement.

The accuracy of DInSAR is generally better than the accuracy of image matching, but the phase has to be coherent between the two acquisitions. This limits the time period over which the displacements can be measured to days, or in some cases up to a month. DInSAR can be used in glacier areas that have no visual contrast because it is not dependent on real physical features, but only on the phase difference. This is an important advantage over image matching. However, DInSAR can only derive displacement in the line of sight.

DInSAR has been used in many glacier studies (e.g. Rignot and MacAyeal, 1998; Joughin, 2002; Luckman et al., 2007; Joughin et al., 2010), especially to measure the displacements of the two ice sheets. It is often used in combination with image matching because the two methods compliment each other. Rott (2009) provides an overview of the use of InSAR within earth sciences.

3

Optical image matching

3.1 Basic concepts

The process of correlating two or more images containing the same image objects is called image matching. This method is used in several different fields besides deriving the velocity of glaciers. Examples of these are photogrammetry, image mosaicking, map updating, face detection, change detection, video coding, tectonics and monitoring of tumor growth. However, different fields often use different names for image matching based on the purpose of the matching. Image registration, motion estimation, particle tracking and optical flow are all words that are used and that essentially mean the same as image matching. Brown (1992) and Zitova and Flusser (2003) provide overviews of image matching.

When the purpose of image matching is to derive glacier velocities, it is important that the time span between the images is long enough to detect significant displacements, but short enough so that the objects are still recognizable. The length of this time span can vary with the velocities of the glaciers, the resolution of the images, the accuracy of the matching method, the amount of surface melt and the strain rates. The longer the time span is, the larger the displacement is compared to the accuracy of the match, but the chance of having too large surface transformation to get a correct match increases. It is the shortest distance that is measured, and this will in cases

with a curved path be different from the real distance traveled. This effect increases when the time span and the displacement increases. Time spans used in glaciological studies range from weeks, for example for matching of 15 m spatial resolution images over outlet glaciers in Greenland (Heid and Kääb, in press), to a decade for matching of for example 250 m spatial resolution images over Antarctic ice shelves (Haug et al., 2010). Typically, yearly velocities are derived, but it is also possible to derive seasonal velocities in areas where the velocity is high (Fig. 3.1), or if the spatial resolution of the images used is high.

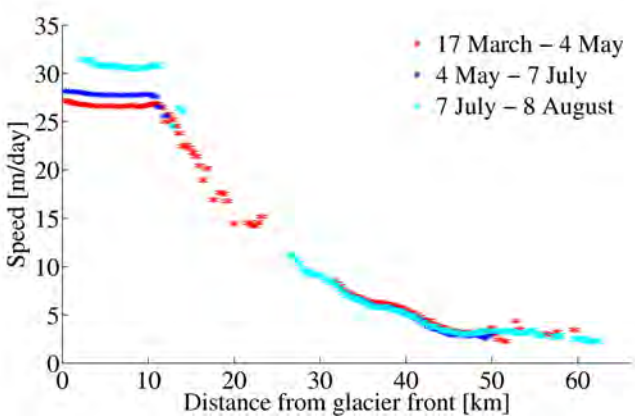

Figure 3.1: Seasonal speed changes in 2001 at Jakobshavn Glacier, western Greenland as points with error bars. This shows that it is possible to observe significant seasonal speed changes using Landsat images in areas with high speeds. (Heid, unpublished.)

Until the 1980s, image matching was done by manually inspecting the images and identifying the same objects in the images from two different times (Brecher, 1985; Lucchitta and Ferguson, 1986; Orheim and Lucchitta, 1987) (Fig. 3.2). This work was very time consuming and there were no possibilities for obtaining subpixel measurements. Bindschadler and Scambos (1991) and Scambos et al. (1992) were the first to do image matching automatically on glaciers. They used image matching algorithms based on

normalized cross-correlation (NCC) and the work of Bernstein (1983). They found that doing this automatically was not just less time consuming, but it was also more accurate than doing it manually. After this first demonstration, different image matching methods have been applied in glaciological studies.

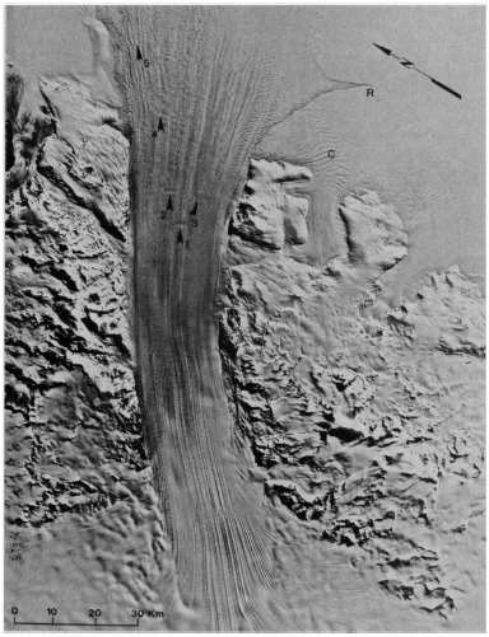

Figure 3.2: Velocity measurements from Byrd Glacier, Antarctica, derived manually using Landsat images. From: Lucchitta and Ferguson (1986).

Image matching methods can be either area-based or feature-based. Area-based methods operate directly on image quantities like brightness or phase. Feature-based methods on the other hand match features that are extracted from the images in a pre-processing step. Such features can be crevasses, stones or other differences in digital numbers (DN).

Image matching methods can also be divided into spatial domain and frequency domain methods. Methods operating in the spatial domain operate

directly in the image space on the intensity values. Here, a small reference template from the first image is searched for in a larger part of the second image. Frequency domain methods benefit from the fact that convolution in the spatial domain equals multiplication in the Fourier domain. This is called the convolution theorem (McClellan et al., 2003). Convolution between two images equals correlation if the intensity values of one of the images are rotated 180° around its center point. When using frequency domain methods the matching itself works differently compared to matching in the spatial domain. Instead of searching for a template of the first image in a larger section of the second image, two equally large areas of the two images are chosen and these are multiplied in the frequency domain to get the displacement.

The size of the windows to be correlated is important in glaciological studies. The window size has to be large enough to ensure that texture and not noise is matched. For small window sizes it is difficult to distinguish between texture and noise. But it is also important that the window size is small enough to avoid much deformation within the window. The optimal window size varies from glacier to glacier depending on glacier characteristics like visual contrast and the amount of deformation within the window. Debella-Gilo and Kääb (in review) created an adaptive algorithm that automatically determines the window size depending on the texture to noise ratio in the images. The optimal window size also depends on whether spatial or frequency domain methods are being used. Frequency domain methods generally require larger window sizes than spatial domain methods. This is because frequency domain methods are less accurate at small window sizes as a consequence of Heisenberg's uncertainty principle.

Which spatial resolution that is wanted on the images to correlate depends on the situation. Commonly, studies aim at images with highest possible spatial resolution, but this is not the best choice in every situation. Higher spatial resolution images cover in general smaller areas. Therefore such images are less likely to cover stable ground that can be used to coregistrate the images. This is particularly an issue for the large ice caps, ice sheets and ice shelves of the world. In such cases, even low resolution images,

like MODIS images with a spatial resolution of 250 m, can be used to derive velocities (Haug et al., 2010). Landsat images are available with both 15 m and 30 m spatial resolution after 1999. Because of a higher noise level for Landsat images with 15 m spatial resolution compared to Landsat images with 30 m spatial resolution (Haug et al., 2010) (Fig. 3.3), it can in some areas with low visual contrast be better to use the 30 m images (Heid and Kääb, in press). The difference between displacements derived using 15 m spatial resolution and 30 m spatial resolution is shown in Fig. 3.4.

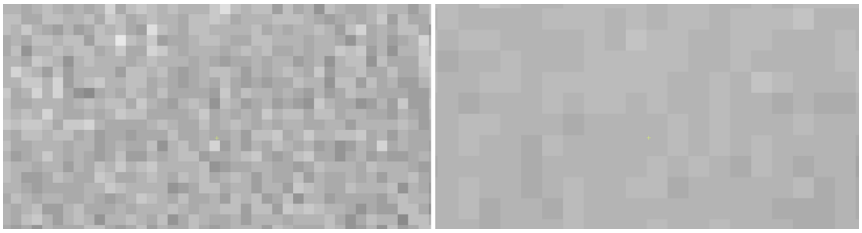

Figure 3.3: Landsat 15 m spatial resolution (left) and Landsat 30 m spatial resolution (right) over an area of Larsen C where the visual contrast is low. The larger differences in digital numbers of the 15 m image most likely shows the higher noise level instead of real texture. Digital numbers vary between 30 and 34 for the 30 m images whereas they vary between 28 and 37 for the 15 m images. Because the variation is greater for the 15 m image but around the same values, this indicates that the variation is due to noise. (Heid, unpublished.)

3.2 Pre-processing

Images used for deriving displacements have to be orthorectified before they are matched, or alternatively the displacements obtained when matching original images that are not orthorectified have to be rectified. This requires that the position of the camera, the look direction of the camera, the lens distortion and the ground topography is known. The quality of the orthorec-

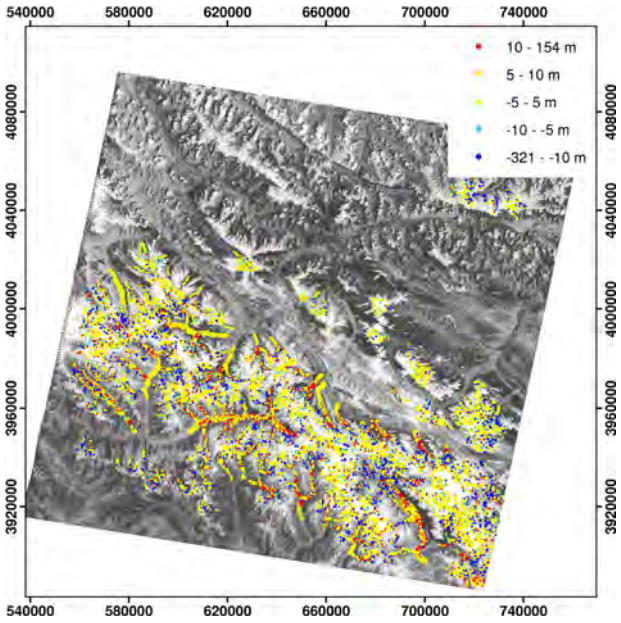

Figure 3.4: Difference between displacements obtained using 30 m and 15 m spatial resolution in Karakoram. Yellow indicates that the displacement is within the 1σ method uncertainty (5 m). From: Heid and Kääb (in press).

tification limits the accuracy of the displacement field. Incorrect values of camera position, look direction, lens distortion and atmospheric effects give horizontal shifts in the orthoimages that can be erroneously identified as displacement. Similarly, vertical errors in digital elevation models (DEMs) used to orthorectify the images translate to horizontal shifts in the orthorectified images (Kääb, 2005) (Fig. 3.5).

Before the matching is conducted the images may be processed to enhance wanted features and depress unwanted features. Scambos et al. (1992) first low-pass filtered the images to remove the variations in DN not connected to topography and matched these low-pass filtered images to coregister the images. Afterwards they high-pass filtered the images to remove the variations in DN connected to topography and matched these to get the dis-

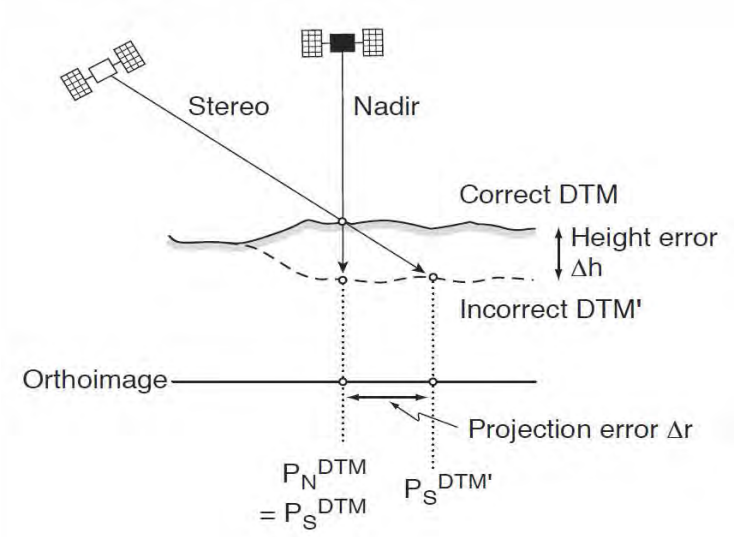

Figure 3.5: DEM errors translate to horizontal errors when images are orthorectified. From: Kääb (2005).

placements. Scambos et al. (1992) also used the first principal component of different visible and near-infrared bands to obtain images with enhanced ice topography, scan-line destriping and gaussian contrast stretching before the matching was conducted.

It is also possible to enhance differences in digital numbers in a preprocessing step. One way of doing this is called orientation correlation (OC) (Fitch et al., 2002). Taking f as the image at time $t = 1$ and g as the image at time $t = 2$, the orientation images f_o and g_o are created from

$$f_o(x,y) = sgn(\frac{\partial f(x,y)}{\partial x} + i\frac{\partial f(x,y)}{\partial y}) \tag{3.1}$$

$$g_o(x,y) = sgn(\frac{\partial g(x,y)}{\partial x} + i\frac{\partial g(x,y)}{\partial y}) \tag{3.2}$$

$$\text{where } sgn(x) = \begin{cases} 0 & \text{if } |x| = 0 \\ \frac{x}{|x|} & \text{otherwise} \end{cases} \tag{3.3}$$

where sgn is the signum function and i is the complex imaginary unit. The

new images f_o and g_o are complex and hence consist of one real and one imaginary part, where the intensity differences in the x direction represent the real matrix and the intensity differences in the y direction represent the imaginary matrix. These orientation images can then be matched using frequency domain methods. OC is an efficient method when it comes to deriving ice shelf velocities (Haug et al., 2010) (Fig. 3.6). Heid and Kääb (in press) showed that the method performs very well in glaciological studies. OC also manages to match Landsat images that have black stripes after a failure of the scan-line corrector (SLC-off) (Fig. 3.7). This is because homogeneous areas get zero values when orientation images are created and therefore these areas are neglected in the matching process.

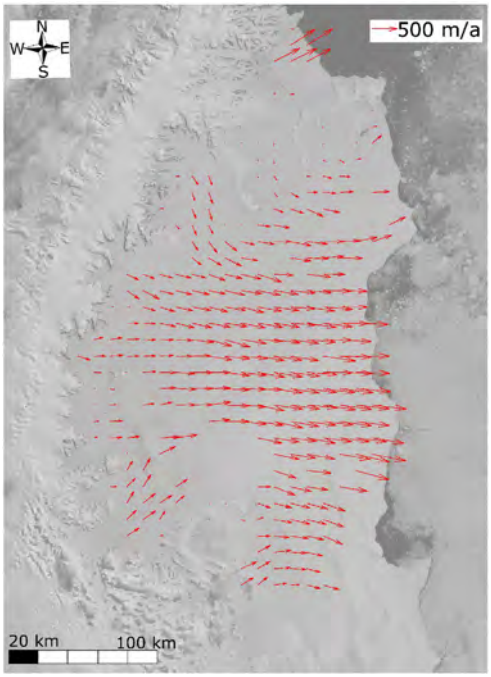

Figure 3.6: Velocity measurements of the Larsen C ice shelf, Antarctic Peninsula, derived using orientation correlation. From: Haug et al. (2010).

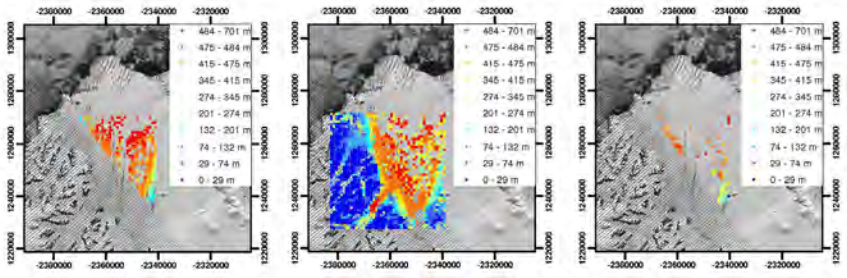

Figure 3.7: Matching of striped Landsat images after a failure of the Scan Line Corrector using normalized cross-correlation (left), orientation correlation (middle) and the matching method from COSI-Corr (right). Only orientation correlation manages to match the striped area. From: Heid and Kääb (in press).

Interest operators can be used to avoid matching areas with too little contrast to obtain a correct match. Förstner and Gülch (1987) developed a method which was mainly meant to extract features in images. However, this method can also be used to select optimal windows for image matching. Schmid et al. (1998) compared different interest operators, and found that a method based on auto-correlation performed best. The adaptive window size algorithm of Debella-Gilo and Kääb (in review) does not only choose the window size depending on the texture to noise ratio in the images, but it also excludes windows with too little texture to noise ratio when an upper window size is reached. However, the amount of texture needed for a matching method to obtain a correct match depends on the matching method. Therefore, the texture to noise ratio at which matching should not be done has to be tuned depending on the matching method.

When large displacements are expected it can be beneficial to align the images according to the expected displacements before the matching is conducted. This is beneficial both for spatial domain methods and for frequency domain methods, but in different ways. For spatial domain methods the search area can be reduced when aligning according to expected displace-

ment is done. This reduces the computing time and increases the likelihood of getting a correct match. For frequency domain methods it is not possible to derive displacements larger than half the window size due to the quadrant ambiguity problem. To be able to derive large displacements without increasing the window size, it is necessary to align the images according to the expected displacement if the expected displacement is larger than half of the wanted window size. In cases where the glaciers flow in different directions and manual aligning is not wanted, it is possible to align images automatically. Matching can first be done using large window sizes. The derived displacements can then be used to align the images, and matching can be done a second time using the wanted final window size (Heid and Kääb, in press). This procedure is best suited for frequency domain methods.

3.3 Different matching methods

There are different mathematical ways to find the best correlation between two images. The most common methods are described below.

Normalized cross-correlation

Normalized cross-correlation (NCC) is a matching method that is very often used when studying glacier velocities due to its simplicity. The first image is taken as the reference image, and a window of this image is searched for in the second image, or the search image. The cross-correlation surface CC is given by

$$\mathrm{CC}(i,j) = \frac{\sum_{k,l}(s(i+k,j+l)-\mu_s)(r(k,l)-\mu_r)}{\sqrt{\sum_{k,l}(s(i+k,j+l)-\mu_s)^2 \sum_{k,l}(r(k,l)-\mu_r)^2}} \tag{3.4}$$

where (i,j) indicates the position in the search area, (k,l) the position in the reference area, r the pixel value of the reference chip, s the pixel value of the search chip, μ_r the average pixel value of the reference chip and μ_s the average pixel value of the search chip. The peak of the cross-correlation surface indicates the displacement between the images. Fig. 3.8 shows the work

flow in the NCC method. This cross-correlation is normalized, which has two effects. Firstly, images with different illumination can be compared, and secondly, the correlation coefficient from different attempts can be compared. Because this method operates in the spatial domain, the process is time consuming compared to processes that operate in the frequency domain using Fast Fourier Transform (FFT).

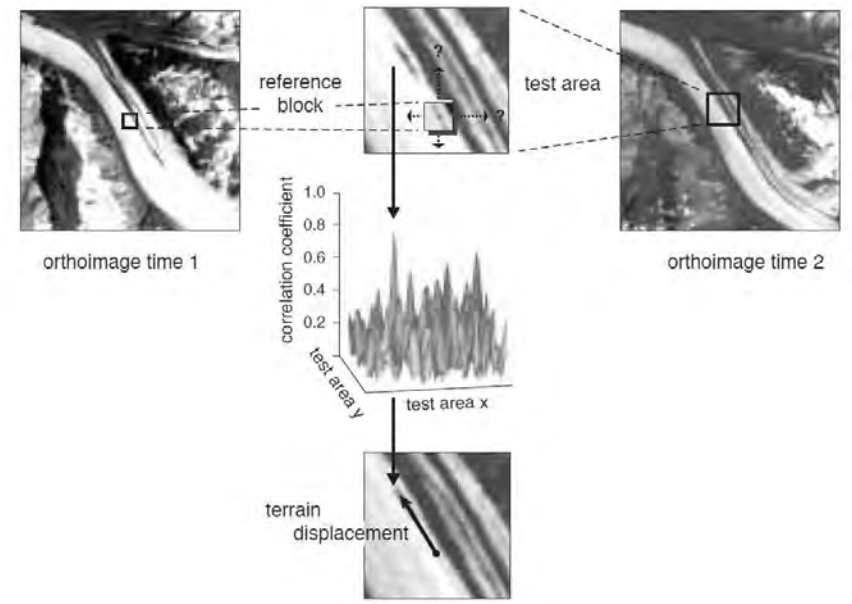

Figure 3.8: The work flow of the NCC method. From: Kääb (2005).

NCC was the first method that was used for deriving glacier velocities, and this was done by Bindschadler and Scambos (1991) and Scambos et al. (1992) based on the work of Bernstein (1983). They developed a program called IMCORR, which has been used in a number of studies deriving glacier velocities (e.g. Skvarca et al., 2003; Berthier et al., 2003; Bindschadler et al., 1996; Dowdeswell and Benham, 2003; Copland et al., 2009). In IMCORR some of the terms in Eq. 3.4 are solved using Fast Fourier Transform (FFT) to

speed up the calculations. Other studies have also used NCC to derive glacier and rock glacier velocities (e.g. Whillans and Tseng, 1995; Kääb and Vollmer, 2000; Evans, 2000; Kääb, 2002; Kaufmann and Ladstädter, 2003; Berthier et al., 2005; Kääb, 2005; Kääb et al., 2005; Debella-Gilo and Kääb, 2011; Huang and Li, 2011). Heid and Kääb (in press) found that NCC generally performs worse on glaciers compared to other methods, but the strength of spatial domain methods like NCC is that they require smaller window sizes than frequency domain methods to produce measurements. Hence, for smaller glaciers, this method can be the best choice.

NCC can be easily dominated by strong differences in DNs in a window (Heid and Kääb, in press). For glacierized areas strong differences in DN are very common due to for example black rocks on white snow. If rocks move with the ice this can generate correct matches in situations that would otherwise be difficult to match, but if the rock rolls on the glacier instead of moving with the ice this can generate mismatches. Also thin clouds and crevasses that are snow-filled in one image and without snow in the other image will generate mismatches for this method.

Cross-correlation operated in the frequency domain

Cross-correlation can be computed in the frequency domain (hereafter abbreviated CCF) by multiplying the Fast Fourier Transform (FFT) of one image and the complex conjugated FFT of the second image (the convolution theorem) (McClellan et al., 2003). This is the same as computing the cross-correlation in the spatial domain. However, the normalization cannot easily be transformed to the frequency domain. In the CCF method, only the cross-correlation is computed, so that this method does not normalize. This implies that a different illumination in the two images can give a mismatch, and also that a wrong match can be chosen if the illumination varies within the section to be matched. In this approach the CC is given by

$$CC(i,j) = IFFT\left(F(u,v)G^{*}(u,v)\right) \tag{3.5}$$

where $F(u, v)$ is the FFT of the matching window from the image at time $t = 1$, $G(u, v)$ is the FFT of the matching window from the image at time $t = 2$, * denotes the complex conjugated and IFFT is the Inverse Fast Fourier Transform.

Since this method does not contain any kind of normalization, it has never been used in glaciological studies alone. But together with pre-processing steps that normalize, it can be a valuable method (Rolstad et al., 1997; Heid and Kääb, in press). In combination with OC it performs very well in glaciological studies, although not as good as COSI-Corr (Heid and Kääb, in press). This method uses the entire matching window to derive a match because it uses phase differences at all frequencies to derive the displacement. It is therefore insensitive to phase differences constrained to a few frequencies, which can be generated for instance if a rock rolls on the glacier. However, in areas with much deformation this method can experience problems since the different frequencies have different phase differences. Noise spread across all frequencies can reduce the accuracy of this method or generate mismatches.

Phase correlation

A common way of approximating a normalization in the Fourier domain is to consider only the phase information. By doing this, differences in image intensity, which show up only in the amplitudes, are ignored. This is done with the PC method. Here the CC is given by

$$CC(i, j) = IFFT\left(\frac{F_o(u, v)G_o^*(u, v)}{|F_o(u, v)G_o^*(u, v)|}\right). \tag{3.6}$$

Also here the peak of the cross-correlation surface indicates the displacement.

Phase correlation (PC) was developed by Kuglin and Hines (1975), but the use of this method within glaciology is very limited. Heid and Kääb (in press) found that this method outperformed NCC in glaciological studies, but that OC and COSI-Corr performed better.

COSI-Corr

COSI-Corr is a highly advanced matching program developed by Leprince et al. (2007). It was originally made for investigating tectonics, but glaciologists soon found that it was also a valuable tool for deriving glacier velocities. It estimates the phase difference in the Fourier domain and does not transform the images back to the spatial domain to find the maximum of the CC. It is weighted by a bell-shaped window to center the matching to the middle of the matching window. This makes it more certain where the match actually comes from within the window, but in cases with little contrast in the image center it can still obtain matches in the outer part. The method obtains more correct matches than other tested methods in areas with little visual contrast and is also generally a very robust method (Heid and Kääb, in press). The code of the program, however, is not publicly available and this makes it difficult to make personal adjustments.

COSI-Corr is starting to become a commonly used program within glaciology. Scherler et al. (2008) did the first study in glaciology with this method (Fig. 3.9), and after that other studies have followed (Quincey and Glasser, 2009; Scherler et al., 2011a,b; Herman et al., 2011).

3.4 Subpixel measurements

All of the methods discussed in Section 3.3 require additional work in order to obtain subpixel velocities except COSI-Corr. There are three possible ways to do this. Firstly, the cross-correlation surface can be interpolated. Secondly, the images can be interpolated before the matching is done. Thirdly, least squares iterations can be used.

The most common way of estimating subpixel displacement is to interpolate the cross-correlation surface from the surrounding points. For spatial domain methods the images should be oversampled by a factor of two to interpolate the cross-correlation surface in order to avoid aliasing (Dvornychenko, 1983). For frequency domain methods, however, this is not necessary. The cross-correlation surface can be interpolated by fitting functions to the sur-

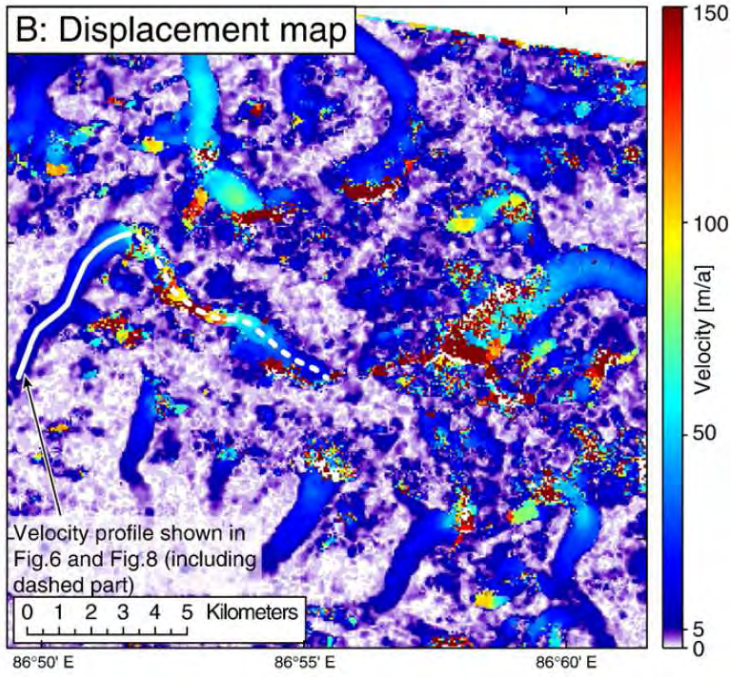

Figure 3.9: Velocity measurements from the Mount Everest region in Nepal derived using COSI-Corr. From: Scherler et al. (2008).

rounding points. Both gaussian and parabolic functions are used for this. For parabolic functions the subpixel displacements in the x direction dx and in the y direction dy are found using

$$dx = \frac{P(x_m + 1, y_m) - P(x_m - 1, y_m)}{2(2P(x_m, y_m) - P(x_m + 1, y_m) - P(x_m - 1, y_m))} \tag{3.7}$$

$$dy = \frac{P(x_m, y_m + 1) - P(x_m, y_m - 1)}{2(2P(x_m, y_m) - P(x_m, y_m + 1) - P(x_m, y_m - 1))} \tag{3.8}$$

where $P(x_m, y_m)$ is the maximum correlation value. For gaussian functions the subpixel displacements in the x direction dx and in the y direction dy

are found using

$$dx = \frac{ln(P(x_m + 1, y_m)) - ln(P(x_m - 1, y_m))}{2ln(2P(x_m, y_m) - P(x_m + 1, y_m) - P(x_m - 1, y_m))} \tag{3.9}$$

$$dy = \frac{ln(P(x_m, y_m + 1)) - ln(P(x_m, y_m - 1))}{2ln(2P(x_m, y_m) - P(x_m, y_m + 1) - P(x_m, y_m - 1))} \tag{3.10}$$

The cross-correlation surface can also be interpolated using bicubic interpolation, which is a standard interpolation technique in MATLAB, for example ('interp2').

It is also possible to interpolate the images before the matching takes place. This can be done using different interpolation techniques, but bicubic is considered to be the most suited interpolation technique (Debella-Gilo and Kääb, 2011).

Least squares matching can also be used to obtain subpixel measurements. This is not a matching method in itself, but it is an iteration process that increases the accuracy of the matchings and makes it possible to obtain subpixel measurements. The initial displacement measurements have to be found using other methods and afterwards least squares iteration is used to minimize the residuals until they converge. Least squares matching can take strain rates and rotation into account and can therefore be valuable when deriving glacier velocities (Whillans and Tseng, 1995; Kaufmann and Ladstädter, 2003; Debella-Gilo and Kääb, in press).

Debella-Gilo and Kääb (2011) compared different subpixel routines for matching using NCC. They found that interpolating images before the matching is done outperformed interpolating the correlation surface after the matching is done (Fig. 3.10). It is however important to notice that this is only valid for NCC. Frequency domain methods have much sharper cross-correlation surfaces that are more suited for interpolation. Images should be oversampled by a factor of two for the interpolation of the cross-correlation surface generated using spatial domain methods to be valid, whereas this is not the case for frequency domain methods.

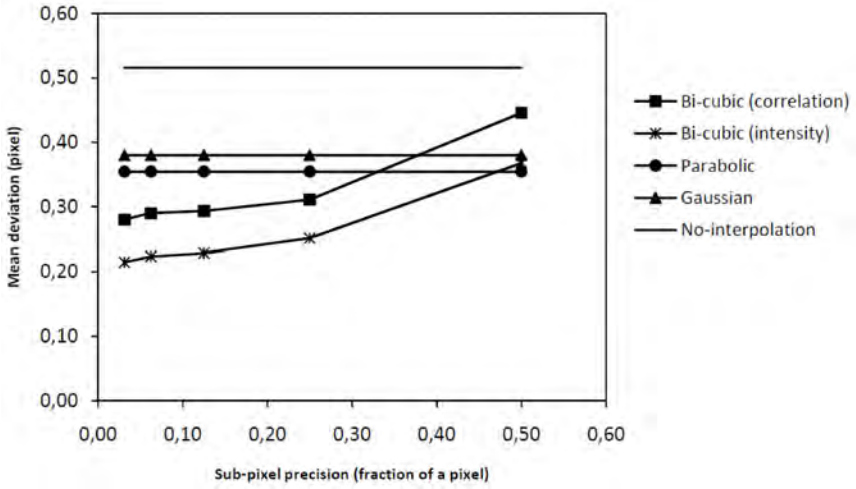

Figure 3.10: The performance of four subpixel algorithms for matching with NCC. Mean deviation indicates the deviation from an assumed correct value. From: Debella-Gilo and Kääb (2011).

3.5 Post-processing

Because the resulting displacement field usually contains a large number of both correct and erroneous matches, editing is needed as a post-processing step. Commonly, the signal-to-noise ratio (SNR) or correlation coefficient is used as the first step (Kääb and Vollmer, 2000; Skvarca et al., 2003; Kääb, 2005; Kääb et al., 2005; Scherler et al., 2008; Quincey and Glasser, 2009). Then matches with low signal-to-noise ratio or low correlation coefficients are removed. This usually leaves some mismatches (and removes some correct matches) and therefore requires more editing afterwards.

More sofisticated methods are also used for filtering the measurements. Scambos et al. (1992) used reverse correlations. They calculated the displacements using first the image from time 1 as the reference image and afterwards the image from time 2 as the reference image. The displacements were then compared, and those that deviated more than a threshold were

rejected. Directional filters have been used in some studies (Kääb, 2005; Kääb et al., 2005; Scherler et al., 2008). In this case, the flow directions are defined from the flow features visible in the images, and then the result of the matching is compared to these flow directions. Filters that look at differences in speed and remove measurements with varying speed over short distances have also been used (Scherler et al., 2008). Heid and Kääb (in press) low-pass filtered the displacement field and compared the original to the filtered version. Measurements that deviated more than a certain threshold were removed (Fig. 3.11). This approach is similar to an approach suggested by Evans (2000). Skvarca et al. (2003) filtered the vectors using a vector median filter developed by Astola et al. (1990). Debella-Gilo and Kääb (in review) actually filtered the measurements as a pre-processing step by investigating the texture in the matching windows and ignoring matching windows with little texture.

For global scale applications it might be more acceptable to remove some correct matches when filtering the displacements. Having stricter thresholds on the automatic filtering methods removes more erroneous matches, but at the same time more correct matches are removed. For global scale applications this might be acceptable, and also necessary because manual filtering of a large number of vectors is too time consuming. For studies of specific glaciers it is often better to use less strict thresholds on the automatic filtering methods and rather filter the results manually in the end to remove the last errors.

All the above mentioned filters have in common that they require manual tuning of thresholds. This is because the glacier characteristics vary considerably both between and within regions. Because of this, it seems unlikely that completely automatic filters ever exist.

3.6 Sources of error

Errors may arise from the pre-processing step, from the matching itself, and from transformation of the surface between the two image acquisitions. Er-

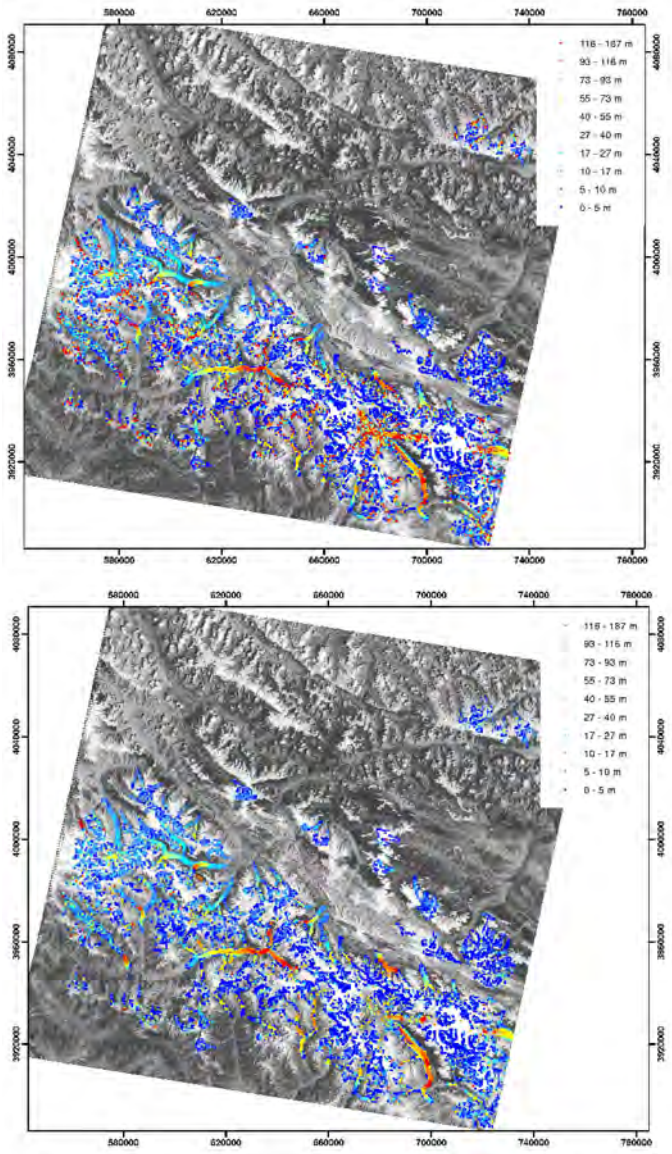

Figure 3.11: Unfiltered velocity measurements (upper panel) and automatically filtered velocity measurements (lower panel) in Karakoram. From: Heid and Kääb (in press).

rors that stem from orthorectification and from the matching are usually the easiest errors to quantify, whereas errors connected to surface transformation are more difficult to quantify.

Orthorectification may, as mentioned earlier, introduce horizontal shifts that are not due to displacement but due to errors in the orthorectification. Such errors can stem from wrong information about the camera position, look direction or lens distortions, atmospheric effects, or errors in the DEM. Errors in the DEM will influence all images obtained from the same point the same way. Therefore, in cases where the two matched images are obtained from the same point, DEM errors create only minor errors in the derived velocities. These errors are created because bumps or depressions in the DEMs that are not real give wrong distances and therefore wrong velocities. Such errors can become more prominent if the velocity field is used to investigate velocity gradients. If the same DEM is used to orthorectify images from different times and the glacier surface elevation changes between image acquisitions, this can create horizontal shifts that are not due to displacement but due to change in elevation. The relationship between elevation changes dz and horizontal position changes dx is given by

$$\frac{dz}{dx} = \frac{z_0 - z}{x} \tag{3.11}$$

where $z_0 - z$ is the sensor height above ground and x is measured as the horizontal distance of a terrain point from the sensor nadir. For Landsat images $z_0 - z = 700\,000\,\mathrm{m}$ and $x = 90\,000\,\mathrm{m}$ in the outer parts of the image. The glacier surface therefore has to change its elevation by 39 m over the time period between the two acquisitions to change the horizontal position 1/3 of a 15 m pixel. In image matching such large changes in elevation will also lead to surface decorrelation, and it will not be possible to obtain correct matches.

The image-to-image registration accuracy of the images used will influence the matching accuracy. Satellite agencies usually investigate the image-to-image registration accuracy of their products and publish the results (e.g. Lee et al., 2004).

The accuracy of the matching algorithm, including the subpixel routine,

also introduces errors. This error can be quantified either by investigating the root mean square error (RMSE) of measurements over assumed stable ground, or by constructing synthetic images with applied displacements and comparing the derived displacements to the applied displacements. To obtain only the accuracy of the matching algorithm, synthetic images should be used because measurements over stable ground also include satellite jitter and errors from the orthorectification if the two images are obtained from different locations.

The match can in theory originate from anywhere inside the window, and where it originates from depends on the matching method. If COSI-Corr is used it is more likely that the match originates from the center because of the weighting with a bell-shaped window. For NCC the match is more likely to come from an area with large differences in DNs. Using frequency domain methods with no weighting window, the match represents the most common displacement within the window. In cases where the displacements have to be attributed to a specific point and not the window, for example if the displacement field is used to derive strain rates or if the displacement field is compared to ground truth data, this can introduce errors.

Undiscovered erroneous matches in the filtered and final displacement field can also be present. Clear mismatches are easy to reject in the post-processing step, but some matches might have both approximately the same direction and magnitude as surrounding matches and incorrectly be classified as a correct match. It can be easier to identify such erroneous matches over stable ground than over moving surfaces, because neighbouring matches should be alike over stable ground whereas neighbouring matches are allowed to vary over surfaces with displacement.

There might be different kinds of surface transformation from one image to the next image that makes the match less correct. Such transformations include deformation, melting, opening or closing of crevasses and debris behaving differently from the glacier. The latter might for example be rocks sliding or rolling on the glacier, or deformation of the debris. As long as the surface transformation is not sufficient enough to generate a mismatch such surface transformations will make the match less accurate.

For independent errors the final error can be calculated as the root sum square (RSS) of the individual error contributions. In image matching of glacier velocities the final error of the measurements E can be given as

$$E = \sqrt{(E_{ort})^2 + (E_{reg})^2 + (E_{mat})^2 + (E_{pos})^2 + (E_{mis})^2 + (E_{tra})^2} \quad (3.12)$$

where E_{ort} is the error from orthorectification, E_{reg} is the error from image-to-image registration, E_{mat} is the error from the matching algorithm, E_{pos} is the error when the match originates from another position in the window than what is assumed, E_{mis} is the error from the mismatches and E_{tra} is the error from the surface transformation.

3.7 Comparison to groundbased measurements

A few studies have compared displacements measured using image matching to displacements measured using ground based surveys. This is usually quite a difficult task because both measurements should ideally represent the same time period. Due to both seasonal and yearly variations in glacier speed, it is easy to capture such differences instead of methodological differences if the measurements do not originate from the exact same period.

The fact that matches can originate from anywhere inside the window can also make the comparison difficult. If the match is attributed to the center point but represents the outer edge of the window, this can give deviations between the ground based measurements and the image matching measurements if there are velocity gradients within the window. This does not mean that the match is incorrect, only that the match is incorrectly said to represent the center of the window.

Lucchitta and Ferguson (1986) compared Landsat derived velocities to velocities derived using ground surveys. They found that there was an agreement of better than 10 %. Frezzotti et al. (1998) compared data from GPS with image matching results obtained using Landsat MSS, Landsat TM and SPOT XS. They found that close to tie points the image matching errors were down to 15 m/a whereas the image matching errors far from tie points

were 70 m/a. Berthier et al. (2005) compared SPOT5 derived velocities to ground truth data obtained using DGPS. The DGPS measurements were from a shorter time period within the period between the two SPOT5 image acquisitions. Differences between the two methods were in the order of 1/5 of the pixel size of 0.5 m, but some of this discrepancy was assumed to stem from the different time periods or uncertainties in the DGPS system. Copland et al. (2009) compared yearly ASTER derived velocities to summer DGPS data. They found that the direction fitted well and that most of the differences in magnitude were within the error of image matching. However, they also found one point with higher magnitude in the DGPS data and they attributed this to higher summer speed. Herman et al. (2011) used COSI-Corr and ASTER images to derive velocities in New Zealand. They found a small bias in the north-south component of the displacements that they attributed to pitch residuals of the spacecraft that were not removed in the orthorectification process.

4

Summary of articles

4.1 Article I

Monitoring ice shelf velocities from repeat MODIS and Landsat data - a method study on the Larsen C ice shelf, Antarctic Peninsula, and 10 other ice shelves around Antarctica

Although many studies have conducted measurements of glacier velocities using image matching of optical images, very few studies have conducted measurements on ice shelves using this method. Bindschadler et al. (1994) and Rack et al. (1999) derived velocities on the relatively small Larsen A ice shelf, Skvarca (1994) and Glasser et al. (2009) measured velocities of small sections of Larsen C ice shelf as part of larger studies. Also, the focus when using image matching to derive glacier velocities has been on medium and high spatial resolution images, and low spatial resolution images have received little attention. Low resolution images however, have several advantages over medium and high spatial resolution images. Firstly, low resolution sensors cover large areas with only one image, which makes it easier to do large-scale monitoring of glacier velocities. This also ensures that there is stable bedrock in most images so that different images can be accurately

coregistered. Secondly, low spatial resolution satellites have high temporal resolution, especially in polar regions where several images can be obtained every day. In cloudy regions this is important because the likelihood of obtaining cloud-free images for a wanted period increases drastically.

In this article velocities are derived using MODIS images (250 m spatial resolution) for two periods for the Larsen C ice shelf on the Antarctic Peninsula. The two periods are 2002-2006 and 2006-2009. The velocities obtained using MODIS images are also validated for two ice shelf sections against velocities obtained using Landsat 7 ETM+ panchromatic images with 15 m spatial resolution. We mainly use orientation correlation to derive velocities, but normalized cross-correlation is also tested.

The uncertainties for the MODIS derived displacements are about one fourth of a pixel, and for Landsat derived displacements the uncertainties are about one pixel. When comparing speeds, the difference between MODIS and Landsat derived speeds is -15.4 m/a and 13.0 m/a for the two different sections on the ice shelf for the first period and -26.7 m/a and 27.9 m/a for the same sections for the second period. We therefore conclude that MODIS images are well suited for measuring ice shelf velocities and also for monitoring their changes over time.

Orientation correlation seems better suited than normalized cross-correlation in this study. Orientation correlation creates fewer mismatches, is able to match images with regular noise and data voids, and is faster. Because it can match images with data voids, it can also be used to match Landsat 7 ETM+ images after the failure of the Scan Line Corrector in 2003 (SLC off).

As a second part of the study we test our method on ten other ice shelves around Antarctica. The method works well on most parts of the ice shelves investigated. The main factor that hinders successful matching during cloud-free conditions is the lack of visual contrast. However, on large parts of the ice shelves it is possible to derive velocities, and this demonstrates that the approach is suitable for large scale monitoring of ice shelf dynamics.

4.2 Article II

Evaluation of different existing image matching methods for deriving glacier surface displacements globally from optical satellite images

There has been little focus on comparing different correlation algorithms to find the correlation algorithm that is best suited for measuring glacier velocities using repeat optical satellite images. However, many different correlation algorithms have been used to derive velocities, so there is a need to compare commonly used correlation algorithms. We hypothesize that since glaciers can be very different depending on where in the world they are situated, it might be that different correlation algorithms work best in different areas of the world.

We test six commonly used matching methods over five glacierized areas spread around the world and with different characteristics, which are though to be globally representative. The matching methods evaluated are (1) normalized cross-correlation operated in the frequency domain, (2) cross-correlation operated in the frequency domain, (3) phase correlation operated in the frequency domain, (4) cross-correlation operated in the frequency domain on orientation images, (5) phase correlation operated in the frequency domain on orientation images, (6) the phase correlation algorithm used in the COSI-Corr software. The five glacierized study regions are Karakoram, the European Alps, Alaska, Pine Island in Antarctica and southwest Greenland. Because the aim of this study also is to open up the possibility to do global-scale mapping and monitoring glacier flow, we use Landsat images. One Landsat image covers a large area on the ground, and also they extend back to 1982 with 30 m spatial resolution.

Cross-correlation on orientation images (CCF-O) outperforms the three similar Fourier methods, both in areas with high and low visual contrast. Normalized cross-correlation (NCC) experiences problems in areas with low visual contrast, areas with thin clouds or changing snow conditions between the images. CCF-O has problems on narrow glaciers where small window

sizes are needed, and it obtains fewer correct matches than COSI-Corr in areas with low visual contrast. COSI-Corr has problems on narrow glaciers and it obtains fewer matches compared to CCF-O when thin clouds cover the surface or if one of the images contains snow dunes. Of the three methods NCC, CCF-O and COSI-Corr, only CCF-O manages to match striped Landsat images after the failure of the Scan Line Corrector (SLC off) in 2003. In total we consider CCF-O and COSI-Corr to be the two most robust matching methods for global-scale mapping and monitoring of glacier velocities.

4.3 Article III

Worldwide widespread decadal-scale decrease of glacier speed revealed using repeat optical satellite images

Because so much focus has been put into developing, improving, automating and comparing different image matching methods over the last years (Leprince et al., 2007; Scherler et al., 2008; Haug et al., 2010; Debella-Gilo and Kääb, 2011, in review; Heid and Kääb, in press), it is now possible to derive glacier velocities over large regions of the world. Such velocity measurements make it possible to improve our knowledge about glacier dynamics both in space and time. In this study we focus on exploring the connection between glacier mass balance and glacier speed changes. Many regions of the world have had a negative mass balance over the last decades (Käser et al., 2006; Lemke et al., 2007; Bahr et al., 2009; WGMS, 2009), and we hypothesize that this has caused the glaciers in these areas to slow down. To test this we select five regions of the world with negative mass balance over the last decades: Pamir, Caucasus, Penny Ice Cap, Alaska Range and Patagonia. For every region the glacier velocities are derived for two different periods and the speeds are compared for these two different periods. We also select Karakoram, which is an area assumed to have positive mass balance (Quincey et al., 2009a) and which also contains many surging glaciers (Hewitt, 1969, 2007; Copland et al., 2009).

We find that the mapped glaciers in the five areas with negative mass balance have reduced their speeds over the last decades. Glaciers in Pamir have reduced their speed by 43 % in average per decade, glaciers in Caucasus by 8 % in average per decade, outlet glaciers from Penny Ice Cap by 25 % in average per decade, glaciers in the Alaska Range by 11 % in average per decade, and outlet glaciers from the Southern Patagonia Ice Field by 20 % per decade.

Glaciers in Karakoram behave differently depending on location. Glaciers in the east have generally increased their speeds as a result of the positive mass balance. In this area there are probably few surging glaciers due to the few observations of surging glaciers and the few looped moraines seen in the satellite images. In the central north many of the glaciers are probably surging due to the low speeds, which indicate surging glaciers in their quiescent phase, and the many observations of glacier surges in this area. In northwest the glaciers have large speed variations from period to period, but because the speeds are high in both periods, sliding must be important in both periods and hence the glaciers cannot be defined as surging glaciers.

5

Conclusions and perspectives

The focus of this thesis has been to further develop optical image matching techniques within glaciology. So far very little focus has been on developing the methods within glaciology, whereas many studies have applied such methods to glaciology. Only medium or high spatial resolution images have been used so far, and studies have only focused on one image matching method. It has therefore been a need to further explore optical image matching within glaciology.

Paper I shows that low resolution images can be of great use within image matching in glaciology. The large ice shelves surrounding Antarctica are difficult to match using high or medium spatial resolution images. This is because they are so large that many high or medium spatial resolution images are needed to match one ice shelf, and because it is difficult to find stable bedrock to orthorectify the images when the ice shelves are so enormous. It can also be easier to find optical images from each year using low resolution images because of the shorter repeat times of such imagery. In this research we used MODIS images with a spatial resolution of 250 m, and obtained an accuracy for MODIS derived displacements of about one fourth of a pixel. Because it is possible to match images several years apart due to the little surface transformation, the yearly uncertainty relative to the yearly displacement is small. Therefore it is possible to monitor ice shelf speed changes using low resolution images.

In Paper II we showed that NCC, which is commonly used to derive glacier displacements, does not perform as well as other methods for most glacier types. In general, COSI-Corr performs best but CCF-O performs almost as well. The main problem with NCC is the low number of correct matches in areas with low visual contrast, but also thin clouds and changing snow conditions are a problem for this method. CCF-O has problems with narrow outlet glaciers, and it obtains fewer correct matches than COSI-Corr in areas with low visual contrast. COSI-Corr has problems on narrow glaciers, when thin clouds cover the surface or if one of the images contains snow dunes. Only CCF-O manages to match striped Landsat images after the failure of the SLC. In total CCF-O and COSI-Corr are considered to be the best methods for global-scale mapping and monitoring of glacier velocities.

Regional glacier velocities give us the opportunity to improve our knowledge about glacier dynamics both in space and time. In this research we investigate the relationship between glacier mass balance and glacier speed. In five regions of the world where the mass balance has been negative over the last decades, glaciers have also reduced their speed. These five areas are Pamir (reduction in glacier speed of 43 % per decade), Caucasus (reduction in glacier speed of 8 % per decade), Penny Ice Cap (reducion in glacier speed of 25 % per decade), Alaska Range (reduction in glacier speed of 11 % per decade) and Patagonia (reduction in glacier speed of 20 % per decade). Karakoram, an area with assumed positive mass balance, shows an increase in glacier speed over the last decades. However, Karakoram is heavily influenced by glacier surges and dynamically instable glaciers, and this is most prominent in this area.

The development of image matching within glaciology done in this research, combined with the development done in other studies (e.g. Kääb, 2005; Leprince et al., 2007; Scherler et al., 2008; Debella-Gilo and Kääb, 2011, in review), makes it easier to derive glacier velocities. In this thesis the focus has been to explore imagery that has never been used to derive glacier velocity before over areas that have never been mapped using image matching. We have also compared commonly used image matching methods to be able to select the best method in every situation. Together with

adaptive window sizes (Debella-Gilo and Kääb, in review) this gives the possibility to automatically derive glacier velocities worldwide. However, using adaptive window sizes is time consuming, and today it is not possible to do this worldwide due to computing time. Filtering of the measurements afterwards to remove mismatches is a task that is difficult to fully automate because all methods require manual tuning of the filtering parameters. The adaptive window size approach may be a solution to this problem because windows with too little texture when the upper window size limit is reached are ignored in the matching.

New image matching methods developed in the future can be tested against the methods tested in this study to investigate whether they perform better over glaciers. It is then important to test the methods over several different glacier surfaces, because it may change from glacier to glacier and glacier region to glacier region which method performs the best. Such a study can be done following the procedure outlined in Paper II.

Image matching of SAR images can also be investigated closer using a similar approach to what is shown for optical images in Paper II. Comparing different SAR-based methods for deriving glacier velocities is more done than comparing different optical methods. However, these studies have focused on the difference between intensity tracking, coherence tracking, speckle tracking and DInSAR (Michel and Rignot, 1999; Strozzi et al., 2002; Luckman et al., 2007) instead of focusing on the difference between different matching methods. Future studies could therefore focus on different image matching algorithms within image matching of SAR images. Fig. 5.1 shows the matching results of NCC, PC and OC using two ERS-1 scenes over Svalbard. Because of the high level of almost random noise in SAR images, PC and OC obtain less correct matches compared to NCC. This is the opposite than for optical images and highlights the importance of testing different image matching methods also for image matching of SAR images.

It is now possible to derive glacier velocities over larger regions, and more effort should be focused on this. Such studies can provide valuable insights in glacier dynamics. Firstly, as shown in Paper III, this can give information about how glaciers respond to climate change. Secondly, regional glacier ve-

locities derived for different periods give the possibility to investigate surge occurrence, surge behaviour and other dynamical instabilities. This can reveal new information on how frequent dynamically instable glaciers actually are. It can also help to solve what the mechanisms behind surging glaciers are. Thirdly, glacier velocities are linked to glacier hazards. The reduction of glacier speed can create glacier lakes, and these may burst and flood lower lying regions. Extending the number of glaciers with velocity measurements can help to point out areas where glacier lakes may form. Such areas can then be monitored closely to avoid or reduce damage when lakes drain. Fourthly, glacier velocities may be tested against glacier inventory parameters such as length, area and hypsometry to point out differences and similarities between areas. Fifthly, glacier velocities can be used to estimate transport times and erosion rates, and thereby contribute to knowledge on landscape development.

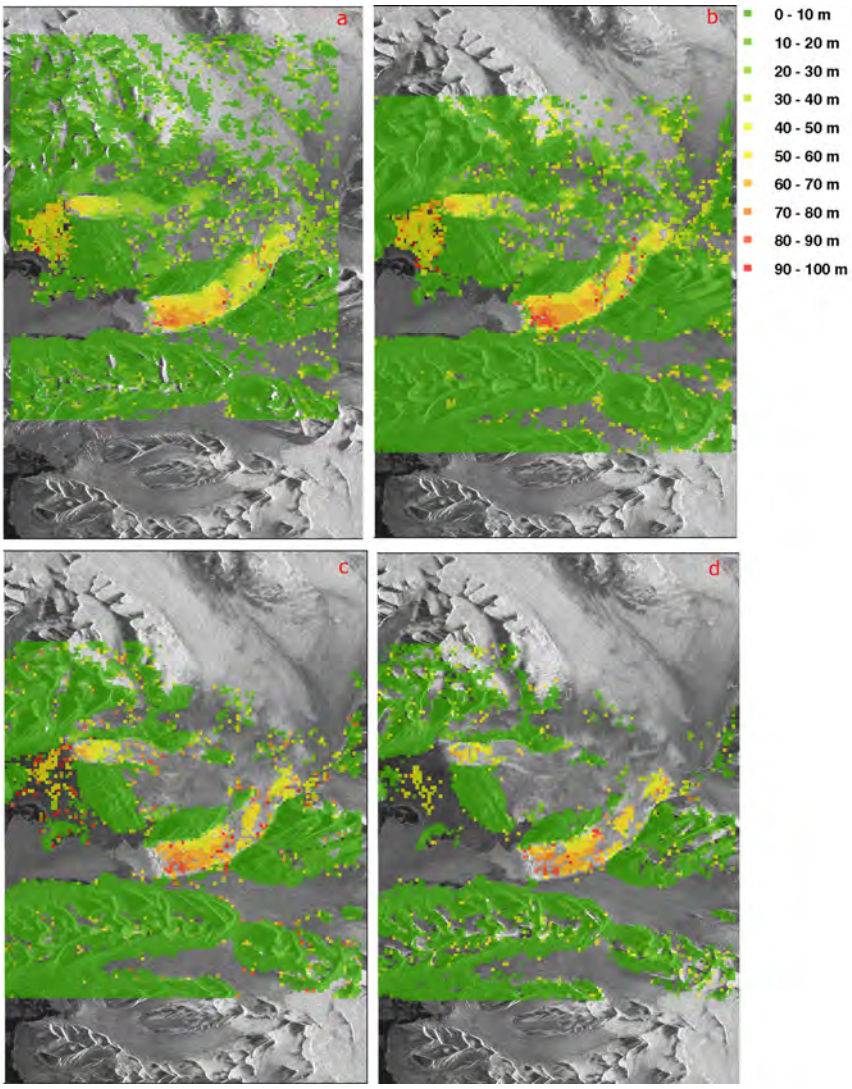

Figure 5.1: SAR intensity tracking using two ERS-1 scenes over Kongsvegen, Kronebreen and Kongsbreen between 5 April 1996 and 10 May 1996. Matching results are obtained using a) the Gamma software developed by Gamma Remote Sensing AG based on normalized cross-correlation, b) own written normalized cross-correlation, c) phase correlation and d) orientation correlation. (Heid, unpublished.)

References

Abdalati, W. and W.B. Krabill, 1999. Calculation of ice velocities in the Jakobshavn Isbrae area using airborne laser altimetry, *Remote Sensing of Environment*, **67**(2), 194–204.

Astola, J., P. Haavisto and Y. Neuvo, 1990. Vector median filters, *Proceedings of the IEEE*, **78**(4), 678–689.

Bahr, D.B., M. Dyurgerov and M.F. Meier, 2009. Sea-level rise from glaciers and ice caps: A lower bound, *Geophysical Research Letters*, **36**, L03501.

Benn, D.I. and D.J.A. Evans, 2010. Glaciers and glaciation, Hodder Education.

Bernstein, R., 1983. Manual of Remote Sensing, American Society of Photogrammetry, Falls Church, VA, chap. Image geometry and rectification, 881–884.

Berthier, E., B. Raup and T.A. Scambos, 2003. New velocity map and mass-balance estimate of Mertz Glacier, East Antarctica, derived from Landsat sequential imagery, *Journal of Glaciology*, **49**(167), 503–511.

Berthier, E., H. Vadon, D. Baratoux, Y. Arnaud, C. Vincent, K.L. Feigl, F. Remy and B. Legresy, 2005. Surface motion of mountain glaciers derived from satellite optical imagery, *Remote Sensing of Environment*, **95**(1), 14–28.

Bindschadler, R.A., M.A. Fahnestock, P. Skvarca and T.A. Scambos, 1994.

Surface-velocity field of the northern Larsen Ice Shelf, Antarctica, *Annals of Glaciology*, **20**, 319–326.

Bindschadler, R.A. and T.A. Scambos, 1991. Satellite-image-derived veolocity field of an Antarctic ice stream, *Science*, **252**(5003), 242–246.

Bindschadler, R., P. Vornberger, D. Blankenship, T.A. Scambos and R. Jacobel, 1996. Surface velocity and mass balance of Ice Streams D and E, West Antarctica, *Journal of Glaciology*, **42**(142), 461–475.

Brecher, H.H., 1985. Surface velocity determination on large polar glaciers by aerial photogrammetry, *Annals of Glaciology*, **8**, 22–26.

Brown, L.G., 1992. A survey of image registration techniques, *Computing Surveys*, **24**(4), 325–376.

Cook, A.J. and D.G. Vaughan, 2010. Overview of areal changes of the ice shelves on the Antarctic Peninsula over the past 50 years, *Cryosphere*, **4**(1), 77–98.

Copland, L., S. Pope, M.P. Bishop, J.F. Shroder Jr, P. Clendon, A. Bush, U. Kamp, Y. B. Seong and L.A. Owen, 2009. Glacier velocities across the central Karakoram, *Annals of Glaciology*, **50**(52), 41–49.

Debella-Gilo, M. and A. Kääb, 2011. Sub-pixel precision algorithms for normalized cross-correlation based image matching of mass movements, *Remote Sensing of Environment*, **115**, 130–142.

Debella-Gilo, M. and A. Kääb, in press. Monitoring slow-moving landslides using spatially adaptive least squares image matching, *Proceedings of the Second World Landslide Forum*.

Debella-Gilo, M. and A. Kääb, in review. Locally adaptive template sizes for matching repeat images of Earth surface mass movements, *ISPRS Journal of Photogrammetry and Remote Sensing*.

Dowdeswell, J.A. and T.J. Benham, 2003. A surge of Perseibreen, Svalbard, examined using aerial photography and ASTER high resolution satellite imagery, *Polar Research*, **22**(2), 373–383.

Dvornychenko, V.N., 1983. Bounds on (deterministic) correlation-functions with application to registration, *IEEE Transactions on Pattern Analysis and Machine Intelligence*, **5**(2), 206–213.

Espizua, L.E. and J.D. Bengochea, 1990. Surge of Grande del Nevado Glacier (Mendoza, Argentina) in 1984 - its evolution through satellite images, *Geografiska Annaler Series A-Physical Geography*, **72**(3-4), 255–259.

Evans, A.N., 2000. Glacier surface motion computation from digital image sequences, *IEEE Transactions on Geoscience and Remote Sensing*, **38**(2, Part 2), 1064–1072.

Fitch, A.J., A. Kadyrov, W.J. Christmas and J. Kittler, 2002. Orientation Correlation, British Machine Vision Conference, 133–142.

Frezzotti, M., A. Capra and L. Vittuari, 1998. Comparison between glacier ice velocities inferred from GPS and sequential satellite images, *Annals of Glaciology*, **27**, 54–60.

Förstner, W. and E. Gülch, 1987. A fast operator for detection and precise location of distinct points, corners and centres of circular features, ISPRS Intercommission Workshop.

Giles, A.B., R.A. Massom and R.C. Warner, 2009. A method for sub-pixel scale feature-tracking using Radarsat images applied to the Mertz Glacier Tongue, East Antarctica, *Remote Sensing of Environment*, **113**(8), 1691–1699.

Glasser, N.F., B. Kulessa, A. Luckman, D. Jansen, E.C. King, P.R. Sammonds, T.A. Scambos and K.C. Jezek, 2009. Surface structure and stability of the Larsen C ice shelf, Antarctic Peninsula, *Journal of Glaciology*, **55**(191), 400–410.

Hagen, J.O., T. Eiken, J. Kohler and K. Melvold, 2006. Geometry changes on Svalbard glaciers: mass-balance or dynamic response?, *Annals of Glaciology*, **42**(1), 255–261.

Haug, T., A. Kääb and P. Skvarca, 2010. Monitoring ice shelf velocities from repeat MODIS and Landsat data - a method study on the Larsen C ice shelf, Antarctic Peninsula, and 10 other ice shelves around Antarctica, *Cryosphere*, **4**(2), 161–178.

Heid, T. and A. Kääb, in press. Evaluation of different existing image matching methods for deriving glacier surface displacements globally from optical satellite imagery, *Remote Sensing of Environment*.

Herman, F., B. Anderson and S. Leprince, 2011. Mountain glacier velocity variation during a retreat/advance cycle quantified using sub-pixel analysis of ASTER images, *Journal of Glaciology*, **57**(202), 197–207.

Hewitt, K., 1969. Glacier surges in Karakoram Himalaya (Central Asia), *Canadian Journal of Earth Sciences*, **6**(4P2), 1009–1018.

Hewitt, K., 2007. Tributary glacier surges: an exceptional concentration at Panmah Glacier, Karakoram Himalaya, *Journal of Glaciology*, **53**(181), 181–188.

Hooke, R.L., 2005. Principles of glacier mechanics, Cambridge University Press, Cambridge.

Huang, L. and Z. Li, 2011. Comparison of SAR and optical data in deriving glacier velocity with feature tracking, *International Journal of Remote Sensing*, **32**(10), 2681–2698.

Joughin, I., 2002. Ice-sheet velocity mapping: a combined interferometric and speckle-tracking approach, *Annals of Glaciology*, **34**, 195–201.

Joughin, I., B.E. Smith, I.M. Howat, T.A. Scambos and T. Moon, 2010. Greenland flow variability from ice-sheet-wide velocity mapping, *Journal of Glaciology*, **56**(197), 415–430.

Kaufmann, V. and R. Ladstädter, 2003. Quantitative analysis of rock glacier creep by means of digital photogrammetry using multi-temporal aerial photographs: two case studies in the Austrian Alps, *Permafrost*, **1&2**, 525–530.

Kuglin, C.D and D.C. Hines, 1975. The phase correlation image alignment method, *Proceedings of the IEEE 1975 International Conference on Cybernetics and Society*, 163–165.

Käser, G., J.G. Cogley, M.B. Dyurgerov, M.F. Meier and A. Ohmura, 2006. Mass balance of glaciers and ice caps: Consensus estimates for 1961-2004, *Geophysical Research Letters*, **33**(19), L19501.

Kääb, A., 2002. Monitoring high-mountain terrain deformation from repeated air- and spaceborne optical data: examples using digital aerial imagery and ASTER data, *ISPRS Journal of Photogrammetry and Remote Sensing*, **57**(1-2), 39–52.

Kääb, A., 2005. Combination of SRTM3 and repeat ASTER data for deriving alpine glacier flow velocities in the Bhutan Himalaya, *Remote Sensing of Environment*, **94**(4), 463–474.

Kääb, A., 2005. Remote sensing of mountain glaciers and permafrost creep, Schriftenreihe Physiche Geographie Glaziologie und Geomorphodynamik. Geographisches Institut der Universität Zürich.

Kääb, A., B. Lefauconnier and K. Melvold, 2005. Flow field of Kronebreen, Svalbard, using repeated Landsat 7 and ASTER data, *Annals of Glaciology*, **42**, 7–13.

Kääb, A. and M. Vollmer, 2000. Surface geometry, thickness changes and flow fields on creeping mountain permafrost: Automatic extraction by digital image analysis, *Permafrost and Periglacial Processes*, **11**(4), 315–326.

de Lange, R., A. Luckman and T. Murray, 2007. Improvement of satellite radar feature tracking for ice velocity derivation by spatial frequency fil-

tering, *IEEE Transactions on Geoscience and Remote Sensing*, **45**(7, Part 2), 2309–2318.

Lee, D.S., J.C. Storey, M.J. Choate and R.W. Hayes, 2004. Four years of Landsat-7 on-orbit geometric calibration and performance, *IEEE Transactions on Geoscience and Remote Sensing*, **42**(12), 2786–2795.

Lemke, P., J. Ren, R.B. Alley, I. Allison, J. Carrasco, G. Flato, Y. Fujii, G. Kaser, P. Mote, R.H. Thomas and T. Zhang, 2007. Observations: Changes in Snow, Ice and Frozen Ground. In: Climate Change 2007: The Physical Science Basis. Contribution of Working Group I to the Fourth Assessment Report of the Intergovernmental Panel on Climate Change (Solomon, S., D. Qin, M. Manning, Z. Chen, M. Marquis, K.B. Averyt, M. Tignor and H.L. Miller (eds.))., Cambridge University Press, Cambridge, United Kingdom and New York, NY, USA.

Leprince, S., S. Barbot, F. Ayoub and J.P. Avouac, 2007. Automatic and precise orthorectification, coregistration, and subpixel correlation of satellite images, application to ground deformation measurements, *IEEE Transactions on Geoscience and Remote Sensing*, **45**(6), 1529–1558.

Lucchitta, B.K. and H.M. Ferguson, 1986. Antarctica - measuring glacier velocity from satellite images, *Science*, **234**(4780), 1105–1108.

Luckman, A., T. Murray, H. Jiskoot, H. Pritchard and T. Strozzi, 2003. ERS SAR feature-tracking measurement of outlet glacier velocities on a regional scale in East Greenland, *Annals of Glaciology*, **36**, 129–134.

Luckman, A., D. Quincey and S. Bevan, 2007. The potential of satellite radar interferometry and feature tracking for monitoring flow rates of Himalayan glaciers, *Remote Sensing of Environment*, **111**, 172–181.

McClellan, J.H, R.W. Schafer and M.A. Yoder, 2003. Signal Processing First, Pearson Education, Inc., Pearson Prentice Hall.

Michel, R. and E. Rignot, 1999. Flow of Glaciar Moreno, Argentina, from repeat-pass Shuttle Imaging Radar images: comparison of the phase correlation method with radar interferometry, *Journal of Glaciology*, **45**(149), 93–100.

Murray, T., K. Scharrer, T.D. James, S. R. Dye, E. Hanna, A.D. Booth, N. Selmes, A. Luckman, A. L.C. Hughes, S. Cook and P. Huybrechts, 2010. Ocean regulation hypothesis for glacier dynamics in southeast Greenland and implications for ice sheet mass changes, *Journal of Geophysical Research*, **115**, F03026.

Orheim, O. and B.K. Lucchitta, 1987. Snow and ice studies by Thematic Mapper and Multispectral Scannar Landsat images, *Annals of Glaciology*, **9**, 109–118.

Paterson, W.S.B., 1994. The physics of glaciers. Third edition, Oxford, etc., Elsevier.

Quincey, D.J., L. Copland, C. Mayer, M. Bishop, A. Luckman and M. Belo, 2009a. Ice velocity and climate variations for Baltoro Glacier, Pakistan, *Journal of Glaciology*, **55**(194), 1061–1071.

Quincey, D.J. and N.F. Glasser, 2009. Morphological and ice-dynamical changes on the Tasman Glacier, New Zealand, 1990-2007, *Global and Planetary Change*, **68**(3), 185–197.

Quincey, D.J., A. Luckman and D. Benn, 2009b. Quantification of Everest region glacier velocities between 1992 and 2002, using satellite radar interferometry and feature tracking, *Journal of Glaciology*, **55**(192), 596–606.

Rack, W., H. Rott, A. Siegel and P. Skvarca, 1999. The motion field of northern Larsen Ice Shelf, Antarctic Peninsula, derived from satellite imagery, *Annals of Glaciology*, **29**, 261–266.

Rees, W.G. and N.S. Arnold, 2007. Mass balance and dynamics of a valley glacier measured by high-resolution LiDAR, *Polar Record*, **43**(227), 311–319.

Rignot, E. and P. Kanagaratnam, 2006. Changes in the velocity structure of the Greenland ice sheet, *Science*, **311**, 986–990.

Rignot, E. and D.R. MacAyeal, 1998. Ice-shelf dynamics near the front of the Filchner-Ronne Ice Shelf, Antarctica, revealed by SAR interferometry, *Journal of Glaciology*, **44**(147), 405–418.

Rolstad, C., J. Amlien, J.O. Hagen and B. Lunden, 1997. Visible and near-infrared digital images for determination of ice velocities and surface elevation during a surge on Osbornebreen, a tidewater glacier in Svalbard, *Annals of Glaciology*, **24**, 255–261.

Rott, H., 2009. Advances in interferometric synthetic aperture radar (InSAR) in earth system science, *Progress in Physical Geography*, **33**(6), 769–791.

Rott, H., W. Rack, P. Skvarca and H. De Angelis, 2002. Northern Larsen Ice Shelf, Antarctica: further retreat after collapse, *Annals of Glaciology*, **34**, 277–282.

Scambos, T.A., M.J. Dutkiewicz, J.C. Wilson and R.A. Bindschadler, 1992. Application of image cross-correlation to the measurement of glacier velocity using satellite image data, *Remote Sensing of Environment*, **42**(3), 177–186.

Scherler, D., B. Bookhagen and M.R. Strecker, 2011a. Hillslope-glacier coupling: The interplay of topography and glacial dynamics in High Asia, *Journal of Geophysical Research*, **116**, F02019.

Scherler, D., B. Bookhagen and M.R. Strecker, 2011b. Spatially variable response of Himalayan glaciers to climate change affected by debris cover, *Nature Geoscience*, **4**(3), 156–159.

Scherler, D., S. Leprince and M.R. Strecker, 2008. Glacier-surface velocities in alpine terrain from optical satellite imagery - Accuracy improvement and quality assessment, *Remote Sensing of Environment*, **112**(10), 3806–3819.

Schmid, C., R. Mohr and C. Bauckhage, 1998. Comparing and evaluating interest points, Proceedings Computer Vision, 230–235.

Schwalbe, E. and H.-G. Maas, 2009. Motion analysis of fast flowing glaciers from multi-temporal terrestrial laser scanning, *Photogrammetrie Fernerkundung Geoinformation*, **1**, 91–98.

Skvarca, P., 1994. Changes and surface features of the Larsen Ice Shelf, Antarctica, derived from Landsat and Kosmos mosaics, *Annals of Glaciology*, **20**, 6–12.

Skvarca, P., H. De Angelis and A.F. Zakrajsek, 2004. Climatic conditions, mass balance and dynamics of Larsen B ice shelf, Antarctic Peninsula, prior to collapse, *Annals of Glaciology*, **39**, 557–562.

Skvarca, P., W. Rack and H. Rott, 1999. 34 year satellite time series to monitor characteristics, extent and dynamics of Larsen B Ice Shelf, Antarctic Peninsula, *Annals of Glaciology*, **29**, 255–260.

Skvarca, P., B. Raup and H. De Angelis, 2003. Recent behaviour of Glaciar Upsala, a fast-flowing calving glacier in Lago Argentino, southern Patagonia, *Annals of Glaciology*, **36**, 184–188.

Strozzi, T., A. Luckman, T. Murray, U. Wegmuller and C.L. Werner, 2002. Glacier motion estimation using SAR offset-tracking procedures, *IEEE Transactions on Geoscience and Remote Sensing*, **40**(11), 2384–2391.

van der Veen, C. and A.J. Payne, 2004. Modelling land-ice dynamics. In: Mass balance of the cryosphere: Observations and modelling of contemporary and future changes, Cambridge University Press, Cambridge.

Vieli, A., A.J. Payne, Z.J. Du and A. Shepherd, 2006. Numerical modelling and data assimilation of the Larsen B ice shelf, Antarctic Peninsula, *Philosophical Transactions Of The Royal Society A-Mathematical Physical And Engineering Sciences*, **364**(1844), 1815–1839.

WGMS, 2009. Global Glacier Change: facts and figures. Zemp, M., Roer, I., Kääb, A., Hoelzle, M., Paul, F. and W. Haeberli (eds.), UNEP, World Glacier Monitoring Service, Zurich, Switzerland, 88 pp.

Whillans, I.M. and Y.H. Tseng, 1995. Automatic tracking of crevasses on satellite images, *Cold Regions Science and Technology*, **23**(2), 201–214.

Zitova, B. and J. Flusser, 2003. Image registration methods: a survey, *Image and Vision Computing*, **21**(11), 977–1000.

Zwally, H. Jay, W. Abdalati, T. Herring, K. Larson, J. Saba and K. Steffen, 2002. Surface melt-induced acceleration of Greenland ice-sheet flow, *Science*, **297**, 218–222.

6

Peer-reviewed articles

I

6.1 Article I

Haug*, T., A. Kääb and P. Skvarca, 2010. Monitoring ice shelf velocities from repeat MODIS and Landsat data - a method study on the Larsen C ice shelf, Antarctic Peninsula, and 10 other ice shelves around Antarctica, *Cryosphere*, 4(2), 161-178.

** last name changed to Heid*

The Cryosphere, 4, 161–178, 2010
www.the-cryosphere.net/4/161/2010/
doi:10.5194/tc-4-161-2010

The Cryosphere

Monitoring ice shelf velocities from repeat MODIS and Landsat data – a method study on the Larsen C ice shelf, Antarctic Peninsula, and 10 other ice shelves around Antarctica

T. Haug[1], **A. Kääb**[1], **and P. Skvarca**[2]

[1]Department of Geosciences, University of Oslo, P.O. Box 1047 Blindern, 0316 Oslo, Norway
[2]Instituto Antártico Argentino, Cerrito 1248, C1010AAZ Buenos Aires, Argentina

Received: 21 December 2009 – Published in The Cryosphere Discuss.: 14 January 2010
Revised: 22 April 2010 – Accepted: 28 April 2010 – Published: 6 May 2010

Abstract. We investigate the velocity field of the Larsen C ice shelf, Antarctic Peninsula, over the periods 2002–2006 and 2006–2009 based on repeat optical satellite data. The velocity field of the entire ice shelf is measured using repeat low resolution MODIS data (250 m spatial resolution). The measurements are validated for two ice shelf sections against repeat medium resolution Landsat 7 ETM+ pan data (15 m spatial resolution). Horizontal surface velocities are obtained through image matching using both orientation correlation operated in the frequency domain and normalized crosscorrelation operated in the spatial domain, and the two methods compared. The uncertainty in the displacement measurements turns out to be about one fourth of the pixel size for the MODIS derived data, and about one pixel for the Landsat derived data. The difference between MODIS and Landsat based speeds is $-15.4\,\mathrm{m\,a^{-1}}$ and $13.0\,\mathrm{m\,a^{-1}}$, respectively, for the first period for the two different validation sections on the ice shelf, and $-26.7\,\mathrm{m\,a^{-1}}$ and $27.9\,\mathrm{m\,a^{-1}}$ for the second period for the same sections. This leads us to conclude that repeat MODIS images are well suited to measure ice shelf velocity fields and monitor their changes over time. Orientation correlation seems better suited for this purpose because it produces fewer mismatches, is able to match images with regular noise and data voids, and is faster. Since it can match images with regular data voids it is possible to match Landsat 7 ETM+ images even after the 2003 failure of the Scan Line Corrector (SLC off) that leaves significant image stripes with no data. Image matching based on the original 12-bit radiometric resolution MODIS data produced slightly better results than using the 8-bit version of the same images. Streamline interpolation from the obtained surface velocity field on Larsen C indicates ice travel times of up to 450 to 550 years between the inland boundary and the ice shelf edge. In a second step of the study we test our method successfully on 10 other ice shelves around Antarctica demonstrating that the approach presented could in fact be used for large scale monitoring of ice shelf dynamics.

Correspondence to: T. Haug
(torborg.haug@geo.uio.no)

1 Introduction

Velocities of glaciers, ice sheets and ice shelves can be measured successfully by remote sensing techniques. The two most commonly used methods so far have been radar interferometry and correlation of repeat images. Radar interferometry measures the phase shifts between two SAR image acquisitions. This relies on phase coherence, and in order to avoid coherence degradation on the rapidly changing snow/ice surface, tandem missions with only a few days between the acquisitions are often required. This limits the application of the radar interferometry method. Image correlation has, in principle, much longer decorrelation times. These can range from about a year for mountain glaciers to more than ten years for Antarctic glaciers and ice streams. The correlation method can be applied to both optical images and to data from synthetic aperture radar (SAR). Image matching can either be done in the spatial domain or the frequency domain (Brown, 1992; Zitova and Flusser, 2003).

Ice velocity studies using the correlation method have among others been conducted in Antarctica (e.g., Scambos et al., 1992), on Svalbard (e.g., Rolstad et al., 1997; Kääb et al., 2005), in the Alps (e.g., Kääb, 2002; Berthier et al., 2005), in New Zealand (e.g., Kääb, 2002; Quincey and Glasser, 2009), in the Himalaya (e.g., Scherler et al., 2008; Kääb, 2005), in Greenland (e.g., Strozzi et al., 2002; Howat et al., 2005), and in Patagonia (e.g., Skvarca et al., 2003). However, very few have studied ice shelf velocities using the correlation method. Bindschadler et al. (1994) and Rack et al. (1999) derived velocities using this method on the relatively small Larsen A ice shelf. Skvarca (1994) and Glasser

et al. (2009) measured the velocities of a small section of the Larsen C ice shelf as part of larger studies.

The purpose of this study is, firstly, to demonstrate that optical sensors with low spatial resolution can be used to measure the velocity fields of Antarctic ice shelves and their changes with satisfactory accuracy. Secondly, the study aims at an initial selection of ice shelves where the method presented could actually be employed for easy and operational monitoring of ice flow. Three major advantages of low resolution optical sensors such as Moderate Resolution Imaging Spectroradiometer (MODIS) or Medium Resolution Image Spectrometer Instrument (MERIS) are: (1) that they cover much larger areas with a single image than medium and high resolution optical and SAR sensors such as Landsat, SPOT, Radarsat, ERS SAR or Envisat ASAR do. This fact allows for large-scale monitoring of ice velocities. In addition, it ensures that one individual scene will in most cases contain stable ground. That helps to accurately co-register the repeat data without having to rely on the satellite-derived geolocation of the data or without having to mosaic scenes that stem from different times and contain only moving targets. (2) The very frequent coverages by low resolution satellite imagery of up to several times per day in polar regions increases drastically the potential for cloud-free scenes compared to medium and high resolution optical sensors with much lower repeat times. (3) Correlation over time for optical data is often much more robust than the phase coherence of SAR data necessary for SAR interferometry or speckle tracking, allowing to cover much larger time steps using optical data.

On the other hand, application of repeat low resolution optical images for ice shelf velocity measurements has also clear disadvantages: (1) image matching accuracy is in general governed by the pixel size so that sensors with higher spatial resolution potentially provide better accuracies. (2) Phase-based methods such as SAR interferometry and SAR speckle tracking will naturally provide a much higher displacement accuracy than image intensity correlation methods as necessary for optical data. (3) Optical sensors are unable to image during (polar) night and through cloud cover. (4) Matching of repeat optical data relies on optical surface contrast features that are naturally scarce over Antarctica. SAR backscatter features suitable for matching will often be denser.

The above list of potential advantages and disadvantages shows that measuring velocity fields on ice shelves using low resolution optical data will not be the optimal method for such work but rather represent a valuable complement to the other methods, which all have different specific benefits and limitations. Correlation of low resolution images with large coverage is a good mean to initially detect regions that have experienced changes and thus to guide where dedicated studies should be performed by collecting time series of higher resolution images.

The potential and accuracy of ice shelf velocities from low resolution optical data (here: MODIS) is assessed using repeat optical images of medium spatial resolution (here: Landsat). For a test site we select the Larsen C ice shelf and the remnants of the Larsen B ice shelf, both located on the Antarctic Peninsula (Fig. 1). The velocity measurements are conducted using two image matching methods, normalized cross-correlation which we operate in the spatial domain and orientation correlation operated in the frequency domain which we operate in the frequency domain, and these two approaches are compared. Velocities are also measured for different periods in order to identify possible velocity changes.

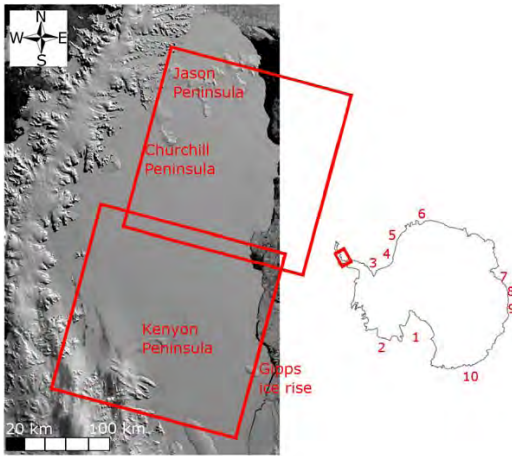

Fig. 1. Sketch map over Antarctica (right) and image of Larsen C ice shelf (left). The position of the MODIS image is indicated as red rectangle in the right panel and it forms the background in the left panel. The position of the Landsat validation images are indicated in red in the left panel (path 216 row 108 and path 216 row 107). The numbers mark the locations of the other ice shelves investigated: 1. Ross, 2. Getz east, 3. Ronne, 4. Filchner, 5. Riiser-Larsen, 6. Fimbul, 7. Amery, 8. West, 9. Shackleton, 10. Mertz. The MODIS image is from 2002 and was preprocessed by Scambos et al. (2009).

Rise in air and sea temperatures around the Antarctic Peninsula over the last decades have impacted on the ice shelves in this area. Turner et al. (2005) found that air temperatures on the western Antarctic Peninsula rose by 0.56 °C decade^{-1} from 1951 to 2000. Meredith and King (2005) reported that the ocean surface temperatures on the western side of the Antarctic Peninsula increased by more than 1 °C in the period 1955 to 1998.

At the same time the ice shelves and glaciers in this area have undergone large changes. As many as seven ice shelves have retreated dramatically or completely disintegrated over the last decades (Cook and Vaughan, 2010). Several studies have shown that the glaciers feeding the ice shelves have increased their velocities after the disintegration. This speed up has been attributed to removal of the buttressing ice shelves

(Rott et al., 2002; Scambos and Bohlander, 2003; De Angelis and Skvarca, 2003; Rignot et al., 2004; Scambos et al., 2004; Rignot et al., 2005). In addition, surge activity has been observed after ice shelf disintegration (De Angelis and Skvarca, 2003). The glaciers on the Antarctic Peninsula have also accelerated because their termini have thinned (Pritchard and Vaughan, 2007). As a result of the velocity increase of glaciers on the Antarctic Peninsula, glaciers in this region were considered to loose $60\pm46\,\mathrm{Gt\,a^{-1}}$ in 2006, which was an increase of 140% since 1996 (Rignot et al., 2008).

Four ice shelves on the northeastern coast of the Antarctic Peninsula have disintegrated between 1986 and 2002. Larsen Inlet started the disintegration process in 1986 and it ended in 1989 (Skvarca, 1993). The ice shelf in Prince Gustav Channel collapsed between 1992 and 1995 (Rott et al., 1996). Larsen A collapsed in 1995 (Rott et al., 1996), and Larsen B followed in 2002 (Rack and Rott, 2004).

It has been observed that several of the ice shelves that disintegrated underwent large changes before they collapsed. Bindschadler et al. (1994) found that Larsen A accelerated by up to 15% from the period 1975–1986 to the period 1986–1989 and Rack et al. (1999) found that it accelerated by 10% from 1986–1989 and 1988–1989 to 1992–1993. Skvarca et al. (1999) measured on Larsen B an acceleration of 13.2% between the periods 1988–1994 and 1994–1997. Rott et al. (2002) also measured an increase in velocity after a calving event in 1995. Furthermore, field measurements carried out along the center flowline of Larsen B revealed that surface ice-velocity which increased by 10% from 1996–1997 to 1997–1999 has augmented to 26% between 1997–1999 and 1999–2001, i.e. just before the final collapse (Skvarca et al., 2004). On the other hand, Vieli et al. (2006) derived from satellite interferometry a maximum increase in ice velocity on Larsen B of about $150\,\mathrm{m\,a^{-1}}$ from 1995/1996 to 1999.

It has been widely discussed whether the penetration of meltwater into crevasses is enhancing the fractures and thereby triggering the disintegration (Scambos et al., 2000; MacAyeal et al., 2003; Scambos et al., 2008). However, as Vieli et al. (2006) point out, this can only explain the final collapse and not the dynamic response that can be seen prior to the collapse. Because the ice shelves that have disintegrated so far have shown a dynamic response prior to the collapse, we suggest that studying changes in ice shelf dynamics can give valuable insight on their stability.

After introducing the satellite data used, we describe the image matching methods applied and their accuracy. Then, the results for Larsen C are presented in detail in order to understand the potential and limitations of the method. Results for ten other ice shelves in Antarctica are also described in order to evaluate the applicability and performance of the method for Antarctic ice shelves in general and to present an initial selection of ice shelves that could be monitored that way. Discussion and conclusions terminate our study.

2 Satellite data

Optical satellite images with two different spatial resolutions are selected for this study. Both the 250 m spatial resolution bands from the NASA's Moderate Resolution Imaging Spectroradiometer (MODIS) images (bands 1 and 2, bandwidths of 620-670 nm and 841–876 nm, respectively) represent the lowest spatial resolution, and NASA/USGS' Landsat 7 Enhanced Thematic Mapper Plus (ETM+) panchromatic images (channel 8, bandwidth of 520-900 nm) with a spatial resolution of 15 m represent the highest. The MODIS images have been preprocessed by the National Snow and Ice Data Center (NSIDC) (Scambos et al., 2009). This preprocessing included orthorecitification, i.e. geocoding and topographic correction using a Digital Elevation Model (DEM). The accuracy of the topographic correction is given as better than 0.2 pixels.

Images from three different times are selected in order to measure both velocities over the two periods and velocity changes between the periods. The periods should be long enough to identify statistically significant displacements, but also short enough to avoid surface changes that hinder the correlation of images. Two areas on Larsen C are chosen to validate the velocities and the velocity changes measured with the MODIS imagery. These areas are hereafter referred to as Larsen C South and Larsen C North. The validation is performed by using the finer spatial resolution imagery from the Landsat ETM+ pan sensor. "Larsen C South" indicates images from path 216 row 108 and "Larsen C North" indicates images from path 216 row 107. Their location is indicated in Fig. 1. The validation areas are selected based on the availability of cloud free images from both the MODIS and the Landsat sensors with as short as possible time separation between both. An overview of the selected images can be found in Table 1.

Until autumn 2005 NSIDC produced images with 8 bit radiometric resolution from the MODIS images. Therefore the MODIS image from 2002 is 8 bit, while the images from 2006, 2008 and 2009 are 12 bit, which is the original radiometric resolution of MODIS. The images from 2006, 2008 and 2009 are also available as 8 bit images, and this gave us also the opportunity to investigate the impact of different radiometric resolutions on image matching.

Due to the small elevation differences on the Larsen ice shelf, there are only minor topographic distortions over the ice shelf caused by elevation differences in the images. These are assessed to be small enough to be neglected in this study. Co-registering the MODIS images using stable ground with varying elevation is possible because the MODIS images from NSIDC are corrected for elevation. In addition, the 2002 and 2008 MODIS data used are from the same orbit, and the 2006 and 2009 data from orbits adjacent to these so that effects from residual topographic distortion are minimized. The matched Landsat images have the same imaging geometry because they are from the same path and row, i.e.

Table 1. MODIS and Landsat satellite images used for the velocity measurements. Larsen C South indicates Landsat images from path 216 row 108 and Larsen C North indicates Landsat images from path 216 row 107.

Larsen C South		Larsen C North	
MODIS	Landsat	MODIS	Landsat
17 Mar 2002 1345	22 Nov 2001	17 Mar 2002 1345	15 Apr 2002
5 Jan 2006 1355	4 Jan 2006	5 Jan 2006 1355	4 Jan 2006
1 Jan 2009 1330	12 Jan 2009	28 Nov 2008 1345	11 Dec 2008

orbit position, and accurate co-registration is thus possible without prior orthorectification.

3 Image matching methods

3.1 Normalized cross-correlation

Matching of two images can be done using the image intensities directly in the normalized cross-correlation method (NCC). The first image is taken as the reference image, and a sub-window of this image is searched for in the second image, or the search image. The cross-correlation surface CC is given by

$$\mathrm{CC}(i,j) = \frac{\sum_{k,l}(s(i+k,j+l)-\mu_s)(r(k,l)-\mu_r)}{\sqrt{\sum_{k,l}(s(i+k,j+l)-\mu_s)^2 \sum_{k,l}(r(k,l)-\mu_r)^2}} \quad (1)$$

where (i,j) indicates the position in the search area, (k,l) the position in the reference area, r the pixel value of the reference chip, s the pixel value of the search chip, μ_r the average pixel value of the reference chip and μ_s the average pixel value of the search chip. The peak of the cross-correlation surface indicates the displacement between the images.

This method has been widely used for measuring the displacement of both glaciers and rockglaciers (e.g., Kääb, 2002, 2005; Kaufmann and Ladstädter, 2003; Debella-Gilo and Kääb, 2010).

3.2 Orientation correlation

The second matching method is based on the orientation correlation method (OC), which is developed by Fitch et al. (2002). We conduct the matching in the frequency domain. Matching in the frequency domain works with the image frequencies instead of working directly with the image intensities. Correlation and convolution are related operations, and convolution in the spatial domain equals multiplication in the Fourier domain (the convolution theorem) (McClelland et al., 2003).

When using OC new orientation images are created from the original images based on the image intensity differences in both the horizontal x direction and in the vertical y direction. Central differences are used, except at the edges where forward and backward differences are used to maintain the image size. Taking f as the image at time $t=1$ and g as the image at time $t=2$, and choosing a complex representation, the orientation images f_o and g_o are created from

$$f_o(x,y) = \mathrm{sgn}\left(\frac{\partial f(x,y)}{\partial x} + i\frac{\partial f(x,y)}{\partial y}\right) \quad (2)$$

$$g_o(x,y) = \mathrm{sgn}\left(\frac{\partial g(x,y)}{\partial x} + i\frac{\partial g(x,y)}{\partial y}\right) \quad (3)$$

$$\text{where } \mathrm{sgn}(x) = \begin{cases} 0 & \text{if } |x| = 0 \\ \frac{x}{|x|} & \text{otherwise} \end{cases} \quad (4)$$

where sgn is the signum function and i is the complex imaginary unit. The new images f_o and g_o are complex and hence consist of one real and one imaginary part, where the intensity differences in the x direction represent the real matrix and the intensity differences in the y direction represent the imaginary matrix. The orientation images are divided into matching windows before the matching is conducted. Such windows should be small enough to avoid having different displacements inside the same window, but large enough to get a clear correlation maximum. In this study we use matching windows of 44×44 pixels (11 000 m) for the MODIS imagery and 350×350 pixels (5250 m) for the Landsat imagery. The spacing between the matching windows is the same as the size of the windows to give a densely populated grid with non-overlapping, independent measurements. The correlation surface $P(x,y)$ is then computed from

$$P(x,y) = \mathrm{IFFT}\left(\frac{F_o(u,v)G_o^*(u,v)}{\left|F_o(u,v)G_o^*(u,v)\right|}\right) \quad (5)$$

where $F_o(u,v)$ is the Fast Fourier Transform (FFT) of the reference window from $f_o(x,y)$, $G_o^*(u,v)$ is the complex conjugate of the FFT of the search window from $g_o(x,y)$ and IFFT is the Inverse Fast Fourier Transform. The shift that is needed to register the two matching windows is found from the position of the maximum of the correlation surface $(P(x,y)_{max})$.

Subpixel accuracy is obtained following the method of Argyriou and Vlachos (2007). Subpixel displacements in the x direction dx and in the y direction dy are found using

$$dx = \frac{P(x_m+1,y_m) - P(x_m-1,y_m)}{2(2P(x_m,y_m) - P(x_m+1,y_m) - P(x_m-1,y_m))} \quad (6)$$

$$dy = \frac{P(x_m,y_m+1) - P(x_m,y_m-1)}{2(2P(x_m,y_m) - P(x_m,y_m+1) - P(x_m,y_m-1))} \quad (7)$$

where $P(x_m,y_m)$ is the maximum correlation value. This means that a parabolic function is fitted to the maximum point and the two surrounding points. When dividing by the amplitude in Eq. (5), only the phase of the FFT is kept. This makes the correlation peak narrower and hence the subpixel accuracy better.

When matching the Landsat images, the orientation images are low pass filtered in the Fourier domain using a Hamming-window based finite impulse response (FIR) filter.

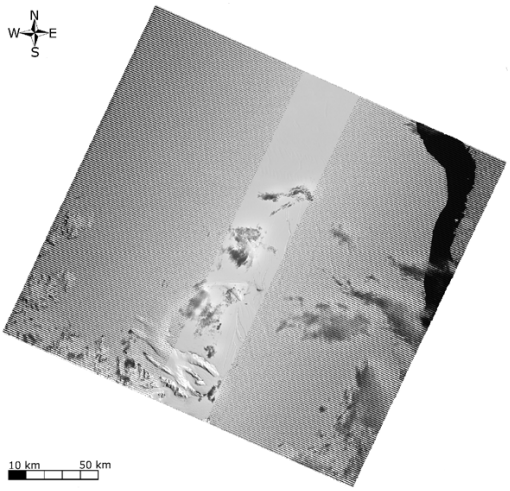

Fig. 2. Landsat 7 ETM+ pan image from 2006 path 216 row 108 used in this study that shows the regular cross-track data voids caused by the failure of the Scan Line Corrector.

This is done to remove the high frequencies, and after this filtering the images can be matched using smaller matching windows than before the filtering is conducted. This implies that the low frequencies contain the displacement information and that the high frequencies represent noise in this particular case.

Fourier domain methods have some constraints. Firstly, displacements larger than half the window size cannot be measured directly due to the quadrant ambiguity problem. If larger displacements are expected, the images should be aligned beforehand based on the expected displacement. Secondly, the window sizes have generally to be larger than if the matching is done in the spatial domain.

The clear advantages of frequency domain over spatial domain methods are that they can be fast if FFT is used, and that they are not sensitive to image information which is constrained to few frequencies. In this study that fact turns out to be particularly useful, because the Landsat 7 ETM+ images from 2003 and onward have regular cross-track data voids, i.e. voids with a very specific frequency (Fig. 2), after a failure of the Scan Line Corrector (SLC).

3.3 Locational accuracy

This section tries to quantify (i) the errors from co-registration and (ii) the errors in areas where no ground control is available.

To quantify the uncertainty of the matching methods, matching points over stable ground are investigated. We searched the shift measurements in both x and y direction for trends. Only zeroth order trends (i.e. mean horizontal shifts) are found to influence our level of accuracy, and these translations are therefore subtracted from the measured pixel shifts. The pixel shifts are in the order of meters for most of the MODIS images. The only exception is the 2002 image which is shifted 465 m relative to the others. For Landsat the shifts range from 6 m to 55 m. The uncertainty of the matching methods is given by the root mean square error (RMS) of the pixel shifts of stable ground, see Table 2. Note, that the pixel location errors resulting from errors in the DEM used for orthorectifying of the MODIS data are systematic in direction (cross-track; roughly east-west), but small (less than 0.2 pixels) and with a random sign from DEM elevations being both too high and too low.

Table 2. Root mean square error (RMS) of displacement measurements obtained using frequency domain matching over stable ground. The number of measurements is indicated by n.

Image pair	RMS_x m	RMS_y m	n
MODIS 2002–2006	28.0	38.7	106
MODIS 2006–2008	24.2	26.0	188
MODIS 2006–2009	21.2	35.9	176
MODIS 2002–2009	30.0	36.1	183
Landsat 2001–2006 South	4.72	8.00	71
Landsat 2006–2009 South	7.75	10.6	47
Landsat 2002–2006 North	–	–	–
Landsat 2006–2008 North	–	–	–

The Landsat images over Larsen C North from Table 1 and Fig. 1 cover not enough stable ground to detrend the data. Instead, images from the neighbour path 217 row 106 are used to co-register the images. These neighbour images are taken on 6 April 2002 and 11 January 2006. They overlap with some of the same grounded, low-velocity ice shelf area as the Larsen C North images. In addition they contain stable ground so that they can be co-registered. These neighbour images (i.e. path 217 row 106) are first co-registered using the stable ground present. Then, the ice velocities over the grounded low-velocity area are found, and these velocities are finally used to co-register the Larsen C North images applied in this study. Because the mean velocity is $12\,\mathrm{m\,a^{-1}}$ the error arising from assuming identical velocity in 2006–2009 is considered small enough for this use. Matching of another neighbour image pair, 3 February 2006 and 25 December 2008 from path 218 row 107, confirmed the 2006–2008 velocities from Larsen C North with a mean difference of $-1.9\,\mathrm{m\,a^{-1}}$. The uncertainty is considered to be somewhat higher than for the Landsat images with stable ground present in the images, and a maximum uncertainty of 15 m in both x and y direction in both periods is assumed.

Outside the areas with stable ground, the attitude variations (variations in the roll, pitch and yaw) of the satellite

may contribute to reduced accuracy. The potential for reduced accuracy can be analyzed based on the characteristics of the sensors. Sensors aboard MODIS and Landsat are whiskbroom sensors that scan pixel by pixel unlike linear array pushbroom sensors. Data from whiskbroom systems are therefore exposed to both along-track and cross-track geometrical distortions due to attitude variations. These errors are not fully accounted for in the RMS of stable ground, because this RMS only comes from limited areas in the images. Wolfe et al. (2002) estimate the geolocation accuracy for MODIS to be 50 m. For Landsat the geolocation accuracy is 250 m and the image-to-image registration accuracy is 7.3 m according to NASA (1996). Lee et al. (2004) confirmed that the image-to-image registration accuracy is within, and actually better, than the pre-launch requirement.

In the measured displacements over stable ground and over the ice shelf, obvious matching outliers are removed manually. Because there is displacement variation over the ice shelf, but not over the stable ground, it is possible that somewhat fewer of the mismatches are filtered out over the ice shelf compared to the stable ground. It is therefore possible that the accuracy decreases slightly over the ice shelf. This effect is, however, difficult to quantify.

Mismatches could also be removed automatically using the signal-to-noise ratio (SNR) because correct matches have generally a stronger correlation peak compared to erroneous matches. In this study, a threshold of approximately RMS > 5 would have removed most of the erroneous matches and left most of the correct matches. However, SNR is not used in this test study because we wanted to have full control over the selection process to avoid removal of any correct matches.

Subsequently, we estimate the total uncertainty of our displacement measurements to be the root sum square (RSS) of (i) the RMS of the matches on stable ground and (ii) the above image-to-image registration accuracy. The RMS from matching over stable ground and the registration accuracy are then assumed to be independent. Since this image-to-image registration accuracy is not known to us for MODIS we use the total geolocation accuracy of 50 m for this sensor instead. That way, our uncertainty estimate for MODIS resembles a worst-case scenario. It is assumed that all the individual displacement matchings are dependent ($n = 1$), which is a second accuracy worst-case scenario.

A further algorithm test could have been performed by resampling the 15 m Landsat data to the 250 m MODIS resolution and comparing the matching results based on both resolution levels of the else identical images. This test was, however, not possible in our study due to the SLC off data voids in the Landsat data that dominated any resampled product.

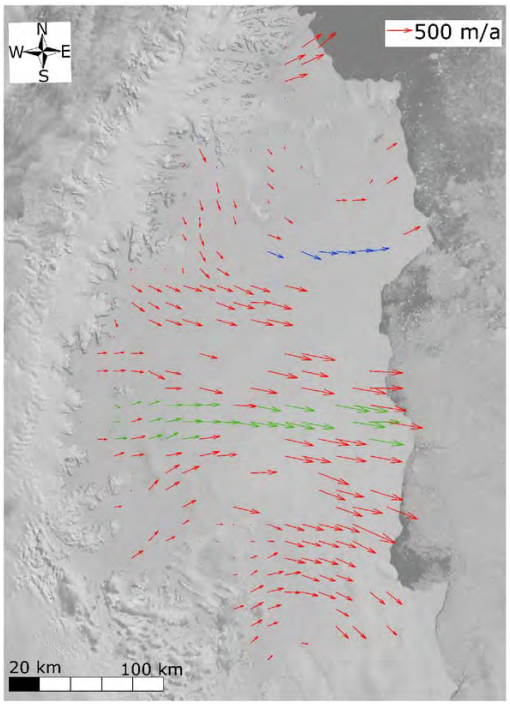

Fig. 3. Average annual velocity between 2002 and 2006 measured with orientation correlation on MODIS images. Blue and green colors indicate that these measurements are compared with Landsat measurements. The underlying MODIS image of 2009 is preprocessed by Scambos et al. (2009).

4 Results for Larsen C

4.1 Orientation correlation

OC produces a densely populated network of correct matches between the MODIS images from 2002 and 2006 (Fig. 3) and in particular between the MODIS images from 2006 and 2009 (Fig. 4). Also the two images from 2002 and 2009, nearly seven years apart, are correctly matched for most of the ice shelf (Fig. 5). The ice flows relatively slowly in the inner parts of the ice shelf and accelerates as it approaches the ice shelf edge to the east, as is to be expected. We found highest velocities for the central to southern outer part of the ice shelf, with velocities of approximately 700 m a^{-1}. The directions of the flow generally fit the crevasse pattern and the peninsulas.

The displacements derived from MODIS images for the period 2002–2006 and the period 2006–2009 are summed up and compared with displacements directly derived from the MODIS images of 2002 and 2009. Only windows that

Table 3. Average velocity and velocity difference measured from MODIS and Landsat images for 6 points in the Larsen C North section and 28 points in the Larsen C South section. The RMS of the average is also given.

	Average velocity 1st period south $m\,a^{-1}$	Average velocity 2nd period south $m\,a^{-1}$	Average acceleration 2nd period–1st period south $m\,a^{-1}$	Average velocity 1st period north $m\,a^{-1}$	Average velocity 2nd period north $m\,a^{-1}$	Average acceleration 2nd period–1st period north $m\,a^{-1}$
MODIS	430.2±177.9	427.1±172.5	−3.1±38.0	383.7±22.9	425.8±39.1	42.0±21.3
Landsat	445.6±157.4	453.8±159.6	8.2±20.9	370.8±20.1	397.9±30.0	27.1±14.5
MODIS – Landsat	−15.4±39.6	−26.7±40.1	−11.3±44.4	13.0±20.5	27.9±33.5	14.9±22.7

Table 4. Uncertainty of the measured MODIS and Landsat displacements and accelerations. The root sum square (RSS) of the uncertainties are also given and can be compared with the deviations given in the lower row of Table 3.

	Uncertainty 1st period south $m\,a^{-1}$	Uncertainty 2nd period south $m\,a^{-1}$	Uncertainty 2nd period–1st period south $m\,a^{-1}$	Uncertainty 1st period north $m\,a^{-1}$	Uncertainty 2nd period north $m\,a^{-1}$	Uncertainty 2nd period–1st period north $m\,a^{-1}$
MODIS	±18.1	±21.8	±28.3	±18.1	±21.1	±27.8
Landsat	±2.86	±4.96	±5.73	±6.01	±7.63	±9.71
RSS	±18.3	±22.4	±28.9	±19.1	±22.4	±29.4

are correctly matched (from manual inspection) in all three matchings are used for the multitemporal comparison. Over the ice shelf the 7-year average displacement difference is −36.3 m with an RMS of 149.6 m ($n = 70$). In the flow direction the average displacement difference is −49.0 m with an RMS of 183.8 m, and in the transverse direction it is 21.5 m with an RMS of 141.4 m. Over stable ground the average pixel shift is 33.5 m and the RMS is 44.9 m. The uncertainty of this comparison, calculated using the RSS of the RMS over stable ground (Table 2) and the image-to-image registration accuracy from literature, is ±117 m.

Velocity measurements on the Landsat images are mostly restricted to the crevassed areas (Figs. 6 and 7). As for the MODIS-derived data, the flow directions obtained from the repeat Landsat images fit the crevasse pattern and flow obstacles, and the velocity increases as the ice moves off the inland boundary. The sections with the highest measured velocities on the MODIS images are also covered by the Landsat images. The latter images also indicate velocities of approximately 700 $m\,a^{-1}$ in this area.

In our procedure it is not possible to directly compare Landsat-derived and MODIS-derived displacements on a point-by-point base because we use different window sizes for Landsat and MODIS, and match the Landsat data in their original geometry, i.e. not geocoded and orthorectified, in order to avoid resampling artifacts. When comparing MODIS and Landsat derived velocities, we first select all MODIS points which have velocity measurements from both periods 2002–2006 and 2006–2009. Then we do the same for the Landsat points, and at last we select a subset of the Landsat and MODIS points that are less than 11 km apart (the length of the sides of one MODIS matching window). This results in 6 MODIS points (see blue colored arrows in Fig. 3) in the Larsen C North section and 28 MODIS points (see green colored arrows in Fig. 3) in the Larsen C South section. For every MODIS point the average of the Landsat points that have this MODIS point as their closest neighbour is calculated. The average Landsat and MODIS derived velocity is then compared. The results of the comparison can be seen in Table 3 and the uncertainties of the results in Table 4. Landsat measures higher average velocities than MODIS in the south, and lower average velocities in the north. In the south the velocities were not significantly different in the two periods, but in the north both sensors measured a velocity increase from the first period to the second period. Due to particularly little longitudinal strain in this area the acceleration observed is considered a real acceleration and not a result of a longitudinal velocity gradient that would bias the results from matching moving target features at stable matching geolocations. The RMS of the average velocities is highest in the south. This reflects the fact that the southern section covers larger velocity gradients.

A difference in average annual velocity between the periods 2002–2006 and 2006–2009 is evident from the MODIS images also for the remnants of Larsen B. The four points measured on this ice shelf reveal a mean speed increase of 135 $m\,a^{-1}$ with an RMS of 26.3 $m\,a^{-1}$. This is an increase of approximately 30%. The uncertainty here is ±28.3 $m\,a^{-1}$. Other velocity changes are not statistically significant (i.e. bigger than the uncertainties given in Table 4) from the MODIS measurements.

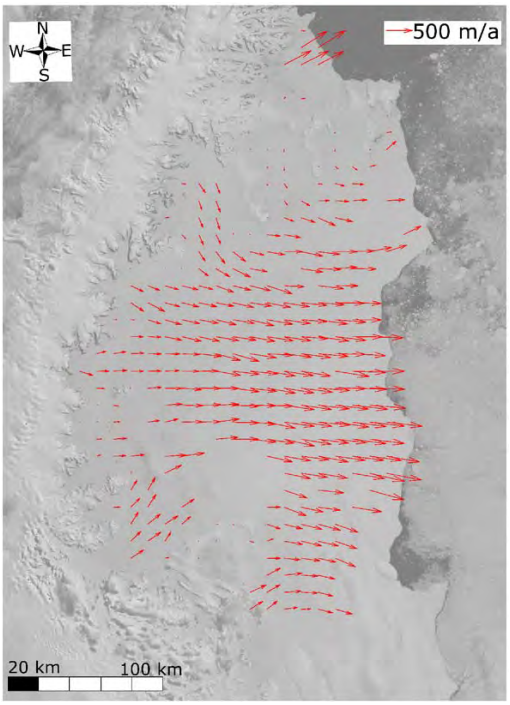

Fig. 4. Average annual velocity between 2006 and 2009 measured with orientation correlation on MODIS images.

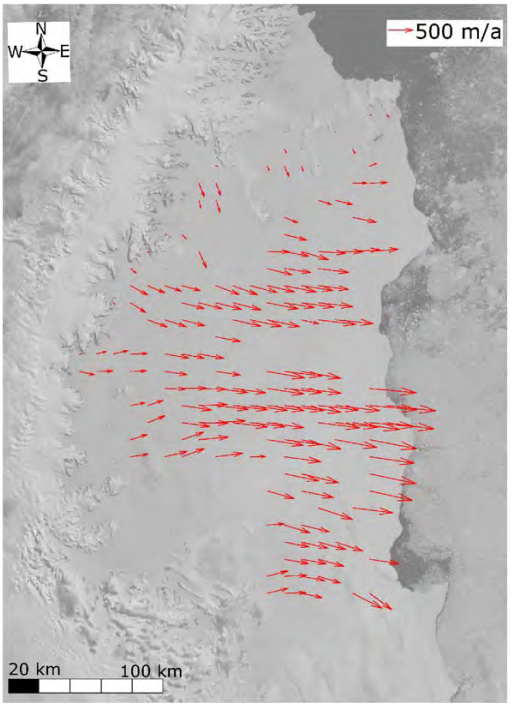

Fig. 5. Average annual velocity between 2002 and 2009 measured with orientation correlation on MODIS images.

4.2 Comparison between orientation correlation and normalized cross-correlation

Normalized cross-correlation (NCC) does not produce such a dense velocity field as OC when the matching is conducted in a regular grid using the same window size as used for OC (44×44 pixels). This can be seen if comparing Fig. 4 showing the velocity field created by the OC and Fig. 8 showing the velocity field created by NCC. These two velocity fields are obtained by matching the same images with the same position and size of the matching windows. OC produces 332 correct velocity vectors out of 471 possible (70%), whereas NCC produces only 129 correct vectors (27%). The RMS of the NCC measurements over stable ground are similar to the RMS of the OC measurements (27.8 m in the x direction and 29.5 m in the y direction). The mean velocity difference for points on the ice shelf measured using both methods is $19.4 \pm 63.4\,\mathrm{m\,a^{-1}}$ ($n = 75$), OC measuring the higher velocities on average. The mean velocity difference over stable ground is $15.1 \pm 6.9\,\mathrm{m\,a^{-1}}$ ($n = 108$), NCC measuring the higher velocities on average. The uncertainty of the OC is ±21.8 m and the uncertainty of the NCC is ±21.5 m.

NCC gives correct matches even if the window size is decreased. On the MODIS images, window sizes of 15×15 pixels still give correct matches in areas with good contrast, for example crevassed areas (Fig. 9). However, the RMS of the measurements over stable ground increases quickly, and when a window size of 15×15 pixels is chosen, the RMS is as high as 75 m. Also this method measures an increase in velocity on the remnants of Larsen B from 2002–2006 to 2006–2009. The velocity increase is $124.4\,\mathrm{m\,a^{-1}}$ with an RMS of $60.1\,\mathrm{m\,a^{-1}}$ ($n = 11$). The uncertainty of this comparison is $43.5\,\mathrm{m\,a^{-1}}$.

4.3 Radiometric resolution

From autumn 2005 and onward, the MODIS images from NSIDC are also available with the original MODIS 12 bit radiometric resolution, in addition to 8 bit that are available for all dates. Both frequency and spatial domain matching methods are therefore tested on images with different radiometric resolution in order to assess matching differences between 12 bit images and 8 bit images. Matching with OC and a window size of 44×44 pixels on the 12 bit images from 5 January 2006 and 28 November 2008 produces 390

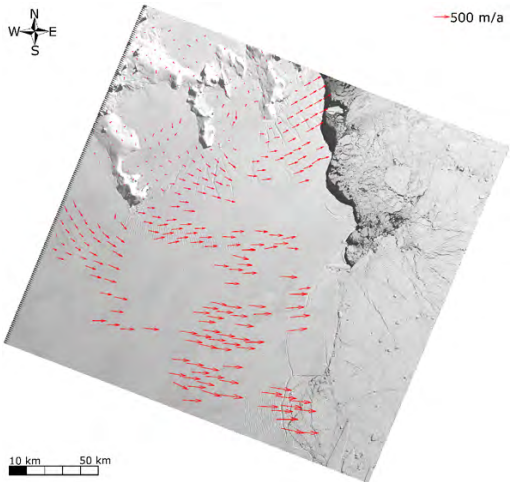

Fig. 6. Average annual velocity between 2006 and 2008 measured with orientation correlation on Landsat 7 ETM+ pan images from path 216 row 107 over Larsen C North. Underlying Landsat image of 2002.

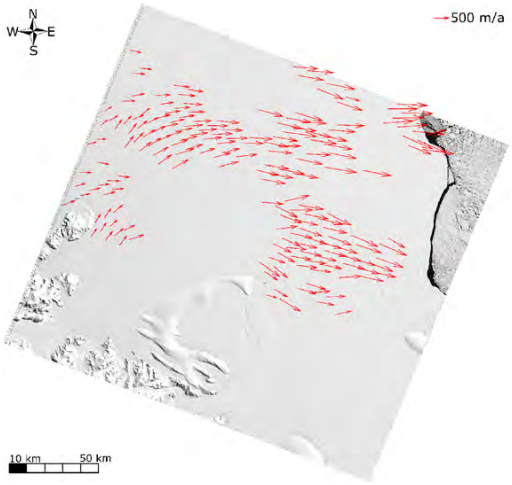

Fig. 7. Average annual velocity between 2006 and 2009 measured with orientation correlation on Landsat 7 ETM+ pan images from path 216 row 108 over Larsen C South. Underlying Landsat image of 2002.

correct matches, whereas the 8 bit images produce 346 correct matches using the same matching windows. This means that the 8 bit images produce 11.3% fewer correct matches than the 12 bit images. A total of 7 points are correctly matched using the 8 bit images but not correctly matched us-

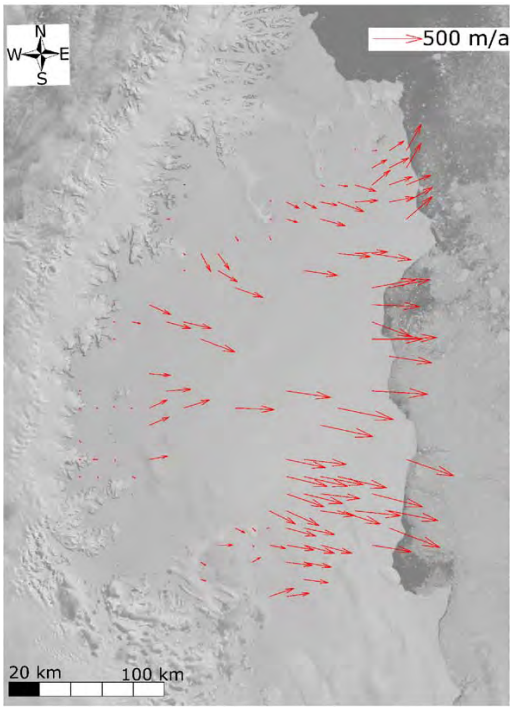

Fig. 8. Average annual velocity between 2006 and 2009 measured with normalized cross-correlation using a window size of 44×44 pixels (the same as used for the orientation correlation) on MODIS images.

ing the 12 bit images. Matching with NCC and a window size of 15×15 pixels at manually pre-selected points with good visual contrast produces 322 correct matches on the 12 bit images. When the matching is repeated at the exact same locations using the 8 bit images, 24 of these points (7.5%) do not produce correct matches. Vice-versa, matching at manually pre-selected points using NCC on the 8 bit images gives 276 correct matches, and when the matching is repeated at the same locations using the 12 bit images, 11 of the points (4.0%) produce mismatches. The RMS of the measurements over stable ground does not change when the 8 bit images are used instead of the 12 bit images, presumably reflecting the good contrast present over the stable areas.

4.4 Streamlines

Streamlines are hypothetical particle tracks interpolated from a velocity field under the assumption that the velocity field does not change over time (Kääb et al., 1998). Here, streamline starting points for time $t(0)$ are selected manually and the algorithm interpolates the velocity at these points. The

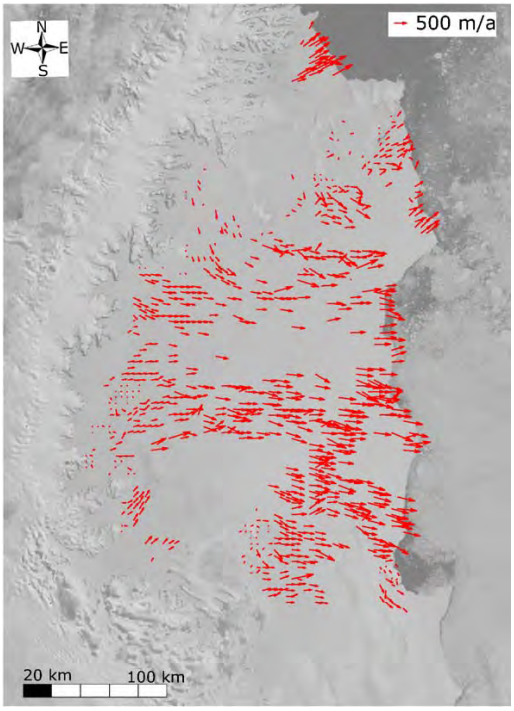

Fig. 9. Average annual velocity between 2006 and 2009 measured with normalized cross-correlation using a window size of 15×15 pixels on MODIS images.

particle position at time $t(1)$ and further for times $t(i+1)$ are computed by adding the interpolated velocity vectors to the particle position obtained from the previous iteration step. Parameters are set for the number of velocity measurements contributing to the interpolation. Thresholds are set for stopping streamline interpolation either when the velocity falls below the above velocity RMS or for an insufficient number of velocity measurements around the interpolation location. The result of the procedure is theoretical particle positions at each time step, i.e. positions with a time marker. Due to the assumption of temporal invariance of the velocity field, streamlines do not necessarily resemble real particle trajectories. Comparing computed streamlines to actual cumulative flow features such as longitudinal flowlines or crevasse patterns is an additional accuracy check, but it can also be used to indicate if and to what extent the assumption of a steady-state velocity field actually reflects reality. Lack of coincidence between the streamlines interpolated from the current velocity field with flow features reflecting past or cumulative flow conditions hints to past changes in the flow field. Streamlines can also, under the restriction that they do not resemble real particle trajectories, be used for surface age estimates.

Here, streamlines are calculated from the 2006–2009 MODIS displacement measurements. The travel time of an ice particle under present-day flow conditions, i.e. a kind of relative age of ice within the Larsen C ice shelf is calculated using inverse streamlines going from the ice shelf edge toward the approximate inland boundary and stopping under above thresholds (not shown). The maximum travel time is ranging from 450 years to 550 years for the central areas of the ice shelf. Along-flow streamlines starting at manual selected points around the inland boundary are also compared to the flowlines of the ice shelf (Figs. 10 and 11) to detect possible changes in the flow field. Computed streamlines and visible flowlines are mostly well aligned, confirming the high accuracy of the velocities matched, and implying at the same time that there has been no or little directional change in the ice-shelf flow over the last decades or few centuries. However, the four southernmost streamlines deviate significantly from the visible flowlines. This could be caused by systematic errors in the measurements only if the systematic errors were twice as large as the measurement uncertainty and localized to one region. The 2006–2009 velocity field has the best quality, but we also investigated the streamlines from the 2002–2006 and 2006–2008 velocity fields to see if the same deviations are present. We found that they were, but the deviations were somewhat smaller. Hence, only systematic errors in this particular part of the 2006 image could have caused the deviations if it is not caused by a real change in flow direction. A possible explanation for a change in flow direction is that one or more of the glaciers Lewis Glacier, Ahlmann Glacier, Bills Gulch and Daspit Glacier have changed their discharge and thus diverted the ice flow from their neighbours. Alternatively, or in addition, it is also possible that considerable changes in calving front position could impact the flow direction on the ice shelf. Closer investigation of this effect would, however, require calving front positions many tens or some hundreds of years back in time because the flow features observed to date might reflect such long time span. During our observational period 2002–2009, the calving front position at the end of the southern streamlines in question constantly advanced, whereas a large iceberg broke off in front of the northern streamlines in late 2004. According to Skvarca (1994), who studied the calving front position between 1975 and 1986–1989, two giant ice bergs calved off in front of the southern and middle streamlines in 1986. Also in front of the northern streamlines an ice berg broke off between 1975 and 1988.

5 Results for other ice shelves

In order to test the applicability and performance of the presented method for monitoring ice shelves dynamics in Antarctica in general, we also match MODIS images of other

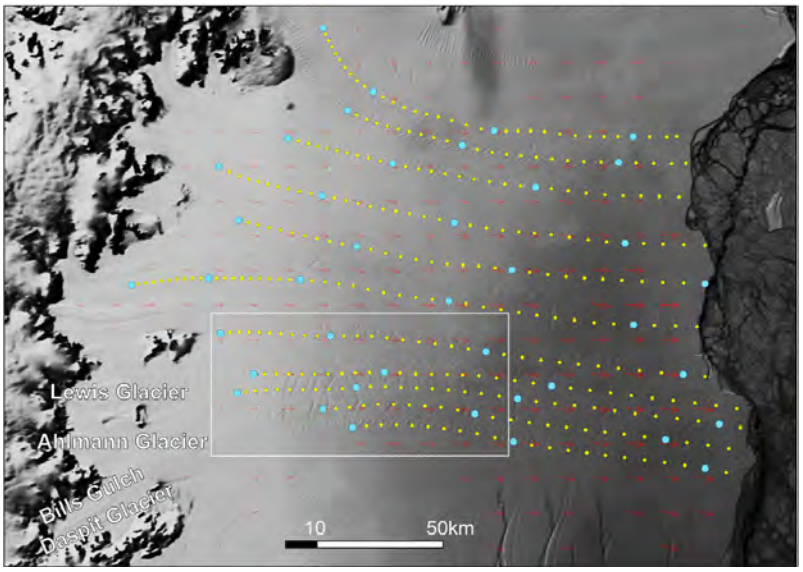

Fig. 10. Streamlines calculated from the 2006–2009 displacement measurements. Yellow dots are separated by 10 years of displacement and blue dots by 100 years of displacement. Underlying MODIS image is from 2008 and is preprocessed by Scambos et al. (2009).

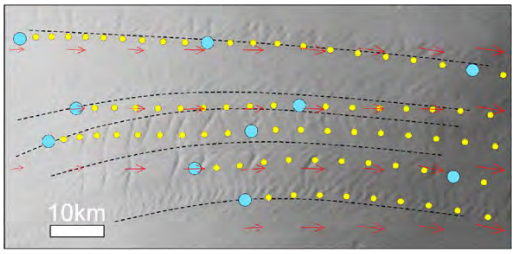

Fig. 11. Zoom-in of streamlines calculated from the 2006–2009 displacement measurements. Yellow dots are separated by 10 years of displacement and blue dots by 100 years of displacement. The black lines mark the flowlines.

Table 5. MODIS images used for deriving velocities and velocity changes for ten other ice shelves in Antarctica.

Ice shelf	Time 1	Time 2	Time 3
Ross West	28 Dec 2001	5 Dec 2005	8 Dec 2008
Ross East	6 Oct 2002	25 Oct 2005	27 Dec 2008
Getz	21 Jan 2003	1 Mar 2006	11 Feb 2009
Ronne	3 Dec 2002	4 Oct 2006	13 Oct 2008
Filchner	3 Dec 2002	23 Feb 2006	9 Mar 2009
Riiser-Larsen	19 Feb 2003	29 Jan 2006	14 Feb 2009
Fimbul	2 Mar 2003	1 Mar 2006	11 Mar 2009
Amery	20 Feb 2002	3 Mar 2006	19 Feb 2009
West	20 Jan 2003	16 Mar 2006	19 Mar 2009
Shackleton	26 Feb 2003	20 Feb 2006	23 Feb 2009
Mertz	15 Mar 2002	11 Mar 2006	2 Mar 2009

ice shelves. The objective of this study step is to indicate for what ice shelves or ice-shelf sections the method works and to characterize the necessary ground conditions. Larsen C exhibits comparably many flow features, which makes the matching successful. In addition, it is also comparably fast flowing, which favours detection of displacements at a statistically significant level. Other ice shelves may be more challenging in these respects.

Velocity fields for the ice shelves Ronne, Filchner, Riiser-Larsen, Fimbul, Amery, West, Shackleton, Mertz, Ross and Getz are derived. This is done for two different periods to also identify possible velocity changes. The images used are listed in Table 5. Velocity fields are shown in Figs. 12 and 13. Displacement matches are generated for the entire images shown, but non-significant displacements (i.e. displacements of the slow moving parts) are removed to improve the readability and so are also clear mismatches as revealed by manual inspection. The parts of the ice shelves not covered by velocity arrows in the figures are hence not matched correctly or show no movement. Generally the method produces densely populated velocity fields for all ice shelves. Gaps in

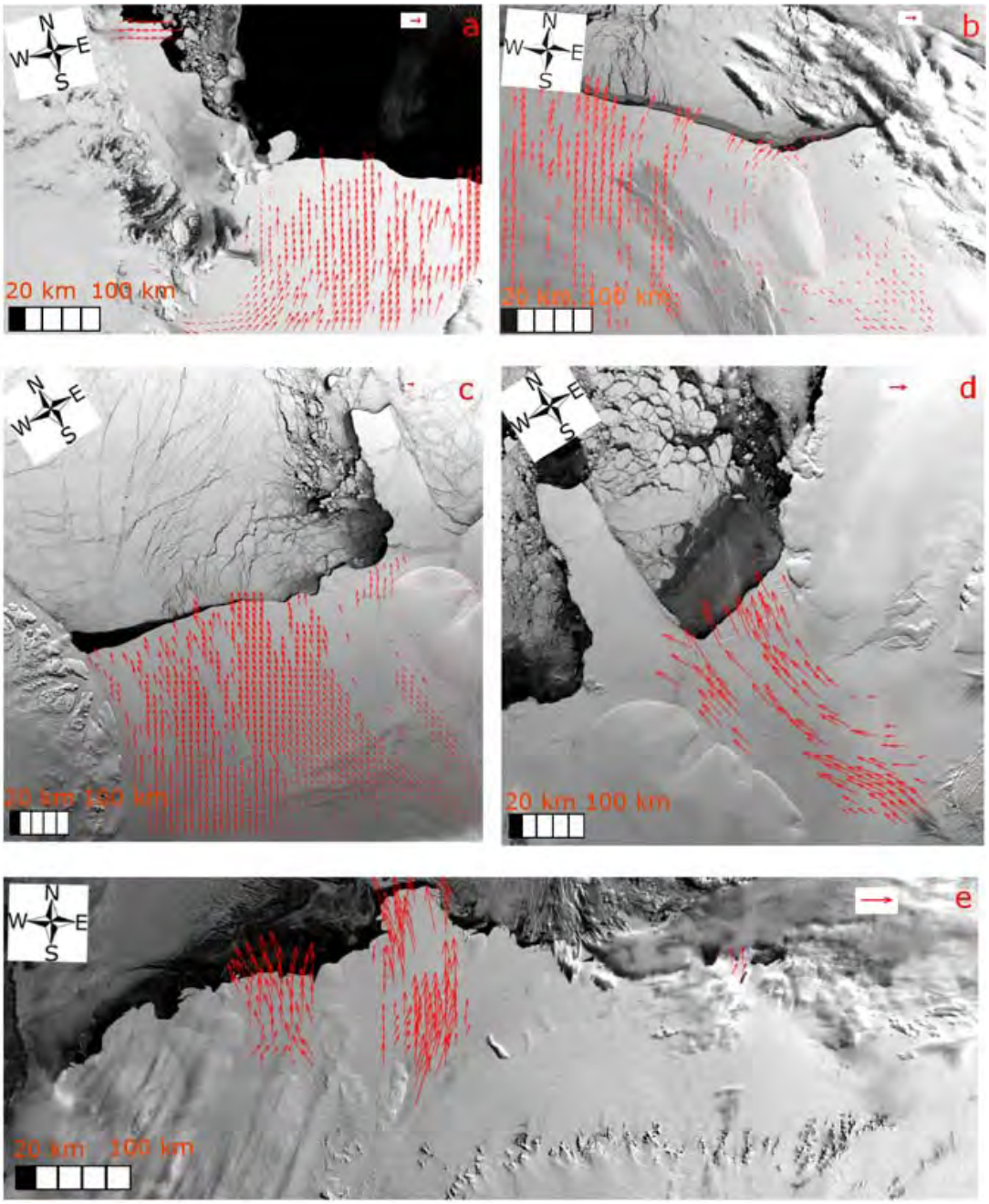

Fig. 12. The velocity fields of four ice shelves in Antarctica derived from repeat MODIS images using orientation correlation. **(a)** Ross (west),**(b)** Ross (east), **(c)** Ronne, **(d)** Filchner, **(e)** Fimbul. The arrow in the upper right corner indicate a velocity of 500 m a^{-1}. Note that the scale of the arrow changes from subfigure to subfigure. The underlying images are preprocessed by Scambos et al. (2009).

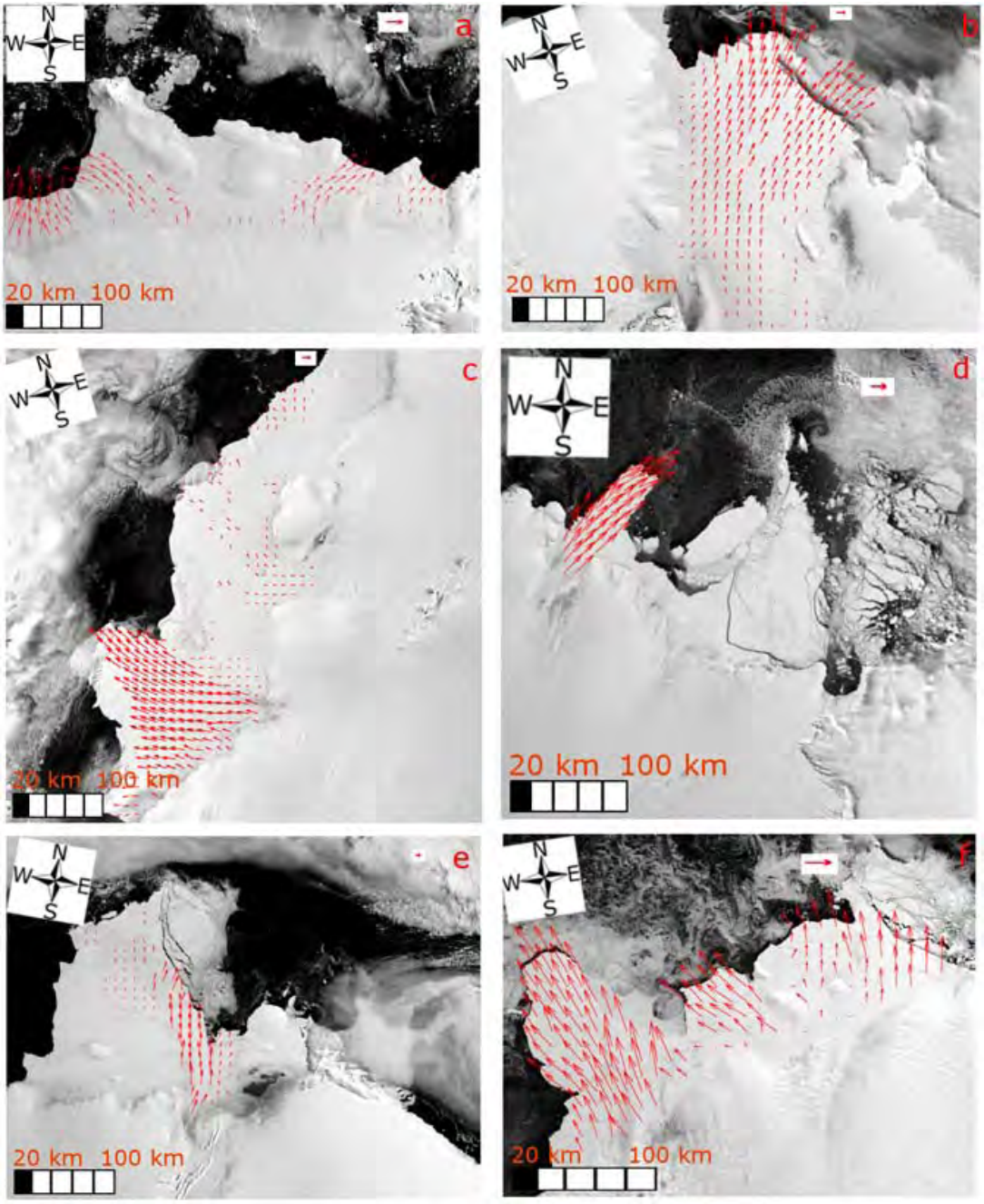

Fig. 13. The velocity fields of six ice shelves in Antarctica derived from repeat MODIS images using orientation correlation. **(a)** Getz (east), **(b)** Amery, **(c)** Riiser-Larsen, **(d)** Mertz, **(e)** Shackleton, **(f)** West. The arrow in the upper right corner indicate a velocity of 500 m a^{-1}. Note that the scale of the arrow changes from subfigure to subfigure. The underlying images are preprocessed by Scambos et al. (2009).

the velocity fields appear mostly where too few radiometric contrast features are present. This is evident for parts of the Fimbul (Fig. 12e), Getz (east) (Fig. 13a), Riiser-Larsen (Fig. 13c) and Shackleton (Fig. 13e) ice shelves. For Ross (east) (Fig. 12b) snow dunes seem to distract the matching and thus cause mismatches, and for Filchner (Fig. 12d) there are some clouds present in the images used. We also tried to match the Wilkins and Sulzberger ice shelves, but most parts of Wilkins had too little radiometric contrast and on Sulzberger most of the velocities were too small to be significant with the level of uncertainty given by the method and image type used. Mean and maximum velocity for the ice shelves is given in Table 6.

Three ice-shelf sections experienced small accelerations from the first period to the second period. Drygalski ice tongue northwest of Ross ice shelf (Fig. 12a) had a mean speed increase of $34.8\,\mathrm{m\,a^{-1}}$ (5%). The uncertainty of this comparison is $\pm 32.4\,\mathrm{m\,a^{-1}}$. The ice to the west of the main ice stream of Shackleton ice shelf (Fig. 13e) increased in speed by $63.8\,\mathrm{m\,a^{-1}}$ (15%) with an uncertainty of $\pm 45.8\,\mathrm{m\,a^{-1}}$. Mertz (Fig. 13d) increased its speed by $51.2\,\mathrm{m\,a^{-1}}$ (4%), with an uncertainty of $\pm 42.1\,\mathrm{m\,a^{-1}}$. Velocity measurements of Drygalski ice tongue from January 1990 to January 1992 (Frezzotti et al., 2000) are available through the Antarctic Ice Velocity Data (VELMAP) project of NSIDC (http://www.nsidc.org/data/velmap). They found that the mean speed of the ice tongue was $719\,\mathrm{m\,a^{-1}}$, but also report that the difference between these measurements and GPS measurements was $\pm 70\,\mathrm{m\,a^{-1}}$. This is comparable to the velocities measured in this study ($647\,\mathrm{m\,a^{-1}}$ from 2001–2005 and $682\,\mathrm{m\,a^{-1}}$ from 2005–2008) because of the large uncertainties.

The western part of the West ice shelf (Fig. 13f) decelerated from the first period to the second. In the first period the mean speed was $762.1\,\mathrm{m\,a^{-1}}$ and in the second period the mean velocity for the same points was $570.7\,\mathrm{m\,a^{-1}}$. This corresponds to a deceleration of approximately 25%. The uncertainty of this comparison is $39.5\,\mathrm{m\,a^{-1}}$. Matching using NCC on the MODIS images and also manual matching of Landsat and ASTER images confirmed the MODIS-derived deceleration.

6 Discussion

The comparison between MODIS and Landsat derived velocities reveals that MODIS derived velocities are accurate enough to derive velocities for ice shelves, even for a few years of separation between the images. These velocities can also be used to study dynamic changes. This is possible, in spite of the large pixel size of 250×250 m, because the accuracy of the measurements is approximately 1/4 pixel using orientation correlation.

Table 6. Mean and maximum velocity for the ten other ice shelves in Antarctica.

Ice shelf	Mean velocity $\mathrm{m\,a^{-1}}$	Maximum velocity $\mathrm{m\,a^{-1}}$
Ross	580	1100
Getz	420	1080
Ronne	660	1420
Filchner	780	1400
Riiser-Larsen	760	1230
Fimbul	450	770
Amery	400	1200
West	460	770
Shackleton	850	1790
Mertz	1100	1340

Both clouds, surface changes and lack of contrast can hinder successful matching. For the MODIS matching on Larsen C in the first period 2002–2006 it is mostly surface change between the two image acquisitions that hinders successful matching, but also lack of radiometric contrast. For the MODIS matching in the second period 2006–2009, the areas that are not correctly matched are mostly obscured by clouds. Successful matching of Landsat images is mainly hindered by the lack of radiometric contrast.

Average difference and RMS between the results when summing up the MODIS measurements from 2002–2006 and 2006–2009, and comparing them to the MODIS measurements directly for 2002–2009, are larger over the ice shelf and smaller over stable ground. The most important reason for this is that the velocity measurements are repeated on points with fixed geolocation, i.e. points that do not follow the ice movement (cf. remark on longitudinal strain in the results section, subsection on orientation correlation). Thus, longitudinal strain happening as the ice moves toward the ice shelf front is not accounted for. Another reason for the larger difference on the ice shelf is that it is easier to identify erroneous matches over stable ground than over the moving ice. It is more difficult to exclude mismatches from a nominally varying velocity field (ice shelf) than from a nominally constant one (stable ground). This is especially a problem where there are few measurements in close vicinity, which is the case for matching of the 2002 and 2009 images.

The difference in measured displacements between OC and NCC probably arises because the two methods match differently. The matching result will for instance be different if there is one strong contrast feature in the image. NCC will then match this feature, but OC is dependent on several features with different frequencies and with the same displacement.

Matching windows have to be chosen to be considerably larger (in pixels) for the Landsat images compared to the MODIS images in order to obtain successful matches. The

main reason for that is due to the typical large wavelength of contrast features on Larsen C such as crevasses. In the case of window sizes smaller than this density, most moving window positions simply contain not enough radiometric contrast to enable successful matching. In addition, the Landsat data have to be filtered to remove high frequencies, because the Landsat 7 ETM+ pan images contain detector noise of several digital numbers (DN), much more than the MODIS data, as can easily be explored over the vast low-contrast areas on the images. This high noise level within the 15 m ETM+ pan data compared to the 250 m MODIS data is a direct consequence of the much smaller instantaneous field of view and related weaker SNR in the detector. The high noise level in the ETM+ pan data requires relatively larger matching window sizes. It will be interesting to test how the potential gain in matching performance from using less noisy 30 m multispectral ETM+ or TM data relates to the potential loss in matching performance due to the reduced spatial resolution of 30 m in contrast to 15 m. In addition, using 30 m data instead of 15 m ones would offer the possibility to applying Landsat TM5 data instead of the SLC off affected ETM+ data. Such recent TM5 data after 2003 are, though, not available for Larsen C.

Deriving velocities from MODIS and Landsat images are both based on tracking of surface features, and are hence not completely independent methods. If surface features change their shape over the observational period in a way that introduces a systematic bias, this bias would affect the displacement measurements from both methods. Only a completely independent method, which was not available to us, could rigorously test the results.

Accuracy relative to pixel size is poorer for the Landsat 7 ETM+ pan images compared to the MODIS images. This is mainly because the accuracy of the Landsat sensor is poorer, and because of the above sensor noise, which requires low-pass filtering. Low-pass filtered images give a less pronounced correlation peak, on which then the derivation of subpixel accuracy has to rely on.

OC operated in the frequency domain is better suited for image matching in this particular study. It produces more correct matches than NCC operated in the spatial domain for the MODIS images. It is capable of matching Landsat images that have regular data voids after the failure of the SLC in 2003. OC is also faster than NCC. The clearest advantage of NCC against OC is that the size of the matching windows can be smaller, and thus more independent, i.e. non-overlapping displacements can be measured. However, reduced window size leads, in turn, to reduced accuracy. When matching low resolution images the best possible accuracy is needed in order to obtain meaningful results. In other studies where better spatial resolution of the velocity field is needed over best possible accuracy, NCC can be a better choice.

Images with 12 bit radiometric resolution are better suited for image matching in this area than images with 8 bit radiometric resolution because they produce more correct matches using both OC and NCC. It is therefore possible that areas that give no correct matches using 8 bit images can give correct matches if 12 bit images are used instead. However, 8 bit images give correct matches in most of the areas, and unless measurements over a relatively featureless area are needed, they produce satisfying results. Some points are even matched with the 8 bit images that are not matched correctly with the 12 bit images. These can be mismatches that are not revealed by our selection procedure. However, the reduced noise level in 8 bit images compared to 12 bit images from the same sensor will also lead to more robust matches in 8 bit data. In the figures, there seems to be a difference in the effect of using 12 bit images instead of 8 bit images between OC and NCC. However, this is just an apparent, not necessarily a real difference because NCC is matched on manually selected points in high-contrast areas, whereas OC is matched in a regular grid where the contrast may also be low. NCC matching in a regular grid with large window sizes gives too few matches for the MODIS images applied in our study.

It is possible that creating a 12 bit radiometric resolution image from the original 2002 MODIS data would have increased the number of MODIS matches in the first period due to more contrast. However, since the difference between 12 bit and 8 bit resolution turned out to be small, this is not done.

Co-registering images before the matching procedure improves the results, both when it comes to the accuracy of the measurements and the number of correct measurements. This is particularly important for the Landsat images which only have an absolute geolocation accuracy of 250 m, or 16.7 pixels (NASA, 1996). In order to get more correct matches on the ice shelf, the images were sometimes also aligned locally based on an assumed first-order displacement or a first matching iteration.

In this study we only use forward tracking when we perform the matching. This means that a window from time 1 is searched for in the image from time 2 and not vice versa, which would be called backward tracking. These two different methods can potentially give different results, especially if the number of surface features is sparse. On Larsen C the surface features are usually clustered, so that where there is enough contrast to get a match, this is based on several surface features. In addition the displacement is very small compared to the window size, so that it is likely that both forward tracking and backward tracking would be based on the same surface features and thus give the same results.

The presented method works well on most parts of the ice shelves investigated. The main factor that hinders successful matching during cloud-free conditions is the lack of radiometric contrast features, mostly flow features. Also snow dunes can be a problem when they cover the flow features in one of the images. Because of the uncertainty of the displacement measurements, some ice shelves actually showed velocities below the significance level.

Both Skvarca (1994) and Glasser et al. (2009) have conducted velocity measurements on Larsen C. Skvarca (1994) found that the heavily crevassed area just north of Kenyon Peninsula (see Fig. 1 for location) moved with velocities ranging from 430 to 550 m a^{-1} between 1975 and 1986, the velocities increasing as the ice moved seawards. In the same area we find velocities ranging from 410 to 630 m a^{-1}. Our results are therefore consistent with previous results in this area. Glasser et al. (2009) measured the velocities between 2002 and 2007 in a crevassed area close to the ice shelf edge in the middle of the ice shelf by an unspecified method. They measured a mean velocity of 640 m a^{-1} in this area. We measure velocities of 670 m a^{-1} in both periods, which is also consistent with their measurements in this area.

The acceleration that is observed at Larsen B and southeast of Churchill Peninsula can be put in context with the elevation decrease that Shepherd et al. (2003) measured between 1992 and 2001. The acceleration is found in the areas where also the largest elevation decrease was found. It is therefore likely that the acceleration can be attributed to the reduced backstress that a thinning ice shelf causes. This has been observed earlier for tidewater glaciers on the Antarctic Peninsula (Pritchard and Vaughan, 2007). Large calving events in front of the accelerating part could also explain the acceleration. Such calving events were searched for in the satellite images, but only a calving event in late 2004 just south of the accelerating area was found.

Glasser et al. (2009), who studied the surface structure of the Larsen C ice shelf from features such as crevasses and flowlines, did not see any large changes in the surface structure of the ice shelf between 1963 and 2007, and concluded that the ice shelf is stable. It is therefore likely that the acceleration seen so far in this northern part is too small to have an impact on the visible surface structures. It is important to keep in mind that Glasser et al. (2009) only looked at changes from 1963 to 2007, whereas when we compare streamlines and flowlines we can possibly see changes from the last centuries, which is the time it takes for ice to flow across the ice shelf.

The most likely explanation for the deceleration of the West ice shelf is that the ice shelf is already detached from its contributing glaciers. The satellite images support this hypothesis because there is a intersection going across the flow direction in the inner part of the ice shelf where there are no flow features. However, the detached part is probably still grounded and therefore not an iceberg.

7 Conclusions and outlook

We have demonstrated that repeat optical MODIS satellite images are well suited for measuring and monitoring velocities on Antarctic ice shelves in spite of their low spatial resolution of 250 m. This is done by comparing velocities derived from MODIS images over the Larsen C ice shelf with velocities derived from Landsat 7 ETM+ pan images with a spatial resolution of 15 m. The results agree well. For the period 2002–2006 the difference between MODIS and Landsat derived velocities are -15.4 m a^{-1} and 13.0 m a^{-1} for two sections on the ice shelf, and for the period 2006–2009 it is -26.7 m a^{-1} and 27.9 m a^{-1} for the same sections. The uncertainties of the method are ± 18.3 m a^{-1} and ± 19.1 m a^{-1} for the first period, and ± 22.4 m a^{-1} and ± 22.4 m a^{-1} for the second period. Uncertainties are calculated as the RSS of the RMS of the displacement measurements over stable ground and the image-to-image registration accuracy from the literature.

It is possible to obtain better results from matching MODIS images than obtained here. In this study we chose MODIS images with small amount of clouds acquired as close as possible in time to the Landsat images. Images with less clouds and of better radiometric quality were available, but then the time separation between the MODIS and the Landsat images would have been larger. Short time separation between MODIS and Landsat images was considered to be more important than maximizing the number of matches for this validation study.

Both OC operating in the frequency domain and NCC operating in the spatial domain are tested for matching the images. OC is faster, gives more correct matches, and can match images with regular noise because it is not sensitive to information restricted to few frequencies. The latter makes it possible to match Landsat 7 images with striped data voids after the failure of the SLC. NCC can match images with smaller matching window sizes than OC. However, this reduces the accuracy of the measurements. In situations where small window sizes are important, for example where the velocity varies over short distances, NCC can produce a higher resolution velocity field, but the accuracy will then be reduced. In this study both accuracy, number of correct matches and insensitivity to information constrained to few frequencies were important. Therefore OC produced the best results both for MODIS and Landsat images. In total, we achieved a sub-pixel accuracy of about 1/4 of a pixel for matching displacements based on repeat MODIS data.

The remnants of Larsen B and one section in the north of Larsen C accelerated from the 2002–2006 period to the 2006–2009 period. These areas also thinned between 1992 and 2001 (Shepherd et al., 2003), which can have reduced the backstress and thereby caused the acceleration. However, these changes have so far not changed the surface structure of the ice shelf in a visually obvious way (Glasser et al., 2009).

From a deviation between calculated streamlines and flowlines visible in the MODIS images of Larsen C we find that there is a possible change in discharge from one or more of the glaciers Lewis Glacier, Ahlmann Glacier, Bills Gulch and Daspit Glacier. The deviation between streemlines and flowlines could also be caused by a considerable change in calving front position. For the rest of the ice shelf the streamlines and flowlines agree well, indicating stable flow direction over

the ice particle travel time. The same streamlines indicate a travel time of the ice of the Larsen C ice shelf between the inland boundary and the ice edge of up to about 450 to 550 years. We applied our method successfully to ten other ice shelves around Antarctica and present an initial selection of ice shelves that could be monitored that way, confirming that the method developed here is, indeed, capable for Antarctic ice shelf velocity monitoring in general.

Our study opens for a new strategy that complements existing approaches, mainly based on SAR interferometry and tracking, to monitor and better understand dynamics, calving rates and stability of ice shelves around Antarctica. In addition to the MODIS data tested here, other low-resolution, but large coverage and high repeat-rate sensors such as ESA's Envisat MERIS are available for this purpose.

Acknowledgements. Special thanks are due to Wolfgang Rack, an anonymous referee, Mauri Pelto, and the paper's editor, Jonathan Bamber, for their detailed, thoughtful and constructive comments. MODIS data are courtesy of NASA, and were prepocessed by Scambos et al. (2009) and obtained from NSIDC through http://www.nsidc.org. Landsat data are courtesy of USGS and were obtained through http://glovis.usgs.gov. We are grateful to these institutions for making their unique data available. We are also grateful to the NASA GSFC MODIS team for their insights into MODIS orbits. This study is funded by The Research Council of Norway (NFR) through the CORRIA project (no. 185906/V30) and serves in addition as test study for the ESA DUE GlobGlacier project and the NFR IPY Glaciodyn project.

Edited by: J. L. Bamber

References

Argyriou, V. and Vlachos, T.: Quad-tree motion estimation in the frequency domain using gradient correlation, IEEE Transactions On Multimedia, 9, 1147–1154, doi:10.1109/TMM.2007.898926, 2007.

Berthier, E., Vadon, H., Baratoux, D., Arnaud, Y., Vincent, C., Feigl, K., Remy, F., and Legresy, B.: Surface motion of mountain glaciers derived from satellite optical imagery, Remote Sens. Environ., 95, 14–28, doi:10.1016/j.rse.2004.11.005, 2005.

Bindschadler, R. A., Fahnestock, M. A., Skvarca, P., and Scambos, T. A.: Surface-velocity field of the northern Larsen Ice Shelf, Antarctica, Ann. Glaciol., 20, 319–326, 1994.

Brown, L. G.: A survey of image registration techniques, Comput. Surv., 24, 325–376, 1992.

Cook, A. J. and Vaughan, D. G.: Overview of areal changes of the ice shelves on the Antarctic Peninsula over the past 50 years, The Cryosphere, 4, 77–98, 2010, http://www.the-cryosphere-discuss.net/4/77/2010/.

De Angelis, H. and Skvarca, P.: Glacier surge after ice shelf collapse, Science, 299, 1560–1562, 2003.

Debella-Gilo, M. and Kääb, A.: Sub-pixel precision algorithms for normalized cross-correlation based image matching of mass movements, Remote Sens. Environ., in review, 2010.

Fitch, A. J., Kadyrov, A., Christmas, W. J., and Kittler, J.: Orientation Correlation, in: British Machine Vision Conference, 133–142, 2002.

Frezzotti, M., Tabacco, I. E., and Zirizzotti, A.: Ice discharge of eastern Dome C drainage area, Antarctica, determined from airborne radar survey and satellite image analysis, J. Glaciol., 46, 253–264, 2000.

Glasser, N. F., Kulessa, B., Luckman, A., Jansen, D., King, E. C., Sammonds, P. R., Scambos, T. A., and Jezek, K. C.: Surface structure and stability of the Larsen C ice shelf, Antarctic Peninsula, J. Glaciol., 55, 400–410, 2009.

Howat, I. M., Joughin, I., Tulaczyk, S., and Gogineni, S.: Rapid retreat and acceleration of Helheim Glacier, east Greenland, Geophys. Res. Lett., 32(22), L22502, doi:10.1029/2005GL024737, 2005

Kaufmann, V. and Ladstädter, R.: Quantitative analysis of rock glacier creep by means of digital photogrammetry using multitemporal aerial photographs: two case studies in the Austrian Alps, Proceedings of the 8th International Conference on Permafrost, 525–530, 2003.

Kääb, A.: Monitoring high-mountain terrain deformation from repeated air- and spaceborne optical data: examples using digital aerial imagery and ASTER data, ISPRS J. Photogr. Remote Sens., 57, 39–52, 2002.

Kääb, A.: Combination of SRTM3 and repeat ASTER data for deriving alpine glacier flow velocities in the Bhutan Himalaya, Remote Sens. Environ., 94, 463–474, doi:10.1016/j.rse.2004.11.003, 2005.

Kääb, A., Gudmundsson, G. H., and Hoelzle, M.: Surface deformation of creeping mountain permafrost. Photogrammetric investigations on Rock Glacier Murtèl, Swiss Alps, Proceedings of the 7th International Conference on Permafrost, 531–537, 1998.

Kääb, A., Lefauconnier, B., and Melvold, K.: Flow field of Kronebreen, Svalbard, using repeated Landsat 7 and ASTER data, Ann. Glaciol. 42, 7–13, 2005.

Lee, D. S., Storey, J. C., Choate, M. J., and Hayes, R. W.: Four years of Landsat-7 on-orbit geometric calibration and performance, IEEE T. Geosci. Remote Sens., 42, 12, 2786–2795, doi:10.1109/TGRS.2004.836769, 2005

MacAyeal, D. R., Scambos, T. A., Hulbe, C. L., and Fahnestock, M. A.: Catastrophic ice-shelf break-up by an ice-shelf-fragment-capsize mechanism, J. Glaciol., 49, 22–36, 2003.

Meredith, M. P. and King, J. C.: Rapid climate change in the ocean west of the Antarctic Peninsula during the second half of the 20th century, Geophys. Res. Lett., 32, L19604, doi:10.1029/2005GL024042, 2005.

McClellan, J. H., Schafer, R. W., and Yoder, M. A.: Signal Processing First, Pearson Education, Inc., Pearson Prentice Hall, ISBN: 0-13-120265-0, 2003

NASA, G.: Landsat 7 System Specification, NASA Goddard Space Flight Center, 1996.

Pritchard, H. D. and Vaughan, D. G.: Widespread acceleration of tidewater glaciers on the Antarctic Peninsula, J. Geophys. Res., 112, F03S29, doi:10.1029/2006JF000597, 2007.

Quincey, D. J. and Glasser, N. F.: Morphological and ice-dynamical changes on the Tasman Glacier, New Zealand, 1990–2007, Global and Planetary Change, 68, 185–197, doi:10.1016/j.gloplacha.2009.05.003, 2009.

Rack, W., Rott, H., Siegel, A., Skvarca, P.: The motion field of

northern Larsen Ice Shelf, Antarctic Peninsula, derived from satellite imagery, Ann. Glaciol., 29, 261–266, 1999.

Rack, W. and Rott, H.: Pattern of retreat and disintegration of the Larsen B ice shelf, Antarctic Peninsula, Ann. Glaciol., 39, 505–510, 2004.

Rignot, E., Casassa, G., Gogineni, P., Krabill, W., Rivera, A., and Thomas, R.: Accelerated ice discharge from the Antarctic Peninsula following the collapse of Larsen B ice shelf, Geophys. Res. Lett., 31, L18401, doi:10.1029/2004GL020697, 2004.

Rignot, E., Casassa, G., Gogineni, S., Kanagaratnam, P., Krabill, W., Pritchard, H., Rivera, A., Thomas, R., Turner, J., and Vaughan, D.: Recent ice loss from the Fleming and other glaciers, Wordie Bay, West Antarctic Peninsula, Geophys. Res. Lett., 32, L07502, doi:10.1029/2004GL021947, 2005.

Rignot, E., Bamber, J. L., Van Den Broeke, M. R., Davis, C., Li, Y., Van De Berg, W. J., and Van Meijgaard, E.: Recent Antarctic ice mass loss from radar interferometry and regional climate modelling, Nature Geosci., 1, 106–110, doi:10.1038/ngeo102, 2008.

Rolstad, C., Amlien, J., Hagen, J. O., and Lunden, B.: Visible and near-infrared digital images for determination of ice velocities and surface elevation during a surge on Osbornebreen, a tidewater glacier in Svalbard, Ann. Glaciol., 24, 255–261, 1997.

Rott, H., Skvarca, P., and Nagler, T.: Rapid collapse of northern Larsen Ice Shelf, Antarctica, Science, 271, 788–792, 1996.

Rott, H., Rack, W., Skvarca, P., De Angelis, H.: Northern Larsen Ice Shelf, Antarctica: further retreat after collapse, Ann. Glaciol., 34, 277–282, 2002

Scambos, T. and Bohlander, J.: Glaciers of Larsen B embayment area show marked speed-up since shelf collapse, Eos Trans. AGU, 86, Fall Meet. Suppl., C11C–0829, 2003.

Scambos, T., Ross, R., Bauer, R., Yermolin, Y., Skvarca, P., Long, D., Bohlander, J., and Haran, T.: Calving and ice-shelf break-up processes investigated by proxy: Antarctic tabular iceberg evolution during northward drift, J. Glaciol., 54, 579–591, 2008.

Scambos, T., Bohlander, J., and Raup, B.: "Images of Antarctic ice shelves", National Snow and Ice Data Center, online available at: http://nsidc.org/data/iceshelves_images/, 2009.

Scambos, T. A., Hulbe, C., Fahnestock, M., and Bohlander, J.: The link between climate warming and break-up of ice shelves in the Antarctic Peninsula, J. Glaciol., 46, 516–530, 2000.

Scambos, T. A., Bohlander, J. A., Shuman, C. A., and Skvarca, P.: Glacier acceleration and thinning after ice shelf collapse in the Larsen B embayment, Antarctica, Geophys. Res. Lett., 31, L18402, doi:10.1029/2004GL020670, 2004.

Scambos, T. A., Dutkiewicz, M. J., Wilson, J. C., and Bindschadler, R. A.: Application of image cross-correlation to the measurement of glacier velocity using satellite image data, Remote Sens. Environ., 42, 177–186, 1992.

Scherler, D., Leprince, S., and Strecker, M. R.: Glacier-surface velocities in alpine terrain from optical satellite imagery - Accuracy improvement and quality assessment, Remote Sens. Environ., 112, 3806–3819, doi:10.1016/j.rse.2008.05.018, 2008.

Shepherd, A., Wingham, D., Payne, T., and Skvarca, P.: Larsen ice shelf has progressively thinned, Science, 302, 856–859, 2003.

Skvarca, P.: Fast recession of the northern Larsen Ice Shelf monitored by space images, Ann. Glaciol., 17, 317–321, 1993.

Skvarca, P.: Changes and surface features of the Larsen Ice Shelf, Antarctica, derived from Landsat and Kosmos mosaics, Ann. Glaciol., 20, 6–12, 1994.

Skvarca, P., Rack, W., and Rott, H.: 34 year satellite time series to monitor characteristics, extent and dynamics of Larsen B Ice Shelf, Antarctic Peninsula, Ann. Glaciol., 29, 255–260, 1999.

Skvarca, P., Raup, B., and De Angelis, H.: Recent behaviour of Glaciar Upsala, a fast-flowing calving glacier in Lago Argentino, southern Patagonia, Ann. Glaciol., 36, 184–188, 2003.

Skvarca, P., De Angelis, H., and Zakrajsek, A.: Climatic conditions, mass balance and dynamics of Larsen B ice shelf, Antarctic Peninsula, prior to collapse, Ann. Glaciol., 39, 557–562, 2004.

Strozzi, T., Luckman, A., and Murray, T.: Glacier motion estimation using SAR offset-tracking procedures, IEEE T. Geosci. Remote Sens., 40(11), 2384–2391, doi:10.1109/TGRS.2002.805079, 2002

Turner, J., Colwell, S. R., Marshall, G. J., Lachlan-Cope, T. A., Carleton, A. M., Jones, P. D., Lagun, V., Reid, P. A., and Iagovkina, S.: Antarctic climate change during the last 50 years, Int. J. Climatol., 25, 279–294, 2005.

Vieli, A., Payne, A. J., Du, Z. J., and Shepherd, A.: Numerical modelling and data assimilation of the Larsen B ice shelf, Antarctic Peninsula, Philos. T. Roy. Soc. A, 364, 1815–1839, doi:10.1098/rsta.2006.1800, 2006.

Wolfe, R., Nishihama, M., Fleig, A., Kuyper, J., Roy, D., Storey, J., and Patt, F.: Achieving sub-pixel geolocation accuracy in support of MODIS land science, Remote Sens. Environ., 83, 31–49, 2002.

Zitova, B. and Flusser, J.: Image registration methods: a survey, Image Vision Comp., 21, 977–1000, doi:10.1016/S0262-8856(03)00137-9, 2003.

II

6.2 Article II

Heid, T. and A. Kääb, in press. Evaluation of different existing image matching methods for deriving glacier surface displacements globally from optical satellite images, *Remote Sensing of Environment*.

Evaluation of existing image matching methods for deriving glacier surface displacements globally from optical satellite imagery

T. Heid[a,*], A. Kääb[a]

[a]*Department of Geosciences, P.O Box 1047 Blindern, 0316 Oslo, Norway*
torborgh@geo.uio.no

Abstract

Automatic matching of images from two different times is a method that is often used to derive glacier surface velocity. Nearly global repeat coverage of the Earth's surface by optical satellite sensors now opens the possibility for global-scale mapping and monitoring of glacier flow with a number of applications in, for example, glacier physics, glacier-related climate change and impact assessment, and glacier hazard management. The purpose of this study is to compare and evaluate different existing image matching methods for glacier flow determination over large scales. The study compares six different matching methods: normalized cross-correlation (NCC), the phase correlation algorithm used in the COSI-Corr software, and four other Fourier methods with different normalizations. We compare the methods over five regions of the world with different representative glacier characteristics: Karakoram, the European Alps, Alaska, Pine Island (Antarctica) and southwest Greenland. Landsat images are chosen for matching because they expand back to 1972, they cover large areas, and at the same time their spatial resolution is as good as 15 m for images after 1999 (ETM+ pan). Cross-correlation on orientation images (CCF-O) outperforms the three similar Fourier methods, both in areas with high and low visual contrast. NCC experiences problems in areas with low visual contrast, areas with thin clouds or changing snow conditions between the images. CCF-O has problems on narrow outlet glaciers where small window sizes (about 16 pixels by 16 pixels or smaller) are needed, and it also obtains fewer correct matches than COSI-Corr in areas with low visual contrast. COSI-Corr has problems on narrow outlet glaciers and it obtains fewer correct matches compared to CCF-O when thin clouds cover the surface, or if one of the images contains snow dunes. In total, we consider CCF-O and COSI-Corr to be the two most robust matching methods for global-scale mapping and monitoring of glacier velocities. If combining CCF-O with locally adaptive template sizes and by filtering the matching results automatically by comparing the displacement matrix to its low pass filtered version, the matching process can be automated to a large degree. This allows the derivation of glacier velocities with minimal (but not without!) user interaction and hence also opens up the possibility of global-scale mapping and monitoring of glacier flow.

Keywords: image matching, optical imagery, glacier, Landsat, surface displacement, global

1. Introduction

Deriving surface velocity fields of glaciers, rockglaciers, ice caps and ice shelves using optical satellite images is an efficient method with low costs, which has been used since mid 1980s. When satellite images were first used for this purpose, the matching was done by manually identifying corresponding objects and their displacement in images from different times (Lucchitta and Ferguson, 1986). Bindschadler and Scambos (1991) and Scambos et al. (1992) were the first to do this process automatically on glaciers. They used image matching algorithms based on normalized cross-correlation and the work of Bernstein (1983). After this first demonstration, different image matching methods have been tested and applied in glaciological studies. This includes normalized cross-correlation (e.g. Bindschadler et al., 1996; Rack et al., 1999; Kääb, 2002; Berthier et al., 2003; Skvarca et al., 2003; Copland et al., 2009), cross-correlation operated in the Fourier domain (Rolstad et al., 1997), least squares matching (Kaufmann and Ladstädter, 2003), phase correlation (Leprince et al., 2008; Scherler et al., 2008; Quincey and Glasser, 2009) and orientation correlation (Haug et al., 2010) (first author's last name meanwhile changed to Heid), developed by Fitch et al. (2002).

A large number of archived and upcoming optical satellite image missions now make it possible to map and monitor glacier flow on a nearly global scale. Deriving glacier displacements globally will give unique glaciological information. It will make it possible to compare spatio-temporal variations of glacier velocities both within regions (Kääb, 2005) and between regions. Such knowledge will enable to better understand a wide range of processes related to glacial mass fluxes, such as glacier response to climate and climatic changes, glacier physics and flow modes, glacier flow instabilities (e.g. surges), subglacial processes (e.g. erosion), supra- and intra-glacial mass transport, etc. Knowledge about glacier ice supply helps

*Corresponding author

to understand the development of glacial lakes and associated hazards. Glacier velocities are also input into numerical glacier models. Mapping and monitoring glacier flow globally perfectly complements current attempts for mapping and monitoring glacier areas and glacier volume changes on a global scale (Zemp et al., 2009; Haeberli, 2004; Bishop et al., 2004; Raup et al., 2007).

Studies based on matching of repeat glacier images have so far mostly concentrated on obtaining the best results using one specific image matching method, and little work has been done on comparing different methods over glaciers. This contrasts to the effort done with comparing different methods in the more technical signal processing community using synthetic tests (Scharstein and Szeliski, 2002; Brown et al., 2003). It is therefore a need to evaluate different existing methods over a globally representative set of glacier surface types in order to recommend an optimal method or set of methods for precise, accurate, robust and broadly applicable measurement of glacier flow over large scales from repeat optical satellite data. The goal of this study is therefore to look into different case studies which together represent the challenges that are often met when doing image matching in glacierized areas. The purpose of the study is not to compare algorithms on the strictly technical level, but to compare algorithms with global scale applications as a focus. The ultimate goal of this study is to contribute the methodological background for operational global-scale mapping and monitoring of glacier flow from repeat optical satellite images.

Here we compare six commonly used image matching algorithms over five glacierized areas spread around the world and with different characteristics, which are thought to be globally representative. The methods evaluated are (1) normalized cross-correlation operated in the spatial domain, (2) cross-correlation operated in the frequency domain, (3) phase correlation operated in the frequency domain, (4) cross-correlation operated in the frequency domain on orientation images, (5) phase correlation operated in the frequency domain on orientation images, and (6) the phase correlation algorithm used in the COSI-Corr software, explained below. Methods 2 to 5 are all based on the same Fourier matching technique, but have different normalizations. The matching method from COSI-Corr is also a Fourier method, but in contrast to the other Fourier methods evaluated here, the result is not transformed back to the spatial domain for getting the correlation surface. Least squares matching is a method that is often used for image matching, in particular in photogrammetry. This method, however, requires initial measurements from other matching methods and is only a way to improve the accuracy. It is therefore not tested in this study. The five glacierized study regions chosen are the Karakoram, the European Alps, Alaska, Pine Island (Antarctica) and southwest Greenland (Figure 1). In addition, for a small section in the Karakoram a method using adaptive window sizes is tested.

Given the scale of glaciers and glacial features considered in this study on the one hand, and the availability and accessibility of suitable data on a global scale on the other hand, we focus here on applying medium resolution satellite imagery (ca. 30 m to 15 m). It should however be noted that even low-resolution

Figure 1: Map showing the location of the five selected glacierized areas.

data can be used for deriving the flow of very large glaciers (typically Antarctica; (Haug et al., 2010)). On the other hand, high-resolution data are able to provide glacier velocity fields for selected sites (e.g. for validation) at very high density and accuracy, but are not yet available and accessible for global-scale applications.

This study is not a complete study investigating all possible image matching methods. There are both more possible matching methods and also more possible implementations of the matching methods evaluated here. But this study evaluates the traditionally and much used normalized cross-correlation and also COSI-Corr that is more and more used. The study also includes other Fourier matching methods that are often used in image matching, and that have also been used in glaciological studies with success.

2. Methods

2.1. Selecting satellite images and glacier regions

This study focuses on Landsat satellite images because one image covers a large area (183 km by 170 km for ETM+, 185 km by 172 km for TM and 185 km by 185 km for MS), and at the same time the spatial resolution for the panchromatic band after 1999 is as good as 15 m. This makes them highly suited for global measurements. The Landsat series extends back to 1982 with 30 m spatial resolution and to 1972 with 68 m by 83 m spatial resolution. This long time series makes it possible to study velocity changes. Landsat images are available at no cost through the U.S. Geological Survey (USGS). Also ASTER images have a spatial resolution of 15 m in the visible and near-infrared spectrum, and are available at no cost for scientific users. However, one ASTER image covers a much smaller section of the Earth than one Landsat image does (60 km by 60 km), so that ASTER images are considered to be less easily used for global mapping of glacier velocities compared to Landsat data. Landsat images have, however, subpixel noise created by the attitude variations. Lee et al. (2004) found that the the image-to-image registration accuracy was better than the requirement of 7.3 m, and that the average was at about 5 m. This noise is impossible to model because it is a whisk-broom system, and therefore the accuracy of the matching reduces to this level. For most glaciological studies this is an acceptable accuracy because the glacier displacements over the time period

that the glacier features are preserved by far exceed this noise level.

Here we select images from Landsat 7 ETM+ before failure of the Scan Line Corrector (SLC). This is because the striped data voids that are present in Landsat images after SLC failure are special for Landsat images, and avoiding these stripes makes our method comparison more valid for images from other sensors. However, we also test selected methods on Landsat images after SLC failure to see how they perform in case of such striped data voids. We use Level 1T images, which are terrain-corrected using ground control points (GCPs) and digital elevation models (DEMs).

We choose a set of glacier regions and glaciers with different characteristics that we think are globally representative in terms of glacier dimensions, topography, surface features, flow rates, climatic setting, etc. The European Alps (Landsat path 195 row 28) are chosen because the glaciers in this area are small valley glaciers with high surface transformation due to intense summer melt. Karakoram (path 148 row 35) is chosen because many of the glaciers in this area have a thick debris cover in their lower parts. Alaska (path 63 row 18) is selected because of the large mass flux and the high velocities. Pine Island in Antarctica (path 233 row 113) is selected because of the very little visual contrast in this area, and because of the very large glacier size. Southwest Greenland (path 9 row 11) is chosen because the velocity differences between fast ice streams and slower moving parts of the ice cap are very large, and because the glaciers here contain very little debris. Table 1 gives an overview of the images used.

2.2. Image matching methods

Six different image matching methods are tested and evaluated: (1) normalized cross-correlation operated in the spatial domain (hereafter referred to as NCC), (2) cross-correlation operated in the frequency domain using Fast Fourier Transform (FFT) (hereafter referred to as CCF), (3) phase correlation operated in the frequency domain using FFT (hereafter referred to as PC), (4) cross-correlation operated in the frequency domain using FFT on orientation images (hereafter referred to as CCF-O), (5) phase correlation operated in the frequency domain using FFT on orientation images (hereafter referred to as PC-O), and (6) the phase correlation algorithm used in COSI-Corr (hereafter referred to as COSI-Corr). When computing the cross-correlation it is assumed that the first and second order statistics are constant (stationarity) and that the noise is random.

NCC is a matching method that is often used when studying glacier velocities. This is much due to its simplicity. The first image is taken as the reference image, and a template out of this image is searched for in the second image, or the search image. The centered cross-correlation surface CC is given by

$$\mathrm{CC}(i,j) = \frac{\sum_{k,l}(s(i+k,j+l)-\mu_s)(r(k,l)-\mu_r)}{\sqrt{\sum_{k,l}(s(i+k,j+l)-\mu_s)^2 \sum_{k,l}(r(k,l)-\mu_r)^2}} \quad (1)$$

where (i, j) indicates the position in the search area, (k, l) the position in the reference area, r the pixel value of the reference chip, s the pixel value of the search chip, μ_r the average pixel value of the reference chip and μ_s the average pixel value of the search chip. The peak of the cross-correlation surface indicates the displacement between the images. This cross-correlation is normalized, which has two effects. Firstly, images with different illumination conditions can be better compared, and secondly, the correlation coefficient from different correlation attempts can be compared. Because this method operates in the spatial domain (as a convolution operation), the computation is time-consuming compared to computations in the frequency domain.

The NCC method is easily dominated by large differences in the digital numbers. If large differences exist within the reference or the search template, large differences also have to exist in the opposite window (i.e. the search or the reference template, respectively). We hypothesize that this is a major drawback with this method for glacier applications. Glacier areas usually contain large differences in digital numbers, because white snow and black rocks etc. are present. This would not be a problem if these differences were present in both images and also represented the displacement. However, it is common that snow patches in one image disappears in the nest image, that rocks move independently of the glacier movement by rolling or sliding at the glacier surface. Situations where large intensity differences are not present in both images or where large intensity differences do not represent the displacement are hence hypothesized to create erroneous matches for the NCC method.

Cross-correlation can also be computed in the frequency domain by multiplying the Fourier transform of one image and the complex conjugated Fourier transform of the second image (the convolution theorem) (McClellan et al., 2003). This procedure is equivalent to computing the cross-correlation in the spatial domain. However, the above normalization cannot easily be transformed to the frequency domain. In the CCF method, only the cross-correlation is computed, so that this method does not normalize. This implies that different illumination conditions in the two images can lead to mismatches. Also, the method can result in a wrong match if the illumination varies within the section to be matched. In this approach the cross-correlation surface CC is given by

$$CC(i,j) = IFFT\left(F(u,v)G^*(u,v)\right) \quad (2)$$

where $F(u, v)$ is the Fast Fourier Transform (FFT) of the matching window from the image at time $t = 1$, $G(u, v)$ is the FFT of the matching window from the image at time $t = 2$, * denotes the complex conjugate and IFFT is the Inverse Fast Fourier Transform.

Since the CCF method does not contain any kind of normalization, it is hypothesized not to outperform other methods. But by including this method, it is easier to evaluate the effect of different normalizations.

A common way of approximating normalization in the Fourier domain is to consider only the phase information. By doing this, differences in image intensity, which show up only in the

Table 1: Overview of the Landsat image pairs used.

Area	Path/Row	Date image t = 1	Date image t = 2	ID image t = 1	ID image t = 2
European Alps	195/28	12 Aug 2000	30 Jul 2001	LE71950282000225EDC00	LE71950282001211EDC00
Karakoram	148/35	16 Jun 2000	21 Jul 2001	LE71480352000168SGS01	LE71480352001202SGS00
Alaska	63/18	31 Aug 2000	03 Sept 2001	LE70630182000244AGS00	LE70630182001246EDC00
Pine Island	233/113	13 Jan 2001	15 Dec 2001	LE72331132001013EDC00	LE72331132001349EDC00
Greenland	9/11	07 Jul 2001	08 Aug 2001	LE0090112001188EDC00	LE70090112001220EDC00

amplitudes, are ignored. In this PC method the *CC* is given by

$$CC(i,j) = IFFT\left(\frac{F_o(u,v)G_o^*(u,v)}{\left|F_o(u,v)G_o^*(u,v)\right|}\right). \quad (3)$$

Also here, the peak of the cross-correlation surface indicates the displacement.

In the PC method the phase differences at every frequency contributes equally, and the dominant phase difference is taken as the displacement (Brown, 1992). Noise limited to one or few frequencies is therefore ignored, whereas noise spread across all frequencies makes the location of the peak inaccurate, and therefore also the final displacement estimate inaccurate. This is hypothesized to effect the matching in both wanted and unwanted ways. Firstly, the method should be robust against different illumination between the images, because this effect is constrained to low frequencies (Brown, 1992). Secondly, it should also be robust to large intensity differences that are hypothesized to create erroneous matches for the NCC method. This is because snow patches and rolling/sliding rocks will be constrained to a few frequencies and thereby ignored in the PC method. Thirdly, this method can be hypothesized to experience problems in areas with deformation, because the phase differences at the different frequencies will not agree.

Fitch et al. (2002) developed a method called orientation correlation. Haug et al. (2010) showed that this method is well suited for deriving ice shelf velocities. Taking f as the image at time $t = 1$ and g as the image at time $t = 2$, the orientation images f_o and g_o are created from

$$f_o(x,y) = sgn\left(\frac{\partial f(x,y)}{\partial x} + i\frac{\partial f(x,y)}{\partial y}\right) \quad (4)$$

$$g_o(x,y) = sgn\left(\frac{\partial g(x,y)}{\partial x} + i\frac{\partial g(x,y)}{\partial y}\right) \quad (5)$$

$$\text{where } sgn(x) = \begin{cases} 0 & \text{if } |x| = 0 \\ \frac{x}{|x|} & \text{otherwise} \end{cases} \quad (6)$$

where sgn is the signum function and i is the complex imaginary unit. The new images f_o and g_o are complex and hence consist of one real and one imaginary part, where the intensity differences in the x direction represent the real matrix and the intensity differences in the y direction represent the imaginary matrix. These orientation images are then matched using cross-correlation operated in the frequency domain (CCF-O) and phase correlation (PC-O).

According to Fitch et al. (2002) orientation correlation is illumination invariant. Because the orientation vector (and hence both orientation images) has zero value in uniform areas and a length of one in non-uniform areas, the correlation is not effected by uniform areas. This is a desired property in glaciological research because uniform areas are common. We also hypothesize this to be important when it comes to matching striped Landsat images after the failure of the scan line corrector (SLC-off) because the stripes are ignored when using orientation correlation.

When it comes to PC-O, two types of normalizations are actually included. Firstly, orientation images are already normalized, and then the amplitudes are removed, which is another normalization. We hypothesize that it is unnecessary to use two kinds of normalizations, and that this actually removes too much of the original signal so that this method obtains less correct matches.

The last matching method that we test is the matching method incorporated in the COSI-Corr software (Leprince et al., 2007). Only the matching algorithm of COSI-Corr is evaluated because the orthorectification and coregistration parts of COSI-Corr are not developed for Landsat and other whiskbroom systems. The matching method in COSI-Corr estimates the phase difference in the Fourier domain as in the above PC, but does not transform the images back to the spatial domain to find the maximum of the CC (Leprince et al., 2007). It also uses a robust function to produce measurements, a method that is less sensitive to outliers.

Matching windows in COSI-Corr are weighted by a bell-shaped function to avoid edge effects. The effect of this is that central parts of the window are given more weight in the matching than the outer parts of the window. The effective size of the matching windows in COSI-Corr are therefore smaller. This, however, will depend on the visual contrast in the windows. COSI-Corr also uses re-weighted least squares in the matching process, and this makes COSI-Corr less sensitive to outliers within the windows. The pixels within the window hence have to move coherently for COSI-Corr to get a correct match. We therefore hypothesize that COSI-Corr can experience problems in areas with much deformation.

All of the frequency domain methods are hypothesized to perform worse compared to the spatial domain method on small window sizes. This follows from the Heisenberg's uncertainty principle. However, small window sizes may in some cases be useful for measuring glacier displacements. This is especially hypothesized to be the case for shear zones or where glaciers flow over obstacles, and for small glaciers where deformation is important over much of the glacier areas.

2.3. Implementations

How image matching methods perform highly depend on how they are implemented. This section therefore explains how the different matching methods are implemented in this study.

For all of the methods except COSI-Corr, we determine the subpixel displacement by fitting orthogonal parabolic functions to the correlation surface. Subpixel displacements in the x direction dx and in the y direction dy are found using

$$dx = \frac{P(x_m + 1, y_m) - P(x_m - 1, y_m)}{2(2P(x_m, y_m) - P(x_m + 1, y_m) - P(x_m - 1, y_m))} \quad (7)$$

$$dy = \frac{P(x_m, y_m + 1) - P(x_m, y_m - 1)}{2(2P(x_m, y_m) - P(x_m, y_m + 1) - P(x_m, y_m - 1))} \quad (8)$$

where $P(x_m, y_m)$ is the maximum correlation value. The parabolic function is therefore fitted using the two nearest neighbours. Debella-Gilo and Kääb (2011) found that when using NCC, this method for determining displacement at subpixel precision performed worse compared to interpolating the image before the matching is conducted. However, for the size of Landsat images, interpolating the images and matching using bigger window sizes would be too computationally expensive at the moment for large-scale applications. In the near future, or using super-computers, it will be possible to use this method instead.

When fitting a parabolic curve to the correlation surface, it is important that the correlation surface approximates a parabola around the peak for the subpixel estimation to be as correct as possible and thereby avoid aliasing. For NCC the images should be oversampled by a factor of two before the matching to avoid aliasing, whereas for frequency domain methods such an oversampling is not necessary. Oversampling by a factor of two is difficult to apply in the case of global glacier matching because of the time consumption associated with both the oversampling process and the matching of two times larger windows in each direction. Biases associated with not oversampling images are usually on the order of 1/10th of a pixel (Dvornychenko, 1983; Kim, 2011), and for Landsat images, with considerable sensor noise, such biases are here not considered significant.

In spatial domain matching, a small reference template is cut out from the reference image (of time 1) and the most similar template within a search window in the search image (of time 2) is found. This procedure requires optimal adjustment of both the reference template size and the search window size (Debella-Gilo and Kääb, 2011, in review). In frequency domain matching, the displacement is found directly without iteration as phase difference from multiplication of the reference template (of time 1) and the search template (of time 2). This procedure requires that the displaced terrain section is well contained both in the reference and search template. Also, in frequency domain matching the displacement cannot be larger than half the window size in each direction for the methods to work correctly. In sum, both spatial and frequency domain matching need selection of optimal window sizes (i.e. reference and search templates and windows; here summarized as the term window). The windows should be big enough to ensure that texture and not noise is matched, but small enough to limit displacement gradients within the window.

Table 2: Size of matching windows and thresholds for the deviation between the raw matching result and the low pass filtered matching result that are used to filter the displacement fields in the different glacierized areas.

Area	Window size, pixels	Filtering threshold, m
Karakoram	32	± 45
European Alps	16	± 45
Alaska	128 - 64	± 300
Pine Island	512 - 64	± 150
Greenland	64	± 100

For each of the five test areas we use a small but representative section of the Landsat images to find the optimal image window sizes. Applying this selection procedure on entire Landsat images would be very time consuming due to the image size of about 15000 pixels by 17000 pixels. The size of the small test sections used is 2000 pixels by 2000 pixels, which translates to 30 km by 30 km. Different window sizes are tested on this section to find a window size that optimizes the matching results. The matching result is considered to be optimized when assumed correct matches are obtained over most of the glacierized areas, but without increasing the window size more than necessary. This is to avoid much deformation in one window. Because only window sizes of 2^n may be used when images are matched using Fourier methods, the choice of window size is very limited for each site, and in practice usually without alternatives. The spacing between the matching windows is kept the same as the matching windows themselves to get completely independent matches. The size of the matching windows is given in Table 2. For Alaska and Pine Island, the images were first matched with large windows but with the wanted final window size as spacing between the windows, then aligned according to the measured initial displacement so that every center pixel has its own vector for aligning, and finally matched with smaller windows to produce the final displacement field. Therefore, for the final match every position has an a priori displacement. For example for Alaska, the images were first matched using windows of 128 pixels but a spacing of 64 pixels, then aligned for every matching using the displacement measured with the 128 pixel window and then matched again with the 64 pixels window.

Because the six matching methods methods work differently, we have to aim for implementations that make the methods as comparable as possible. As mentioned in the above paragraph, frequency domain methods find the displacements directly without iterating, whereas spatial domain methods require iterations to locate the highest correlation. This is one fundamental difference that makes it impossible to design completely identical implementation cases for all the matching methods. Instead we have to make sure that the search area in the NCC method allows for matches half the window size away to be most like the frequency domain methods. Another important issue is that COSI-Corr weights the window using a bell-shaped function making the effective window size smaller, as men-

tioned before. However, in areas with low visual contrast in particular, it is clear that also COSI-Corr can get matches from the outer parts of the window. We therefore decide to use the same matching windows for COSI-Corr as we use for the other methods. However, this should be kept in mind especially when it comes to the accuracy of the matching methods, because larger matching windows normally give higher accuracy. This topic will be discussed in the Discussion section.

We compare the image matching methods based on two criteria: 1) their accuracy and 2) their ability to obtain correct matches for each of the five glacier areas. The first criterion, the accuracy of the different matching methods, is evaluated based on the root mean square error (RMSE) of the assumed correct matches over a section containing stable ground in the Landsat image over the European Alps (path 195 row 28) with a window size of 16 pixels by 16 pixels. The size of the section is 14 km by 14 km and the number of possible correct matches is 3481. The window size used for the accuracy evaluation is the smallest window size that is used when matching the different areas, and will therefore represent a worst case matching accuracy. Since the accuracy is down to fractions of a pixel, also attitude variations and accompanying pixel geolocation errors of the Landsat sensor, and erroneous topographic corrections may influence the RMSE. To test the RMSE of images without geometric distortion between the two images we also generate a synthetic image over the Alaska site (path 63 row 18). To the original image we apply scaling and first and second order analytical displacements ranging from 0 m to 200 m, and match it to the original image without distortions to see how the accuracy is influenced by deformation. We also introduce modelled systematic radiometric noise. The noise model used is among others common in least squares matching, where systematic radiometric differences are accounted for by gain (λ) and offset (η). Here, the digital numbers $F(x, y)$ at time $t = 1$ are given by

$$F(x, y) = G(x', y')\lambda + \eta + e \tag{9}$$

where $G(x', y')$ is the digital numbers at time $t = 2$ over the same area and e is random noise. In this study we generate λ and η randomly for windows of 10 pixels by 10 pixels. λ has a mean of 1 and a standard deviation of 0.3, whereas η has a mean of 0 and a standard deviation of 8. The synthetic image and the original image are matched using window sizes of 32 pixels by 32 pixels. Because the focus of this study is global image matching of glacierized areas using Landsat images, the accuracy cannot be better than the whisk-broom sensor noise, since this noise cannot be modelled. The second criterion, the ability to obtain correct matches for each of the five glacier areas, is evaluated by filtering the raw image matching results in the glacierized area to remove erroneous matches. Then, the percentage of correct matches for each matching method for each area is calculated.

The filtering method to filter erroneous matches over the glacierized area should require little user interaction. The large number of displacement vectors makes it too time consuming to filter the results completely manually. A directional filter is useless in most cases over large scales because the multiple glaciers flow in different directions within the same scene. Filtering by the length of the displacement vectors is possible, but this requires that the user first identifies a maximum velocity. This maximum velocity has to be set for every of the five glacierized areas because both the displacements and the window sizes change from test study to test study. This filtering method will only remove some of the erroneous matches. Signal-to-noise ratio (SNR) and correlation coefficient make it possible to filter depending on the quality of the match. However, the values of SNR and correlation coefficient also vary depending on the matching method. These filtering methods will therefore not be independent of the matching methods, and we therefore consider them to be inappropriate for this study.

Following basic glacier physics, in particular stress transfer, we choose to filter the obtained vectors depending on the neighbouring vectors, so that vectors are assumed correct if they agree to a certain extent with their neighbouring vectors. First, all vectors outside glacierized areas are removed manually or using digital glacier outlines. Then the assumed real maximum displacement is found by manually investigating the vectors. All vectors larger than the assumed real maximum displacement are removed. Using only the remaining vectors, the displacement field in both x and y direction is filtered using a 3 by 3 mean low-pass filter. Individual original vectors that deviate more than a certain threshold from this low-pass filtered displacement field are removed. The threshold varies between the five different areas depending on the displacement variations within the areas. Table 2 lists the different thresholds. Figure 2 shows the unfiltered displacement field and Figure 3 shows the automatically filtered displacement field for Karakoram. Some manual editing is still needed in the end to remove erroneous vectors without neighbours and clusters of erroneous matches of the same size in both x and y direction. The final overview of how many assumed correct matches are produced by the different matching methods is therefore not only a result of the matching methods used, but also, to some extent, a result of the filtering methods used. But by selecting a filtering method that is independent of the matching method used, we assume that the filtering method has the same effect on all the displacement fields.

Also a median low-pass filter could have been used to filter erroneous matches. A mean filter takes better care of areas with velocity gradients, but also removes some correct matches in the outer areas of patches with correct matches. A median filter tends to remove more of the erroneous matches than a mean filter does.

It should be noted that we believe that, in order to receive glaciologically sound and useful glacier displacements, the automatic results should undergo in any case an expert check and, potentially, editing, as is for instance well acknowledged and good practice in multispectral glacier mapping Paul et al. (2009). Thus, the aim of displacement filters becomes to support the analyst to remove as much as possible obvious errors to let focus on details that require glaciological expert judgment. For instance, gradients in glacier velocities are very different from area to area due to the large variety of glaciers, so by manually tuning the filtering, raw displacement fields might be

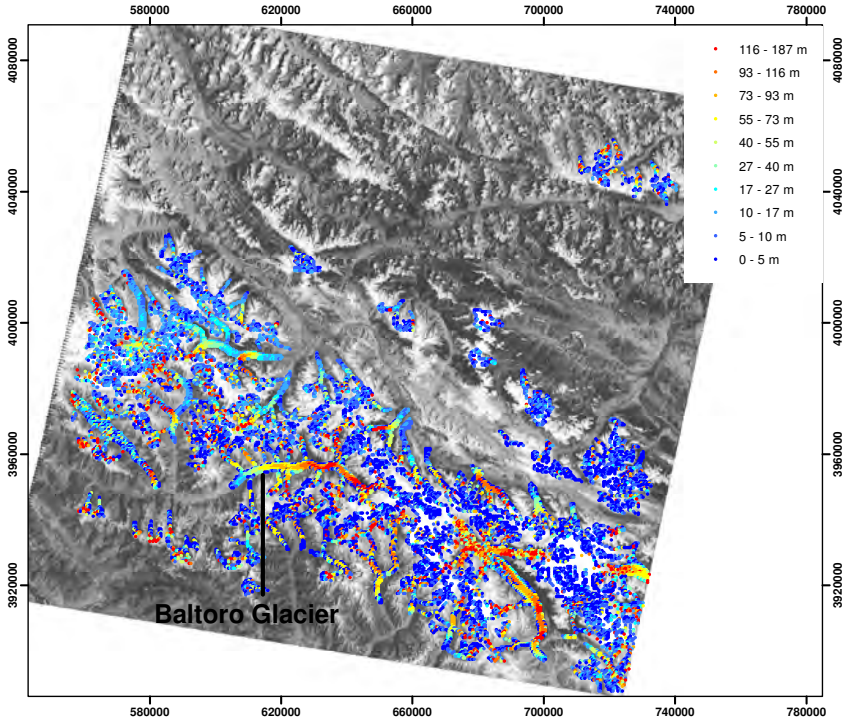

Figure 2: The unfiltered displacement field for Karakoram using CCF-O. Underlying image is from 21 July 2001.

better filtered. To filter the displacements based, for instance, on the assumption that glaciers flow downslope is considered to be impossible globally, because the required accurate elevation models are not available in all glacierized areas, and because of physical reasons where this assumption does not simply hold, such as in confluence areas or for supraglacial ice topography.

It would be very beneficial to compare our velocity measurements to velocity measurements obtained using completely independent methods. However, due to the variability of glacier flow, this is a very difficult task. Glacier flow may vary significantly on daily, seasonal and yearly scales. To be able to compare velocities obtained using different sources it is therefore important that the periods overlap completely. Very few studies have compared velocities derived using optical remote sensing with other methods, and in most of the cases the time periods have not been overlapping. With the global focus of this study it was not possible to compare the velocities with data from independent sources. This is only possible for specific points on a limited number of glaciers where continuous field measurements are available.

3. Case studies

Table 3 shows the percentage of assumed correct matches over glacierized areas for the different matching methods. The results vary both from method to method and from area to area. Generally, COSI-Corr obtains the highest percentage of assumed correct matches, whereas NCC and PC-O obtain the lowest. Alaska is the area which obtains the highest percentage of assumed correct matches, whereas Pine Island obtains the lowest percentage of assumed correct matches.

3.1. Stable ground and synthetic displacements

The RMSE of the matching measurements in both x and y directions over stable ground in the European Alps is given in Table 4. The results are comparable and better than 1/10 of a pixel for NCC, PC and PC-O. CCF and CCF-O perform slightly worse, but still close to 1/10 of a pixel. The matching method from COSI-Corr has the highest RMSE with about 1/4 pixel. Due to several small clouds in the Landsat scene from 2001 the number of erroneous matches is relatively high. NCC and CCF have more erroneous matches than the other matching methods.

The results of the synthetic displacement test is given in Table 5. COSI-Corr obtains the best results and NCC the worst results both when it comes to average error and RMSE. CCF has the highest number of mismatches.

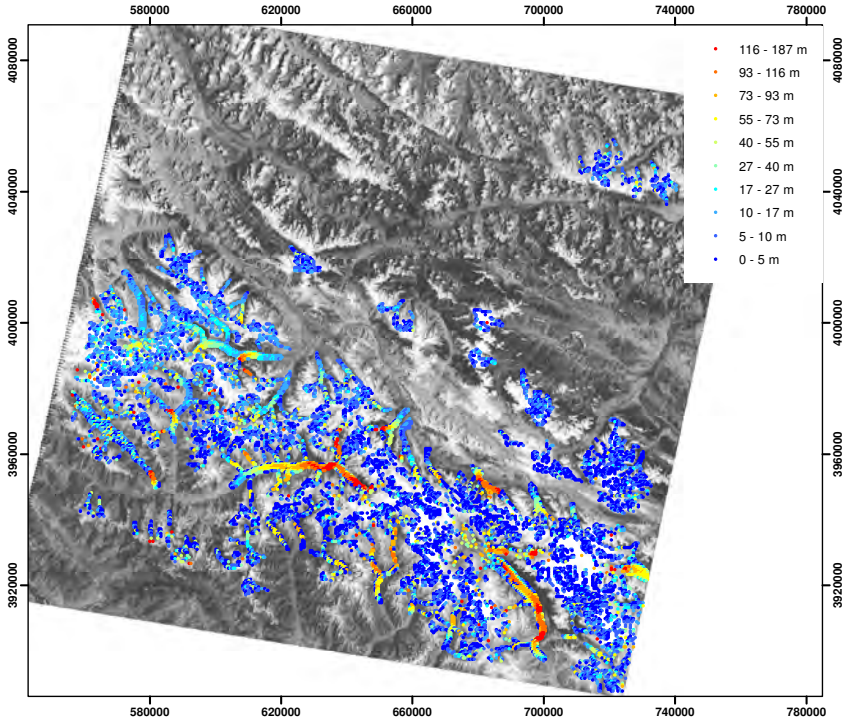

Figure 3: The automatically filtered displacement field for Karakoram using CCF-O. Underlying image is from 21 July 2001.

Table 3: Percentage of assumed correct matches over glacierized areas for the different matching methods. Maxima by region is bold, maxima by method is italics.

Area	NCC	CCF	PC	CCF-O	PC-O	COSI-Corr	n
Karakoram	46 %	59 %	56 %	61 %	54 %	**67 %**	21950
European Alps	49 %	56 %	51 %	57 %	48 %	**67 %**	5476
Alaska	*76 %*	*86 %*	*83 %*	*87 %*	*73 %*	***91 %***	13393
Pine Island	16 %	**18 %**	17 %	17 %	11 %	13 %	28822
Greenland	14 %	25 %	22 %	23 %	17 %	**30 %**	23790

Table 4: RMSE of the matching measurements for the 6 different matching methods over stable ground in the European Alps.

Matching method	σ_x, m	σ_y, m	n
NCC	1.2	1.2	2917
CCF	1.5	1.7	3128
PC	1.0	1.2	3271
CCF-O	1.4	1.7	3288
PC-O	1.1	1.4	3252
COSI-Corr	2.9	3.9	3260

3.2. Karakoram

Figure 4 shows the displacement measurements from CCF in Karakoram. The difference between this matching method and CCF-O (shown in Figure 3) is striking. CCF-O obtains assumed correct measurements over most of the glacierized areas, whereas CCF has problems revealing that the fast valley glaciers have moved over the time period. This means that instead of matching the moving glacier features, it matches the stationary patterns that do not move while the glaciers flow. The displacement field created by CCF is therefore very coherent, but wrong. However, in the upper and slower moving parts of the glaciers, the performance of the two methods is similar.

The performance of NCC is comparable to the performance of CCF-O on the lower parts of the glaciers where the visual contrast is good (not shown). However, as can be seen in Table 3, NCC produces fewer correct matches compared to the CCF-

Table 5: Average and RMSE between derived displacements and actual displacements in a synthetic test.

	Average x-direction *m*	Average y-direction *m*	RMSE x-direction *m*	RMSE y-direction *m*	Number of mismatches
NCC	0.0	-4.9	7.4	5.6	5
CCF	0.7	0.0	5.2	3.8	46
PC	1.4	0.0	4.5	3.8	4
CCF-O	1.3	0.0	3.3	2.3	0
PC-O	1.1	0.0	4.5	3.7	1
COSI-Corr	0.1	0.0	0.9	0.8	0

O over all. This is mainly because NCC produces fewer correct matches above the snowline where the visual contrast is poor.

PC performs similarly to CCF, which means that it does not capture the velocity of the fast valley glaciers. Instead of matching the moving glacier features also this method matches the stationary patterns. The other glacierized parts are, however, well matched. The number of correct matches in total is, however, lower compared to CCF. PC-O manages, like CCF-O, to capture the displacement both of the fast valley glaciers and of the glacierized area with poor visual contrast, but the number of correct matches is lower for PC-O compared to CCF-O.

COSI-Corr performs similarly to CCF-O on the glacier tongues, which have good visual contrast, but above the snowline COSI-Corr obtains a higher number of assumed correct matches than CCF-O. Therefore, the percentage of assumed correct matches for COSI-Corr is higher than the percentage of assumed correct matches for CCF-O.

The sections with highest glacier speeds in the part of the Karakoram studied here show displacements of up to about 150 m over the 13 months investigated (138 m/a). Not only the largest glaciers in the area turn out to be fast flowing, but also some of the smaller ones. Since this is an area that is known to include surging glaciers (Hewitt, 1969; Copland et al., 2009), it is likely that these small but fast moving glaciers are in an active phase of a surge cycle. The pattern of speed variation derived here for Baltoro Glacier fits well with the pattern derived by Quincey et al. (2009) for the period 2003-2008.

3.3. European Alps

NCC is the only matching method to match most of the area below the snowline of the glaciers in this region (Figure 5, left). COSI-Corr creates fewer assumed correct matches below the snowline, but above the snowline, where the visual contrast is poor, COSI-Corr creates more assumed correct matches than NCC. When it comes to the number of assumed correct matches in total, COSI-Corr outperforms both NCC and the other four matching methods. This is because of its superior performance in the areas with low visual contrast. CCF-O obtains more correct matches than the three other similar Fourier methods.

The displacement field in the European Alps needs more manual editing than the displacement fields in Karakoram because the matching methods produce fewer correct matches. Aletsch Glacier (see Figure 5 for location) is the fastest glacier in this area, moving up to 150 m over the 11.5 months studied. However, maximum displacement in both x and y direction is less than half the window size, 120 m.

Since we know that the effective window size for COSI-Corr is less than the actual window size, we also try to match the images from the European Alps using COSI-Corr and a window size of 32 pixels by 32 pixels (Figure 5, right). NCC still performs better using a window size of 16 pixels by 16 pixels than COSI-Corr does using window sizes of 32 pixels by 32 pixels.

3.4. Alaska

In this region, NCC experiences trouble not just with areas with poor visual contrast, but also with thin clouds and snow in crevasses. Figure 6 shows the displacements measured using NCC and Figure 7 show the displacements measured using CCF-O. In the 2001 image there is a thin cloud covering parts of Malaspina Glacier (see Figure 6 for location). CCF-O and to some extent also COSI-Corr manage to match this area in spite of the thin cloud, whereas NCC does not succeed. At Bering Glacier (see Figure 6 for location) some of the crevasses are filled up with snow in the 2000 image but not in the 2001 image. This also causes the NCC method to fail, whereas CCF-O and COSI-Corr succeed.

CCF-O performs better than the three similar Fourier methods also in this area. It both captures the displacement of the outlet glaciers better than the other methods and obtains more correct matches above the snowline.

The most striking velocity feature in this area is the fact that the speed of Bering Glacier is much smaller compared to the speed of Malaspina Glacier (maximum displacement of about 200 m for Bering versus 800 m for Malaspina over the 12 months studied), even though their sizes are comparable. These two glaciers are both known to surge (Post, 1969; Lingle et al., 1997), and they are clearly in different modes during our study period.

3.5. Pine Island

Since the displacement of the front of Pine Island Glacier is close to 3000 m over this time period (approximately 1 year), large window sizes are needed in this area in order to capture the movement. The ice stream itself is therefore matched with a window size of 512 pixels, aligned depending on the measured displacements, and matched again using a window size of 64 pixels. The area outside of the ice stream is matched using a window size of 64 pixels since the movement here is much smaller.

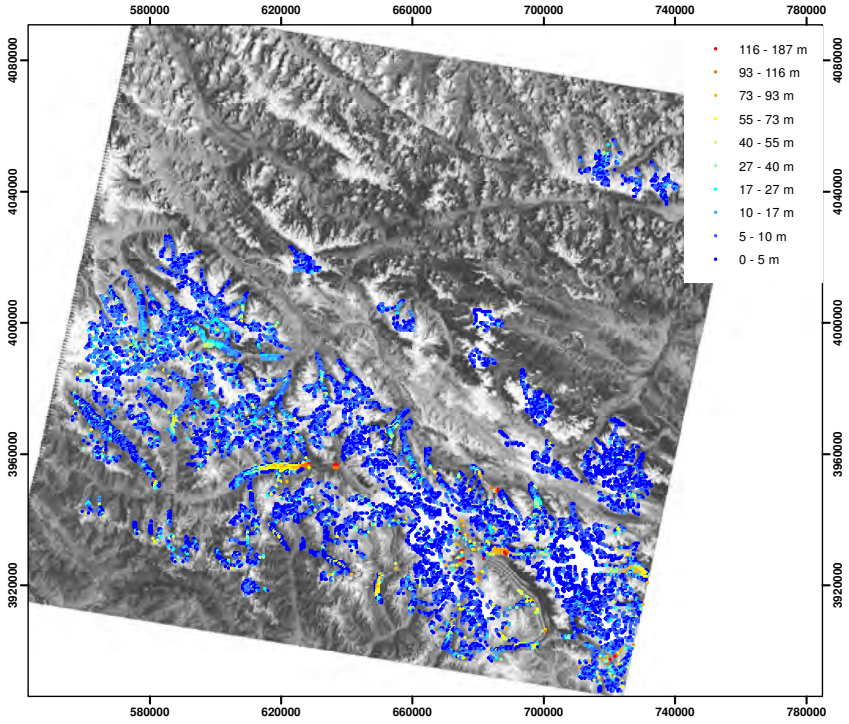

Figure 4: Displacements measured using CCF in Karakoram. Underlying image is from 21 July 2001.

All six of the methods manage to match Pine Island Glacier relatively well (not shown). This is an area with many crevasses that makes it easy to match. The parts surrounding Pine Island Glacier, however, lack visual contrast and are hence more difficult to match. This is the reason for the low percentage of correct matches in this area. The performance of the different matching methods is relatively similar.

CCF obtains the highest percentage of assumed correct matches in this area according to Table 3. However, many of these matches come from the slow flowing area surrounding Pine Island Glacier. On the ice stream itself, this method obtains fewer correct matches compared to the other methods. Because CCF measures smaller displacements over parts of the slow flowing area compared to other methods, we strongly suspect that many of the assumed correct matches are actually incorrect because the method does not normalize. It is therefore possible that instead of capturing small displacements it captures stagnant features. It is however difficult to quantify this effect and filter the measurements correctly because of the similar magnitudes.

The different window sizes that are used in the matching over Pine Island Glacier make it possible to investigate the difference in the displacements derived (Figure 8). At the margins of the ice stream, the largest window size measures a larger displacement than the smaller window size, as can be seen in the figure as arrows pointing upglacier. The difference between the methods is in the most extreme cases more than 400 m. This indicates that there is a strong velocity gradient in this area. In the middle of the ice stream the two window sizes perform much more similarly, indicating small velocity gradients in this area.

Joughin et al. (2003) have studied the velocity of Pine Island Glacier using InSAR, and also they found maximum velocities of about 3000 m/a.

3.6. Greenland

Also in our Greenland case study, the percentage of assumed correct matches is relatively low because a large section of the images contain areas above the snowline and hence has poor visual contrast. As can be seen in Figure 9, COSI-Corr resolves the velocity differences between the fast flowing ice streams and the slower flowing parts of the ice cap better than CCF-O (Figure 10). COSI-Corr also has the highest percentage of assumed correct matches in total.

CCF obtains a high percentage of assumed correct matches compared to the three other similar Fourier methods also here, but many of these matches stem from the slower flowing parts above the snowline. Many of these matches are therefore, as for the areas surrounding Pine Island Glacier, probably incorrect.

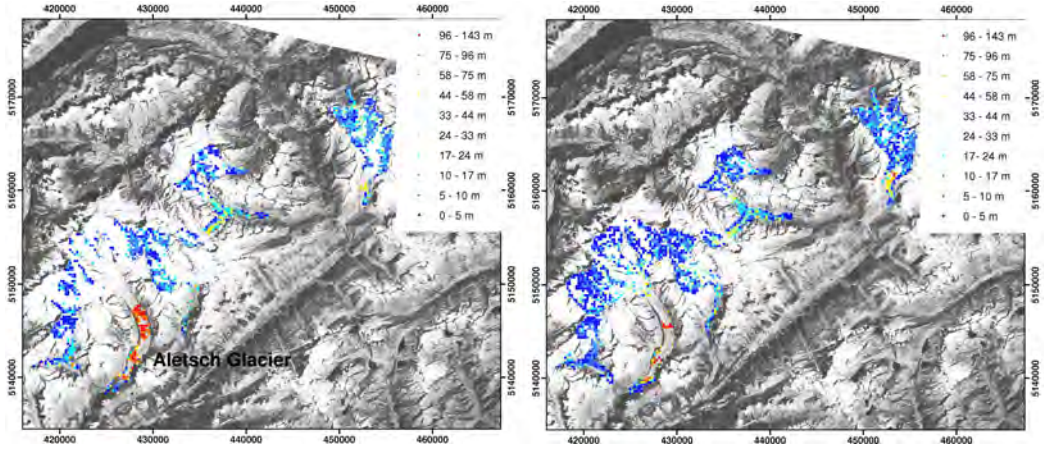

Figure 5: Displacements for a section in the European Alps measured using NCC with window sizes of 16 pixels by 16 pixels (left) and COSI-Corr with window sizes of 32 pixels by 32 pixels (right). Underlying image is from 30 July 2001.

Obtaining cloud free images in this area was difficult, and in the image from 8 August 2001 a cloud is covering large parts of Jakobshavn Glacier (see Figure 9 for location). Therefore, this area lacks correct matches.

In some areas it is difficult to identify the ice streams in the Greenland images visually before the matching is conducted. There are large velocity variations over short distances, and velocity measurements are necessary to separate fast flowing areas from more stagnant areas. Maximum displacement over the one month period is about 350 m. The pattern of speed variation fits well with the pattern derived by Joughin et al. (2010) using InSAR.

3.7. Other tests: SLC-off images, 15 m vs. 30 m resolution, adaptive windows

To test how the three methods NCC, CCF-O and COSI-Corr perform on striped Landsat images from 31 May 2003 and onwards after a failure of the Scan Line Corrector (SLC-off), two images covering Larsen B, Antarctic Peninsula, are chosen. The images are from path 217 row 106, taken on 8 January 2005 and 11 January 2006. Figure 11 shows the matching result using windows of 64 pixels by 64 pixels for a 43 km by 43 km section covering both an area with stripes and an area without stripes. Both NCC and COSI-Corr fail in the striped area, whereas CCF-O ignores the stripes and obtains correct matches. The striped area contains strong visual contrast features like a crevassed glacier and several nunataks, so all methods are expected to perform well in this area if the images lacked stripes. In addition, COSI-Corr obtains very few correct matches outside the striped area, whereas NCC and CCF-O return approximately the same number of assumed correct matches. This area has some surface transformation because the 2005 image contains many small-scale snow dunes that are not present in the 2006 image. Also several melt ponds are present in the 2006 image but not in the 2005 image.

We also match the Karakoram images with CCF-O and COSI-Corr using Landsat band 4 (near infrared) which has a spatial resolution of 30 m. This is both to test how the performance is on Landsat images obtained before 1999, which are only available with 30 m spatial resolution, and also to test how the higher noise level in the panchromatic band with 15 m spatial resolution Haug et al. (2010) influences the results. Using a window size of 16 pixels, compared to 32 pixels for the panchromatic images with 15 m spatial resolution, it is possible to obtain matches using windows covering the same ground sections. The matches are compared based on the difference in displacement between the assumed correct matches using 15 m and the displacement obtained for the same ground section using images with 30 m spatial resolution. Assuming an uncertainty using CCF-O of about 1/9 of a pixel, as Table 4 indicates, and statistically completely dependent matches ($n = 1$) , the two methods are assumed to measure the same displacement if the displacement difference is within ± 5 m (Figure 12). A total of 59 % of the matches (n=13438) are within this range. Extending this threshold to ± 10 m (2σ), 75 % of the matches are within this range. For COSI-Corr the accuracy is about 1/3 of a pixel, therefore the methods are assumed to measure the same displacement if the displacement difference is within ± 15 m. A total of 57 % of the matches (n=14765) are within this range, and 70 % are within the 2σ range.

Debella-Gilo and Kääb (2011) present displacements for Baltoro Glacier in Karakoram (see Figure 2 for location) using the same images as we use in the current study. They obtain the displacements using normalized cross-correlation and adaptive matching window sizes based on the signal-to-noise ratio (SNR) of the digital numbers in the image and the cross-correlation coefficient. The SNR of the digital numbers is the variance of the signal divided by the noise variance. This means that the window sizes are varying over the image based on the level of noise in the images and the maximum correlation coef-

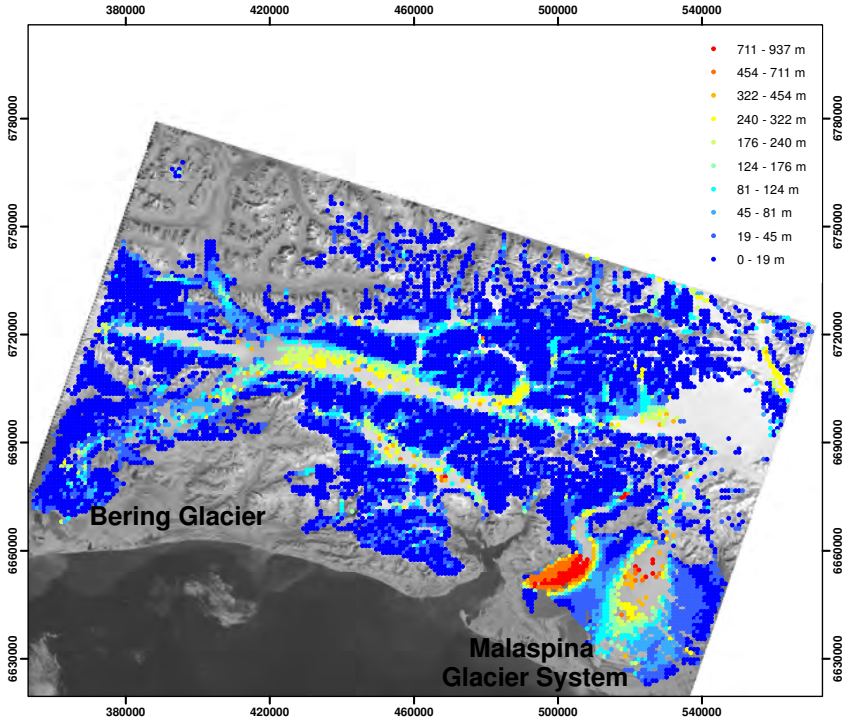

Figure 6: Displacements in Alaska measured using NCC. Underlying image is from 31 August 2000.

ficients for each location. If the SNR is lower than a given threshold even at maximum window sizes, the method does not match. Hence, filtering is performed automatically before the matching is conducted. Comparing the results from the adaptive matching and COSI-Corr reveals that 89 % of the matches (n = 640) agree within ± 15 m. For CCF-O and the adaptive method 90 % agree within ± 15 m (n=617). Mean size of the reference image for all the matchings is 29 pixels by 29 pixels. All of the matches that do not agree within 15 m are situated at the glacier margins or on the small tributaries to Baltoro. For almost all of these cases, the adaptive method measures higher velocities than the two other methods, due to less susceptibility to velocity gradients. In total, CCF-O and COSI-Corr give a higher number of assumed correct matches than the adaptive method does. CCF-O returns 1124 assumed correct matches, COSI-Corr 1175 assumed correct matches and the adaptive method 701 assumed correct matches in this area. The lower number for the adaptive method is mainly because it is, here, based on the NCC and returns hence fewer matches in the areas with low visual contrast (cf. above for NCC).

4. Discussion

Matching methods with high RMSE values over stable ground are in general considered to be less accurate than matching methods with low RMSE values. However, since the accuracy is down to fractions of a pixel, also attitude variations and accompanying pixel geolocation errors of the Landsat sensor, and erroneous topographic corrections influence the RMSE in the nonsynthetic case. The higher RMSE of COSI-Corr in the nonsynthetic case can both be because COSI-Corr captures the geolocation errors and because the effective window size is smaller. The small RMSE of COSI-Corr in the synthetic case suggests that COSI-Corr is the most accurate matching method, but that geolocation errors increase the RMSE of this method in the nonsynthetic case. The RMSE of NCC is higher than for CCF-O and COSI-Corr in the synthetic displacement case. This is because NCC is easily dominated by large differences in digital numbers, and can therefore match features away from the center of the window. Large deformations can therefore make the measurements less accurate. It is clear that both CCF-O and COSI-Corr obtain higher accuracies than what is possible to get using Landsat images due to the sensor noise. Therefore, the sub-pixel level accuracies of these methods are dominated by the sensor noise and not the accuracy of the matching methods. For the four other methods the accuracy of the matching

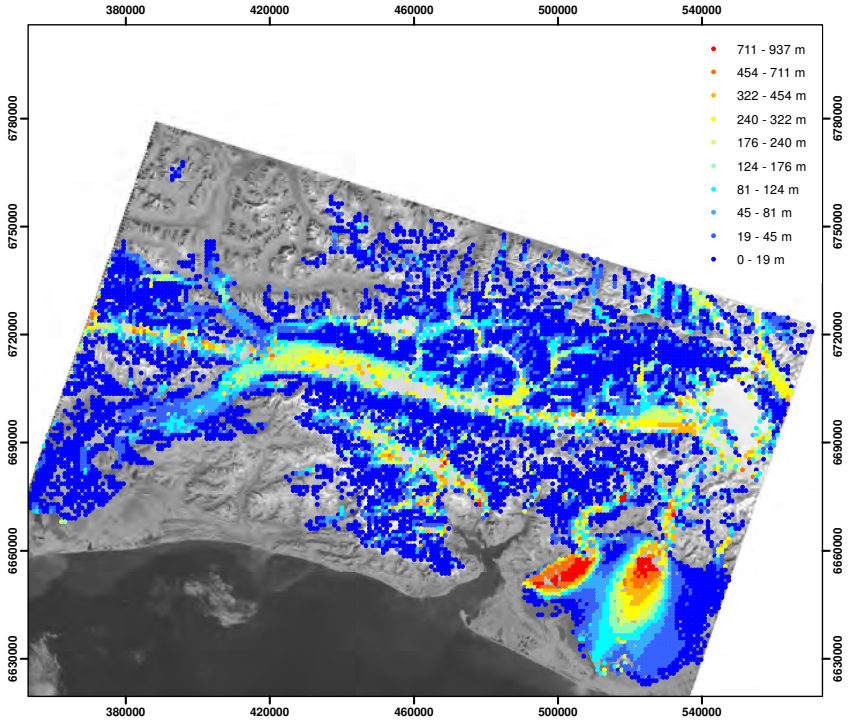

Figure 7: Displacements in Alaska measured using CCF-O. Underlying image is from 31 August 2000.

methods and the geolocation errors in Landsat images are comparable.

Surprisingly, the unnormalized matching method CCF gives more correct matches than the normalized matching methods PC and PC-O (Table 3). This is probably because it performs well above the snowline where the surface is very homogeneous, both spatially and temporally. Normalization is therefore not so important in this area. Below the snowline and outside of the glacier area it experiences problems, and it therefore proves that normalization is important in areas that are not homogeneous. This is especially clear in Karakoram where CCF matches the stationary patterns instead of the moving glacier features. This is also the case for PC. Crevasses at one geographical place are more like the crevasses at the same geographical place the year after than the corresponding but displaced crevasses, probably due to different illumination conditions and surface degradation. Since CCF does not capture movement well, it is also difficult to use in slower flowing areas where it seems to return correct results, because there will always be transitions between fast and slow flowing areas. In zones where there is a transition from slow to faster flow it is difficult to know at which value to start filtering the matches. For the same reason there might also be erroneous matches that are not discovered in the present study. This could be part of the reason why the percentage of correct matches for this method is so high, especially for the Pine Island and Greenland studies.

CCF-O performs best compared to the three other Fourier methods (CCF, PC and PC-O) that are operated in the same way but with different normalizations. PC has problems capturing the displacement of fast outlet glaciers, so this kind of normalization seems to have little effect in such areas. In addition it in general gives fewer correct matches compared to CCF-O. PC-O does not have any clear weaknesses compared to CCF-O, but in general gives fewer correct matches.

A previous study on the Larsen C ice shelf on the Antarctic Peninsula showed that few correct matches could be obtained in this area using the NCC method (Haug et al., 2010). The Larsen C ice shelf has a relatively homogeneous snow surface with few surface features like crevasses and flowlines. The present study confirms that the NCC method performs worse than other tested methods in areas with poor visual contrast. Hence, other methods should be chosen for matching such areas. COSI-Corr gives the most correct matches in low visual contrast areas, and this is mainly the reason why COSI-Corr obtains a higher percentage than other matching methods in Table 3.

In areas of high visual contrast, the performance of NCC is comparable to the performance of CCF-O and COSI-Corr. In the European Alps, where the glaciers are small, NCC outper-

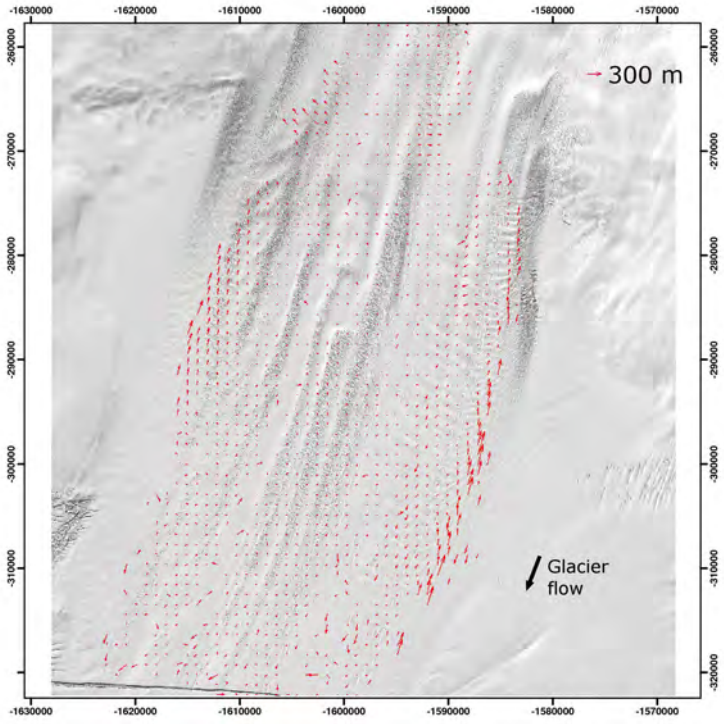

Figure 8: The measured displacements after aligning the images with displacements obtained using a window size of 512 pixels. The vectors therefore indicate the difference in the matching between a window of 512 pixels and a window of 64 pixels. The glacier flow is downwards (south). Arrows pointing upstream (north) indicate that a matching window of 512 pixels obtains higher velocities than a matching window of 64 pixels. The matching method used here is CCF-O. Underlying image is from 31 January 2001.

forms CCF-O and COSI-Corr in the narrow parts of the glaciers that are being channelized down the valleys. This is because NCC performs better with small window sizes, and in this case increasing the window size does not improve the results because the velocity varies significantly over short distances. For small glaciers where small window sizes are preferred, NCC can be a better choice than CCF-O and COSI-Corr. COSI-Corr performs better than CCF-O in such cases because it mainly uses the center part of the window to match due to weighting of the central pixels, whereas CCF-O uses the entire window with equal weight. Large velocity gradients within the window therefore make it more difficult for CCF-O to match, whereas COSI-Corr and especially NCC are less sensitive in such cases.

Increasing the window size from 16 pixels by 16 pixels to 32 pixels by 32 pixels in the European Alps did not improve the COSI-Corr displacement measurements much. We tried this because of the smaller efficient window size of COSI-Corr. It is still difficult to get correct measurements on small glaciers with much deformation because COSI-Corr is less sensitive to outliers, as explained in the Methods section. This method therefore needs the window to move coherently, which is not the case in areas with deformation.

Not only poor visual contrast, but also thin clouds and snow filled crevasses in one of the images can disturb the NCC method. CCF-O and to some extent also COSI-Corr are more robust under such conditions. This difference, like the difference between the methods for the small glaciers in the European Alps, arises because the matching methods work differently. Because CCF-O uses the entire window to match, it is less sensitive to noise. NCC, however, is easily dominated by large spatial gradients in digital numbers, like the difference between dark ice and bright snow for windows with snow filled crevasses, and searches for a similar jump in digital number in the image without snow filled crevasses. Since this difference in digital number is not present at the same feature in the image without snow filled crevasses it may find another feature with a similar difference in digital numbers and hence create a mismatch. Because COSI-Corr mainly uses the center part of the window to match due to weighting of the central pixels, this method is more sensitive to noise constrained to few frequencies compared to CCF-O, but less sensitive to noise constrained to few frequencies compared to NCC. The example with snow filled crevasses and clouds is therefore connected to the example from the small glaciers in the European Alps, but the

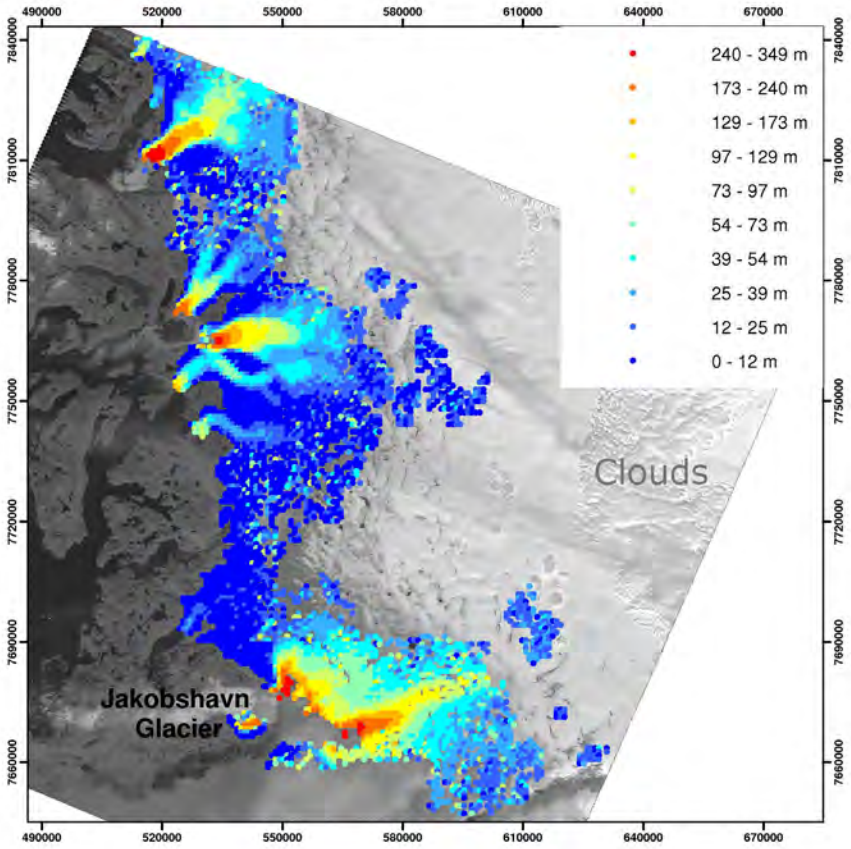

Figure 9: Displacements in southwest Greenland measured using COSI-Corr. Underlying image is from 8 August 2001.

sensitivity of NCC therefore has an unwanted effect and the insensitivity of CCF-O has a wanted effect. This highlights the fact that one single matching method can not be expected to perform well under all circumstances.

All the methods obtain a relatively similar number of assumed correct matches in the Pine Island area. This is probably because this area has too little visual contrast in most areas for the methods to obtain correct matches. But in the areas where the methods obtain assumed correct matches the visual contrast is very good due to crevasses, and all the methods manage to match these areas. As discussed above, normalization is not so important here because the area is very homogeneous.

The difference in the velocity derived using a large and a small window size over Pine Island Glacier highlights how important it is to use the smallest window size possible to avoid large velocity gradients within one window. The derived velocity may stem from anywhere inside the window depending on the digital numbers and the velocity distribution. It is therefore important to be aware of the fact that the displacement derived is not necessarily the displacement for the center pixel of the window. This gets even more important when using the displacement measurements to derive strain rates. The smaller the windows are and the smaller the velocity gradients are, the more correct it will be to assume that the displacement derived is actually the displacement for the center pixel of the window (Debella-Gilo and Kääb, in review).

Of the three matching methods NCC, CCF-O and COSI-Corr, only CCF-O manages to match striped Landsat images successfully. Hence, only this method is considered to be useful on Landsat images from the ETM+ sensor after 31 May 2003 (SLC-off).

COSI-Corr obtains fewer assumed correct matches than CCF-O and NCC on the non-striped section of Larsen B. The 2005 image here contains many small-scale snow dunes that are not present in the 2006 image. These features are likely to corrupt the phase differences at many of the frequencies and hence inhibit successful matching. NCC is less sensitive to this kind of noise because other features represent a greater difference in

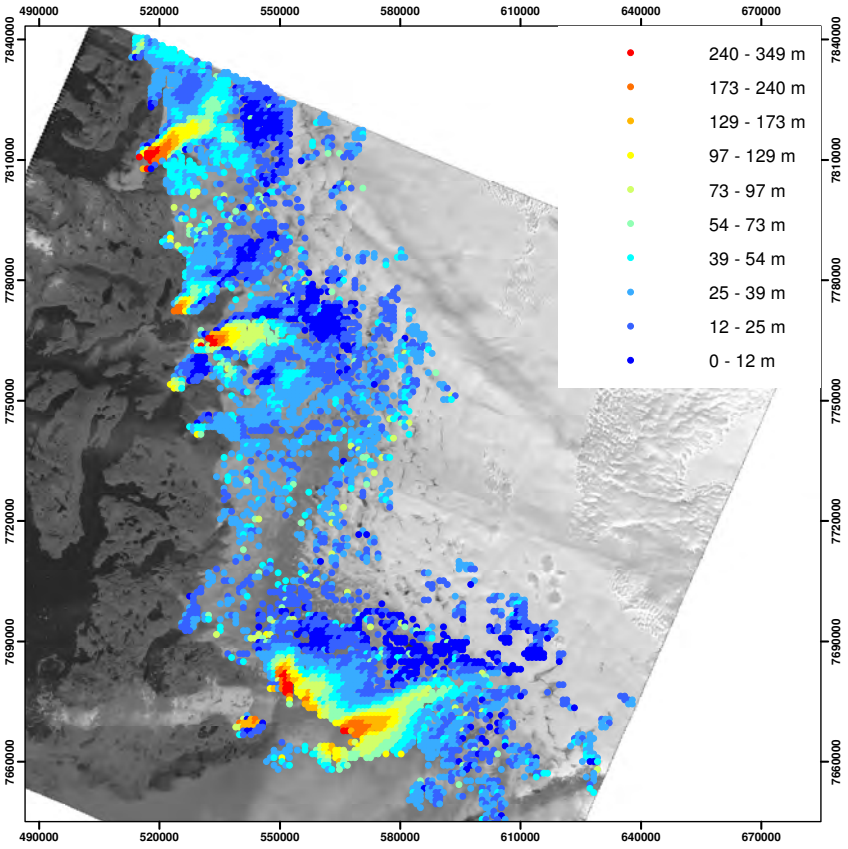

Figure 10: Displacements in southwest Greenland measured using CCF-O. Underlying image is from 8 August 2001.

digital numbers. The performance of CCF-O was assumed to be lower because of these snow dunes since it normally outperforms NCC in areas with low visual contrast, but still it performs as well as NCC.

The difference between using images of 15 m spatial resolution and 30 m spatial resolution is generally within the 1σ uncertainty of the methods. According to statistical theory, 68 % of the differences are expected to be within this range, and since 59 % are within this range for CCF-O and 57 % for COSI-Corr the results are slightly worse than expected. There can be several reasons for this. Firstly, the different spatial resolutions may enhance or suppress different features so that actually different features are matched in 30 m spatial resolution images compared to 15 m spatial resolution images. If velocity gradients are present within the windows, this may also result in different displacements at different resolutions. Many of the glacier tongues in Figure 12 show larger displacements using 15 m spatial resolution compared to 30 m spatial resolution. It is likely that small scaled features on glacier surfaces are better captured using finer spatial resolution so that especially for glacier margins, where the velocity gradients are large, images with finer resolution capture the displacement of the glacier whereas images with courser resolution capture the more stagnant areas. Secondly, erroneous matches are present in both displacement fields. Most of the erroneous matches stem from the 30 m spatial resolution matching since this result is not filtered. But it is also possible that not all erroneous matches are filtered in the 15 m spatial resolution displacement field. However, since the general agreement is good, both CCF-O and COSI-Corr can be expected to provide accurate displacement measurements for images with 30 m spatial resolution. For areas with low visual contrast the results can actually be better using 30 m spatial resolution, because the noise level is known to be higher for Landsat images with 15 m spatial resolution compared to Landsat images with 30 m spatial resolution (Haug et al., 2010). This is the case for some areas with low visual contrast in Karakoram.

The reason why the adaptive NCC method disagrees with

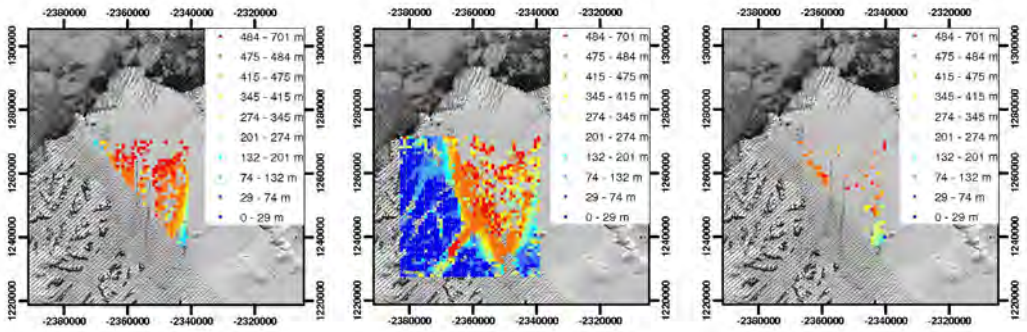

Figure 11: Displacements over Larsen B for a pair of Landsat images with SLC-off. NCC is shown to the left, CCF-O in the middle and COSI-Corr to the right. Underlying image is from 11 January 2006.

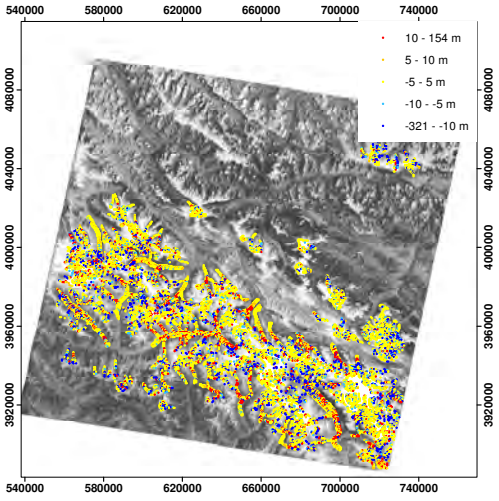

Figure 12: Difference between displacements obtained using spatial resolution of 30 m and 15 m for CCF-O. Yellow indicate that the displacement is within the 1σ method uncertainty (5 m). Underlying image is from 21 July 2001.

COSI-Corr and CCF-O by more than 15 m for some points at the glacier margins is probably because the adaptive method uses smaller window sizes in this area compared to the other methods. The windows then include smaller velocity gradients so that the displacements measured are more representative for the center pixel. Since the adaptive method implemented here is based on NCC, it is not surprising that it returns fewer matches than CCF-O and COSI-Corr in areas with low visual contrast. In the future, or using faster computers, the adaptive method can certainly be used for deriving glacier displacements globally. If SNR thresholds are tuned, locally adaptive window sizes can also be used in combination with other methods than the NCC. This will probably increase the number of correct matches in areas with low visual contrast, and at the same time areas containing large velocity gradients can be matched with smaller window sizes so that the velocities obtained are more representative for the center pixel. However, it is difficult to use the adaptive method in combination with COSI-Corr since the latter method only accepts window sizes of 2^n where n is an integer. For all window sizes used in typical glaciological studies the difference from one window size to the next possible window size will probably be too large.

5. Conclusion

In this study we have tested and assessed six existing image matching methods with as similar as possible implementations on a set of five glacier regions on Earth with different, globally representative glacier characteristics. The methods have been evaluated according to their applied suitability for global-scale mapping and monitoring of glacier flow using repeat medium-resolution optical satellite imagery, rather than evaluated on a strict technical level. Landsat data have been used for matching as they are probably the best suited data source for such global-scale application at present. The matching methods investigated are the normalized cross-correlation, the phase correlation algorithm used in COSI-Corr, and four other Fourier methods with different normalizations.

Of the four Fourier methods with different normalizations, CCF-O outperforms the other methods, both in areas with good and poor visual contrast. NCC is outperformed in areas of poor visual contrast, areas with thin clouds or changing snow conditions from one image to the next, but it performs well in high visual contrast areas and performs better than all other tested methods on narrow glaciers where small window sizes (about 16 pixels by 16 pixels) are needed. CCF-O has problems on narrow outlet glaciers. It also obtains fewer correct matches than COSI-Corr in areas with poor visual contrast, but more correct matches than NCC. COSI-Corr has problems on narrow outlet glaciers where small window sizes (about 16 pixels by 16 pixels) are needed, when snow dunes cover one of the images and also to some extent where thin clouds cover the surface. Of the three methods CCF-O, NCC and COSI-Corr, only

CCF-O manages to match the striped Landsat images that are available after the failure of the SLC in May 2003.

The most robust matching method of the six matching methods tested in this study is the matching method in COSI-Corr. CCF-O performs almost as well as COSI-Corr, but produces fewer correct matches above the snowline, making COSI-Corr better, although COSI-Corr has more problems with areas covered with thin clouds and snow dunes. The COSI-Corr program also has a coregistration processor where some push-broom sensors are included to model the imaging geometry. For cases where sensors included in the coregistration processor of COSI-Corr are being used, the accuracy of COSI-Corr will be higher because also the coregistration between the images to be matched is improved. Since COSI-Corr mainly uses the central part of the window to match due to weighting of the central pixels, the velocities derived using this method are more representative for the center coordinates of the window. Users can therefore also be relatively confident that the matches are independent even when using overlapping windows.

This study does not give a complete overview of all matching methods and all variations of the different matching methods, but it focuses on methods that are commonly used and that have performed well in published glaciological studies. Other matching methods might theoretically perform equally or better than the matching methods tested here, and in the future new matching methods will be developed that should also be tested against existing methods.

In sum, our study suggests that no one matching method clearly outperforms all others investigated under all circumstances, but rather that a set of two or three methods should be combined depending on the image conditions and the glacier characteristics. Further improvement can be achieved using locally adaptive template sizes as proposed by Debella-Gilo and Kääb (in review) combined with CCF-O and filtering the matching results automatically by comparing the displacement matrix to its low-pass filtered version as proposed here. Thus, future improvements of glaciological image matching should also focus more on the algorithm implementation and intelligent post-processing and filter procedures, rather than the pure algorithms itselves. Matches over stable ground can be used to check and improve the co-registration between the images compared. Using all these approaches, the matching process can be automated to a large degree for deriving glacier velocities with minimal user interaction, a prerequisite for being able the measure ice velocities over large areas and many regions. Though, we believe that a final expert check and edit of displacements should be performed and will still be necessary for some time to come in order to obtain glaciologically sound and useful results. Spatio-temporal variations of glacier velocities measured over large areas or even globally will soon be possible, and will provide new insights in, for example, glacier response to climate, glacier physics, ice and sediment fluxes, erosion and landscape development, glacial geomorphology, or glacial hazard development.

Acknowledgments

COSI-Corr is developed by S. Leprince, S. Barbot, F. Ayoub and J.P. Avouac and is available for download from the website http://www.tectonics.caltech.edu/slip_history/spot_coseis/index.html. We thank S. Leprince for insightful comments. Landsat images are downloaded from http://glovis.usgs.gov/. Comments and suggestions from B. Raup and three anonymous reviewers greatly improved the paper. The study is supported by The Research Council of Norway through the Precise analysis of mass movements through correlation of repeat images (CORRIA) project (No. 185906/V30) and the ESA Climate Change Initiative (project Glaciers_CCI). The study is also a contribution to the "Monitoring Earth surface changes from space" study by the Keck Institute for Space Studies at Caltech/JPL. Misganu Debella-Gilo derived the displacements using the adaptive approach and created synthetic displacement images.

References

Bernstein, R., 1983. Manual of Remote Sensing. American Society of Photogrammetry, Falls Chyrch, VA, Ch. Image geometry and rectification, pp. 881–884.

Berthier, E., Raup, B., Scambos, T., 2003. New velocity map and mass-balance estimate of Mertz Glacier, East Antarctica, derived from Landsat sequential imagery. Journal of Glaciology 49 (167), 503–511.

Bindschadler, R., Scambos, T., 1991. Satellite-image-derived veolocity field of an Antarctic ice stream. Science 252 (5003), 242–246.

Bindschadler, R., Vornberger, P., Blankenship, D., Scambos, T., Jacobel, R., 1996. Surface velocity and mass balance of Ice Streams D and E, West Antarctica. Journal of Glaciology 42 (142), 461–475.

Bishop, M., Olsenholler, J., Shroder, J., Barry, R., Raup, B., Bush, A., Copland, L., Dwyer, J., Fountain, A., Haeberli, W., Kääb, A., Paul, F., Hall, D., andB.F. Molnia, J. K., Trabant, D., Wessels, R., 2004. Global land ice measurements from space (GLIMS): remote sensing and GIS investigations of the Earth's cryosphere. Geocarto International 19, 57–85.

Brown, L. G., 1992. A survey of image registration techniques. Computing Surveys 24 (4), 325–376.

Brown, M., Burschka, D., Hager, G., 2003. Advances in computational stereo. IEEE Transactions on Pattern Analysis and Machine Intelligence 25 (8), 993–1008.

Copland, L., Pope, S., Bishop, M., Jr, J. S., Clendon, P., Bush, A., Kamp, U., Seong, Y. B., Owen, L., 2009. Glacier velocities across the central Karakoram. Annals of Glaciology 50 (52), 41–49.

Debella-Gilo, M., Kääb, A., 2011. Sub-pixel precision algorithms for normalized cross-correlation based image matching of mass movements. Remote Sensing of Environment 115, 130–142.

Debella-Gilo, M., Kääb, A., in review. Locally adaptive template sizes for matching repeat images of Earth surface mass movements. ISPRS Journal of Photogrammetry and Remote Sensing.

Dvornychenko, V., 1983. Bounds on (deterministic) correlation-functions with application to registration. IEEE Transactions on Pattern Analysis and Machine Intelligence 5 (2), 206–213.

Fitch, A. J., Kadyrov, A., Christmas, W. J., Kittler, J., 2002. Orientation correlation. In: British Machine Vision Conference. pp. 133–142.

Haeberli, W., 2004. Glaciers and ice caps: Historical background and stratergies of world-wide monitoring. In: Mass Balance of the Cryosphere. Cambridge University Press, Cambride.

Haug, T., Kääb, A., Skvarca, P., 2010. Monitoring ice shelf velocities from repeat MODIS and Landsat data - a method study on the Larsen C ice shelf, Antarctic Peninsula, and 10 other ice shelves around Antarctica. Cryosphere 4 (2), 161–178.

Hewitt, K., 1969. Glacier surges in Karakoram Himalaya (Central Asia). Canadian Journal of Earth Sciences 6 (4P2), 1009–&.

Joughin, I., Rignot, E., Rosanova, C., Lucchitta, B., Bohlander, J., 2003. Timing of recent accelerations of Pine Island Glacier, Antarctica. Geophysical Research Letters 30 (13).

Joughin, I., Smith, B., Howat, I., Scambos, T., Moon, T., 2010. Greenland flow variability from ice-sheet-wide velocity mapping. Journal of Glaciology 56 (197), 415–430.

Kaufmann, V., Ladstädter, R., 2003. Quantitative analysis of rock glacier creep by means of digital photogrammetry using multi-temporal aerial photographs: two case studies in the Austrian Alps. Permafrost, 525–530.

Kim, J., 2011. Bias-error reduction in nanometer resolution microscopic motion tracking vision systems. International Journal of Precision Engineering and Manufacturing 12 (2), 267–274.

Kääb, A., 2002. Monitoring high-mountain terrain deformation from repeated air- and spaceborne optical data: examples using digital aerial imagery and ASTER data. ISPRS Journal of Photogrammetry and Remote Sensing 57 (1-2), 39–52.

Kääb, A., 2005. Combination of SRTM3 and repeat ASTER data for deriving alpine glacier flow velocities in the Bhutan Himalaya. Remote Sensing of Environment 94 (4), 463–474.

Lee, D., Storey, J., Choate, M., Hayes, R., 2004. Four years of Landsat-7 on-orbit geometric calibration and performance. IEEE Transactions on Geoscience and Remote Sensing 42 (12), 2786–2795.

Leprince, S., Barbot, S., Ayoub, F., Avouac, J., 2007. Automatic and precise orthorectification, coregistration, and subpixel correlation of satellite images, application to ground deformation measurements. IEEE Transactions on Geoscience and Remote Sensing 45 (6), 1529–1558.

Leprince, S., Berthier, E., Ayoub, F., Delacourt, C., Avouac, J., 2008. Monitoring Earth surface dynamics with optical imagery. EOS, Transactions, American Geophysical Union 89 (1), 1–2.

Lingle, C., Fatland, D., Voronina, V., Ahlnas, K., Troshina, E., 1997. Dynamic behavior of the Bering Glacier-Bagley Icefield system during a surge, and other measurements of Alaskan glaciers with ERS SAR imagery. In: Third ERS symposium on space at the service of our environment, vols. II & III. Vol. 414. pp. 995–1000.

Lucchitta, B., Ferguson, H., 1986. Antarctica - measuring glacier velocity from satellite images. Science 234 (4780), 1105–1108.

McClellan, J., Schafer, R., Yoder, M., 2003. Signal Processing First. Pearson Education, Inc., Pearson Prentice Hall, ISBN 0-13-120265-0.

Paul, F., Barry, R. G., Cogley, J. G., Frey, H., Haeberli, W., Ohmura, A., Ommanney, C. S. L., Raup, B., Rivera, A., Zemp, M., 2009. Recommendations for the compilation of glacier inventory data from digital sources. Annals of Glaciology 50 (53), 119–126.

Post, A., 1969. Distribution of surging glaciers in western North America. Journal of Glaciology 8 (53), 229–240.

Quincey, D., Copland, L., Mayer, C., Bishop, M., Luckman, A., Belo, M., 2009. Ice velocity and climate variations for Baltoro Glacier, Pakistan. Journal of Glaciology 55 (194), 1061–1071.

Quincey, D. J., Glasser, N. F., 2009. Morphological and ice-dynamical changes on the Tasman Glacier, New Zealand, 1990-2007. Global and Planetary Change 68 (3), 185–197.

Rack, W., Rott, H., Siegel, A., Skvarca, P., 1999. The motion field of northern Larsen Ice Shelf, Antarctic Peninsula, derived from satellite imagery. Annals of Glaciology 29, 261–266.

Raup, B., Kääb, A., Kargel, J., Bishop, M., Hamilton, G., Lee, E., Paul, F., Rau, F., Soltesz, D., Khalsa, S., Beedle, M., Helm, C., 2007. Remote sensing and GIS technology in the global land ice measurements from space (GLIMS) project. Computers & Geosciences 33 (1), 104–125.

Rolstad, C., Amlien, J., Hagen, J. O., Lunden, B., 1997. Visible and near-infrared digital images for determination of ice velocities and surface elevation during a surge on Osbornebreen, a tidewater glacier in Svalbard. Annals of Glaciology 24, 255–261.

Scambos, T. A., Dutkiewicz, M. J., Wilson, J. C., Bindschadler, R. A., 1992. Application of image cross-correlation to the measurement of glacier velocity using satellite image data. Remote Sensing of Environment 42 (3), 177–186.

Scharstein, D., Szeliski, R., 2002. A taxonomy and evaluation of dense two-frame stereo correspondence algorithms. International Journal of Computer Vision 47 (1-3), 7–42.

Scherler, D., Leprince, S., Strecker, M. R., 2008. Glacier-surface velocities in alpine terrain from optical satellite imagery - Accuracy improvement and quality assessment. Remote Sensing of Environment 112 (10), 3806–3819.

Skvarca, P., Raup, B., De Angelis, H., 2003. Recent behaviour of Glaciar Upsala, a fast-flowing calving glacier in Lago Argentino, southern Patagonia. Annals of Glaciology 36, 184–188.

Zemp, M., Hoelzle, M., Haeberli, W., 2009. Six decades of glacier mass-balance observations: a review of the worldwide monitoring network. Annals of Glaciology 50 (50), 101–111.

III

6.3 Article III

Heid, T. and A. Kääb, 2011. Worldwide widespread decadal-scale decrease of glacier speed revealed using repeat optical satellite images, *Cryosphere Discussions*, 5, 3025-3051.

The Cryosphere Discuss., 5, 3025–3051, 2011
www.the-cryosphere-discuss.net/5/3025/2011/
doi:10.5194/tcd-5-3025-2011

The Cryosphere Discussions

Worldwide widespread decadal-scale decrease of glacier speed revealed using repeat optical satellite images

T. Heid and A. Kääb

Department of Geosciences, University of Oslo, Box 1047 Blindern, 0316 Oslo, Norway

Received: 17 October 2011 – Accepted: 20 October 2011 – Published: 31 October 2011

Correspondence to: T. Heid (torborgh@geo.uio.no)

Published by Copernicus Publications on behalf of the European Geosciences Union.

Abstract

Matching of repeat optical satellite images to derive glacier velocities is an approach that is much used within glaciology. Lately, focus has been put into developing, improving, automating and comparing different image matching methods. This makes it now possible to investigate glacier dynamics within large regions of the world and also between regions to improve knowledge about glacier dynamics in space and time. In this study we investigate whether the negative glacier mass balance seen over large parts of the world has caused the glaciers to change their speeds. The studied regions are Pamir, Caucasus, Penny Ice Cap, Alaska Range and Patagonia. In addition we derive speed changes for Karakoram, a region assumed to have positive mass balance and that contains many surge-type glaciers. We find that the mapped glaciers in the five regions with negative mass balance have decreased their speeds over the last decades, Pamir by 43 % in average per decade, Caucasus by 8 % in average per decade, Penny Ice Cap by 25 % in average per decade, Alaska Range by 11 % in average per decade and Patagonia by 20 % in average per decade. Glaciers in Karakoram have generally increased their speeds, but surging glaciers and glaciers with flow instabilities are most prominent in this area.

1 Introduction

Deriving glacier surface velocities from optical satellite images using image matching is well established within glaciology. In the beginning manual methods were used (Lucchitta and Ferguson, 1986), but later automatic techniques took over. Bindschadler and Scambos (1991) and Scambos et al. (1992) were the first to use automatic image matching techniques to derive glacier velocities. They used normalized cross-correlation (NCC) based on the work of Bernstein (1983). Later, different image matching techniques have been applied for this purpose. Most studies have used the NCC technique (e.g. Scambos et al., 1992; Kääb, 2002; Copland et al., 2009; Skvarca et al., 2003; Berthier et al., 2005), some have used least square matching (Kaufmann and

Ladstädter, 2003; Debella-Gilo and Kääb, 2011b), and lately frequency domain methods have become more common (Rolstad et al., 1997; Scherler et al., 2008; Haug et al., 2010; Herman et al., 2011; Quincey and Glasser, 2009) especially after the development of COSI-Corr (Leprince et al., 2007).

Most studies have focused on specific glaciers or smaller glacier regions, and only a few studies so far have focused on deriving glacier surface velocities for larger regions and comparing those (Kääb, 2005; Copland et al., 2009; Scherler et al., 2011b,a). However, since much focus is put into developing, improving and automating image matching techniques to make them well suited for image matching of glaciers (e.g. Leprince et al., 2007; Debella-Gilo and Kääb, 2011a,c; Haug et al., 2010; Heid and Kääb, 2011; Scherler et al., 2008) and also on comparing image matching techniques to find the methods that produce best results for glaciers (Heid and Kääb, 2011), it is now possible to focus on comparing glacier velocities within large regions and also between regions to improve our knowledge about glacier dynamics and its variation in space and time.

Using repeat optical satellite images to investigate annual glacier speed changes has one important advantage over using differential interferometric synthetic aperture radar (DInSAR), a technique that has immensely progressed our understanding of glacier flow (Rott, 2009). Because the coherence time is much longer for optical images than the phase coherence time is for SAR images, it is in most areas of the world possible to derive annual speeds using optical satellite images taken one year apart. DInSAR usually requires images days or at the maximum two months apart. Using optical satellite images it is thus less need to take seasonal speed variations into account when investigating whether annual glacier speeds are changing. Concerning coherence times, offset tracking based on repeat radar magnitude images lies in between optical matching and radar interferometry, but has else also a very large potential for global-scale mapping and monitoring of glacier flow (Quincey et al., 2009).

Glacier velocities are connected to mass balance because the mass flux through a cross section of a glacier equals the mass balance upstream of the cross section

when a glacier is in balance (Paterson, 1994). In theory, negative mass balance therefore gives reduced ice flux under equilibrium conditions. Mass balance estimates have been strongly negative over large parts of the world for the last decades (e.g. Käser et al., 2006; Lemke et al., 2007; Bahr et al., 2009; WGMS, 2009), and we hypothesize that this negative mass balance has caused glaciers in many regions to slow down, at least on regional averages. To test this hypothesis, we select five glacier regions where the mass balance has been negative over the last decades. These regions are Pamir with a mass balance of Abramov glacier of $-0.53\,\mathrm{m\,w.e.\,a^{-1}}$ from 1980 to 1997 (WGMS, 1999), Caucasus with a mass balance of Djankuat glacier of $-0.13\,\mathrm{m\,w.e.\,a^{-1}}$ from 1966/67 to 2002/03 (Shahgedanova et al., 2007), Penny Ice Cap in the Canadian Arctic with a mass balance of the Southern Canadian Arctic Archipelago of $-0.57\,\mathrm{m\,w.e.\,a^{-1}}$ as calculated from mass losses derived by Gardner et al. (2011) for the 2004–2009 period, Alaska Range with a mass balance of $-0.30\,\mathrm{m\,w.e.\,a^{-1}}$ from 1953 to 2004 (Berthier et al., 2010), and Southern Patagonia Ice Field with a mass balance of $-0.93\,\mathrm{m\,w.e.\,a^{-1}}$ as calculated from elevation changes by Rignot et al. (2003) for the period 1975 to 2000. Other mass balance estimates also exist for some of these regions, but we choose the most recent estimates. In addition we also select Karakoram in Himalaya, where modelled climate data indicate positive mass balance over the last decades, and measured glacier speed increases at Baltoro glacier are assumed to be associated with this mass surplus (Quincey et al., 2009).

The aim of this study is to test if, and to what degree, glacier speeds have decreased on regional scales due to negative mass balance. Such a relationship is well expected, but it has never been observed on regional scales before. It has been observed for individual glaciers using ground observations (Haefeli, 1970; Span and Kuhn, 2003; Vincent et al., 2009), but also the opposite has been observed (Vincent et al., 2000). Because glaciers may behave very differently even though they experience the same climatic conditions, the relationship between mass balance and speed should not only be studied for individual glaciers, but also for entire regions.

2 Methods

All previous studies that have investigated glacier velocities on regional scales using optical images have used ASTER images. In this study however, we use Landsat images, because they have several advantages compared to ASTER images in studies like the present. One Landsat image covers an area of 183 km by 170 km for ETM+, 185 km by 172 km for TM and 185 km by 185 km for MSS, whereas one ASTER image covers an area of only 60 km by 60 km. The Landsat series also extends long back in time, to 1982 with 30 m spatial resolution and to 1972 to 1982 with 68 m by 83 m spatial resolution. This makes it possible to study long-term velocity changes. ASTER only extends back to 1999. (We should however note that it is also possible to combine ASTER and Landsat data in the kind of study performed here, Kääb et al., 2005b). Landsat images are also used in other studies of global glacier changes, like Global Land Ice Measurements from Space (GLIMS) (Bishop et al., 2004; Kargel et al., 2005; Raup et al., 2007), GlobGlacier and Glacier_CCI. The use of Landsat data for glacier velocity measurements thus ensures a consistency in source data for the various glacier parameters derived, and a larger combined automation potential. The spatial resolution is 15 m for both panchromatic Landsat images after 1999 and visible and near-infrared ASTER images. Landsat images are available at no cost through the US Geological Survey (USGS), and ASTER images are available at no cost for scientific users. The disadvantage with Landsat images however, is subpixel noise created by attitude variations. Lee et al. (2004) found that the image-to-image registration accuracy was better than the requirement of 7.3 m, and that the average was at about 5 m for the ETM+ sensor. For the TM sensor the accuracy is approximately 6 m (Storey and Choate, 2004). This noise is impossible to model because TM and ETM+ are whisk-broom systems, and therefore the accuracy of the image-to-image registration reduces to this level. For most glaciological studies this is an acceptable accuracy because the glacier displacements over the time period that the glacier features are preserved by far exceed this noise level. The attitude variations of ASTER images can

be modelled and removed, as is done in the COSI-Corr matching software, and therefore displacements derived using ASTER can be more accurate than displacements derived using Landsat. In consideration of the above aspects and our primary goal, worldwide decadal-scale glacier velocity changes, we use images from both Landsat TM and Landsat ETM+, depending on the availability of data. The images used in this study are listed in Table 1.

We mainly use cross-correlation operated in the frequency domain on orientation images (CCF-O), a method developed by Fitch et al. (2002), to derive glacier displacements in this study. This method was one of the methods that performed the best on most glacier surfaces in a worldwide evaluation study by Heid and Kääb (2011). COSI-Corr performed slightly better in general, especially in areas with low visual contrast, but COSI-Corr cannot match striped Landsat images. Landsat7 images are striped from May 2003 and onwards because of a failure of the scan line corrector (SLC-off). To also be able to use these striped images we select CCF-O instead of COSI-Corr. However, in Caucasus we use normalized cross-correlation (NCC) because this method performs the best on smaller glaciers with good visual contrast (Heid and Kääb, 2011).

First we derive orientation images from the original images. Taking f as the image at time $t = 1$ and g as the image at time $t = 2$, the orientation images f_o and g_o are created from

$$f_o(x,y) = \mathrm{sgn}\left(\frac{\partial f(x,y)}{\partial x} + i\frac{\partial f(x,y)}{\partial y}\right) \quad (1)$$

$$g_o(x,y) = \mathrm{sgn}\left(\frac{\partial g(x,y)}{\partial x} + i\frac{\partial g(x,y)}{\partial y}\right) \quad (2)$$

$$\text{where}\,\mathrm{sgn}(x) = \begin{cases} 0 & \text{if } |x| = 0 \\ \frac{x}{|x|} & \text{otherwise} \end{cases} \quad (3)$$

where sgn is the signum function and i is the complex imaginary unit. The new images f_o and g_o are complex and hence consist of one real and one imaginary part, where the intensity differences in the x direction represent the real matrix and the intensity

differences in the y direction represent the imaginary matrix. These orientation images are then matched using cross-correlation operated in the frequency domain. The cross-correlation surface CC is given by

$$\mathrm{CC}(i,j) = \mathrm{IFFT}\left(\frac{F_\mathrm{o}(u,v)G_\mathrm{o}^*(u,v)}{|F_\mathrm{o}(u,v)G_\mathrm{o}^*(u,v)|}\right). \quad (4)$$

The peak of the cross-correlation surface indicates the displacement. Subpixel displacements are derived by fitting orthogonal parabolic functions to the correlation surface. Subpixel displacements in the x direction dx and in the y direction dy are found using

$$dx = \frac{P(x_\mathrm{m}+1,y_\mathrm{m}) - P(x_\mathrm{m}-1,y_\mathrm{m})}{2(2P(x_\mathrm{m},y_\mathrm{m}) - P(x_\mathrm{m}+1,y_\mathrm{m}) - P(x_\mathrm{m}-1,y_\mathrm{m}))} \quad (5)$$

$$dy = \frac{P(x_\mathrm{m},y_\mathrm{m}+1) - P(x_\mathrm{m},y_\mathrm{m}-1)}{2(2P(x_\mathrm{m},y_\mathrm{m}) - P(x_\mathrm{m},y_\mathrm{m}+1) - P(x_\mathrm{m},y_\mathrm{m}-1))} \quad (6)$$

where $P(x_\mathrm{m},y_\mathrm{m})$ is the maximum correlation value. The parabolic function is therefore fitted using the two nearest neighbors.

For each of the five study areas we use a small but representative section of the Landsat images to find the optimal matching window size. Applying this selection procedure on entire Landsat images would be very time consuming due to the ETM+ image size of about 15 000 pixels by 17 000 pixels. The size of the small test sections used is 30 km by 30 km. Different window sizes are tested on this section to find a window size that optimizes the matching results. The matching result is considered to be optimized when assumed correct matches are obtained over most of the glacierized areas, but without increasing the window size more than necessary. This is to avoid much deformation in one window (Debella-Gilo and Kääb, 2011c). The spacing between the matching windows is half the window size, which means that the matchings are not completely independent. The size of the matching windows used is given in Table 2.

Following basic glacier physics, in particular stress transfer, we choose to filter the obtained vectors depending on the neighboring vectors, so that vectors are assumed correct if they agree to a certain extent with their neighboring vectors. First, all vectors outside glacierized areas are removed using digital glacier outlines from GLIMS if available or we digitize such outlines from Landsat images. Then the assumed real maximum displacement is found by manually investigating the vectors. All vectors larger than the assumed real maximum displacement are removed. Using only the remaining vectors, the displacement field in both x and y direction is filtered using a 3 by 3 mean low-pass filter. Individual original vectors that deviate more than a certain threshold from this low-pass filtered displacement field are removed (Heid and Kääb, 2011). The threshold varies between the different areas depending on the displacement variations within the areas. Such filtering is not conducted in Caucasus and Patagonia because of the few correct matches derived in these areas. Table 2 shows the different thresholds.

For Pamir, Alaska Range and Karakoram the velocity fields derived are dense enough for comparing velocities derived for points closest to the centerline. However, for Caucasus, Penny Ice Cap and Patagonia the derived velocity fields are more patchy, and therefore also points further away from the centerline are accepted. In all cases the automatically derived results are checked manually in the end and points with mismatches in one or both of the two periods are removed. Thus, only points with accepted matches in both periods are used for computing velocity changes.

The accuracy of the measurements is in theory determined by the image-to-image registration accuracy of the Landsat images and the accuracy of the matching method. But, because the accuracy of the matching method is much smaller than the image-to-image registration accuracy, the accuracy is dominated by the image-to-image registration accuracy (Heid and Kääb, 2011). The uncertainty of single measurements is ± 5 m for ETM+ (Lee et al., 2004) and ± 6 m for TM (Storey and Choate, 2004), whereas the accuracy of the matching method is around 1/10 of a pixel (Heid and Kääb, 2011). We matched stable ground in all of the image pairs, and for all image pairs the root mean square error (RMSE) was between 1.8 m and 5.7 m. For comparison of two different

displacement measurements, the uncertainty will be ± 8 m for ETM+ and ± 9 m for TM using root sum square (RSS). Since time spans are about one year, but in some cases slightly shorter, speed changes of more than ± 10 m a^{-1} are considered significant speed changes in this study.

3 Results

Changes in glacier speed in the areas with negative mass balance are derived for the 2000/2001–2009/2010 period for Pamir, the 1986/1987–2010/2011 period for Caucasus, the 1985/1987–2009/2010 period for Penny Ice Cap, the 1986/1987–2009/2010 period for Alaska Range, and the 1984/1986–2001/2002 period for Patagonia. Speed changes from the first to the second period are shown in Figs. 1 and 2 and are also summed up in Table 3. We compute the mean speeds and their changes from the means of each individual glacier, not from all measurements directly. This normalization is necessary because some glaciers are large or have good visual contrast and allow thus for many measurements, whereas others do not. However, it is important to notice that the numbers in Table 3 are not area averages since not all glaciers and all parts of glaciers are covered. Thus, the numbers from our study are indicative for speed changes but do not quantitatively reflect overall ice flux changes. The largest reduction in speed per decade is found in Pamir where the speed decreased by 43 % per decade. Caucasus has the smallest reduction in speed with only 8 % reduction per decade. Decadal reduction in glacier speed is calculated by simply dividing total change through number of decades, not as compound interest due to the short time intervals involved.

In Pamir we derive speed changes for parts of 50 glaciers. The majority of the glaciers reduced their speed or showed no significant speed changes over the time period, but two glaciers, Bivachnyy and Grum-Grzhimailo, also increased their speeds (Fig. 1a). Pamir is a region with surging glaciers, hence also surge activities potentially influence the results. In total the speed decrease is of about 39 % or 43 % per decade.

In Caucasus we derive speed changes for parts of 16 glaciers. Most glaciers reduced their speed over the time period (Fig. 1b), but the largest glacier in the area, Bezengi glacier, increased its speed over large parts of the glacier. In total, the areas we map show a general decrease in glacier speed of about 19 % over the time period, which translates to about 8 % per decade.

Speed changes are derived for parts of 12 of the outlet glaciers of Penny Ice Cap. Generally all glaciers decreased their velocity from the first period to the second (Fig. 1c). The total speed decrease over the areas we map is about 59 % or 25 % per decade.

The matching in the Alaska Range gives us speed changes for parts of 9 glaciers. All but one glacier, Ruth Glacier, have reduced their speed or had constant speed over the time period (Fig. 1d). Also this is an area with surging glaciers. In total the speed decrease is about 26 %, or 11 % per decade.

In Patagonia speed changes are derived for 10 of the northern outlet glaciers of the Southern Patagonia Ice Field. All the outlet glaciers that we map have reduced their speed over the time period (Fig. 1e), and the total percentage of speed reduction is 34 %, or 20 % per decade.

We also derive changes in glacier speed for Karakoram for the 2001/2002–2009/2010 period (east) and for the 2000/2001–2009/2010 period (west) (Fig. 3). Glaciers in this area are assumed to have had a positive mass balance over the last years (Quincey et al., 2009) and the Karakoram area is also known for its many surging glaciers (Hewitt, 1969, 2007; Copland et al., 2009).

As Fig. 3 shows, the pattern of velocity changes in Karakoram is complex. In the east, glaciers are mainly increasing their speeds, but the difference in speed between the first and the second period is generally less than 25 m a^{-1}. Two exceptions are Stanghan glacier and Skamri glacier, which have low speeds in the first period and very high speeds in the second period. In the west, the speed changes are dramatic for glaciers flowing into the Shimshal valley and also for Khiang glacier and Batura glacier. However, there is no clear pattern in the velocity changes, and both accelerating and

decelerating glaciers are found. In Shimshal valley the speeds are high in both periods, but they are extremely high in one of the periods. Khiang glacier has high speeds in the first period, but in the second period the speed is close to zero. Batura glacier has high speeds in both periods, but the speed is increasing from the first to the second period.

4 Discussion

All the glacier regions with negative mass balance that we investigate in this study show a clear sign of glacier deceleration on a regional scale. This indicates that indeed less ice mass is transported down the glaciers so that the glaciers are thinning and retreating in their lower parts as a response to the negative mass balance. However, there is a lag expected between changes in mass balance and changes in glacier speeds due to the response time of glaciers (Johannesson et al., 1989). The response time is related to the altitudinal mass balance gradient, the mean surface slope of the glacier and the length of the glacier (Oerlemans, 2005).

It is not possible to see a clear correlation between the magnitude of the mass balance in a study region and the percentage speed change on a regional level. This might be due to several factors. Firstly, and most importantly, it can be due to the response times of the glaciers in the different regions. The regions are different when it comes to the factors influencing the response time, hence very different response times must be expected. Secondly, the mass balance estimates and the speed reduction estimates might not be representative for the same regions. Speed differences are not derived for all parts of the glaciers or for all glaciers within one region, and mass balance is sometimes derived for single glaciers within the regions or sometimes for larger regions than what we have investigated. Thirdly, the mass balance estimates and the speed change estimates are from different time periods. Fourthly, glaciers could have changed their amount and way of sliding, i.e. their flow mode, independently of mass balance changes. Or similar, surge-type activities, at lower magnitudes

than full surges, though, may have influenced our measurements. Fifthly and finally, one should have in mind that our measurements represent speed changes between two annual periods, and not necessary steady changes in ice flux on a decadal scale.

Some of the glaciers are accelerating from the first to the second period. In Pamir two glaciers are accelerating, in Caucasus one glacier is accelerating and one glacier is also accelerating in the Alaska Range. Both Pamir and the Alaska Range contain surging glaciers. It is therefore not surprising that some glaciers in these areas are accelerating. The Bivachnyy Glacier in Northwestern Pamir is clearly a surge type glacier in its quiescent phase in the first period, due to velocities close to zero. In the second period this glacier is moving much faster with maximum speed of about $100\,\mathrm{m\,a^{-1}}$. These speeds probably reflect a surge or surge-type movement. Looped moraines on this glacier as visible in the satellite images also confirm that it is a surge-type glacier. The Grum-Grzhimailo Glacier to the southeast in Pamir and the accelerating glacier in Alaska Range, Ruth Glacier, cannot be defined as surge type glaciers from the velocity measurements obtained in this study. These glaciers have speeds of more than $100\,\mathrm{m\,a^{-1}}$ in both periods, and in addition no looped moraines can be seen in the satellite images. It is however likely that it is flow instabilities that are causing these increased speeds since the glaciers are situated in areas containing surging glaciers and because they are behaving differently from their neighbouring glaciers. The accelerating glacier in Caucasus, Bezengi Glacier, can possibly be accelerating as a reaction to positive mass balance values. Mean mass balance here was close to zero for the period 1966/67 to 2002/03 (Shahgedanova et al., 2007), but the mass balance measurements were only done on one glacier, the Djankuat Glacier, so mass balance might have been positive for Bezengi Glacier.

Although Penny Ice Cap and Patagonia have a smaller decrease in glacier speed per decade than Pamir, these are the two areas that show the most homogeneous speed decrease from the first period to the second. No glacier in these two areas accelerates, and in Patagonia almost all compared points show a speed decrease of more than $20\,\mathrm{m\,a^{-1}}$ from the first to the second period. This is probably because all

investigated glaciers in these two areas are dynamically stable and hence only have velocity variations that can be attributed to changes in mass balance.

The moderate increase in glacier speeds in Eastern Karakoram indicates that these glaciers are increasing their speeds as a response to the positive mass balance in this area. Quincey et al. (2009) found that Baltoro accelerated due to positive mass balance, and the present study shows that this is also the case for Siachen Glacier. Staghan Glacier and Skamri Glacier are clearly surge-type glaciers in their quiescent phase in the first period due to their low speeds. In the second period the glaciers are surging according to derived speeds of more than 200 m a^{-1} and also large areas where the speed cannot be measured probably due to very high speeds and much surface transformation.

Many of the glaciers flowing into the Shimshal valley are glaciers with flow instabilities. They cannot be characterized as surge type glaciers from the speed changes derived in this study. This is because they have large speeds in both periods, hence sliding is clearly an important component of the surface speed although the velocities are lower than in the other period. A previous study has speculated that many glaciers in the Karakoram have flow instabilities instead of being of classical surge type (Williams and Ferrigno, 2010). The results in the present study for glaciers flowing into Shimshal valley support this.

Khiang Glacier was in the first period moving more than 100 m a^{-1}. In the second period its speed was close to zero. This glacier has not been identified as a surging glacier before. A tributary of Batura Glacier in the west is surging in the last period, influencing also the speed of Batura Glacier in the confluence zone.

The velocity measurements obtained here indicate that glaciers in Karakoram behave differently depending on location. Glaciers in the east seem to by dynamically stable and their speed changes are linked to changes in mass balance. This is also supported by the very few observations of glacier surges in this area, and few looped moraines. The Central North Karakoram probably contains many surging glaciers because of the very low speeds that are measured in this area. This indicates that these

are surging glaciers in their quiescent phase. Many of these glaciers have also been identified as surging glaciers in previous studies (Hewitt, 1969, 2007; Copland et al., 2009). The area in northwest contains many dynamically instable glaciers that cannot be defined as surging glaciers in the classical sense. This is because their speed is always high, and therefore sliding seems very important at all times. This area also contains some classical surging glaciers.

5 Conclusions and perspectives

In this study we derived speed changes using repeat optical satellite images for five large glacier regions of the world with negative mass balance: Pamir, Caucasus, Penny Ice Cap, Alaska Range and Patagonia. We also derived speed changes for Karakoram, which is an area with positive mass balance and that contains a large number of surging glaciers. In general, all the five regions with negative mass balance had a mean speed decrease in mapped areas from the first period to the second period. Glaciers in Pamir reduced their speed by 43 % per decade, glaciers in Caucasus by 8 % per decade, outlet glaciers from Penny Ice Cap by 25 % per decade, glaciers in the Alaska Range by 11 % per decade and outlet glaciers from the Southern Patagonia Ice Field by 20 % per decade.

On regional scales and over longer time periods, the glacier speeds are expected to decrease because less mass accumulates and therefore also less mass will be transported down to lower elevations. We have shown that this regional speed decrease is taking place. However, we could not observe a relationship between magnitude of negative mass balance and percent speed decrease. This may be because the response time of glaciers is different from area to area, and within the areas, and due to other reasons such as the uncertain representativeness of our velocity measurements. Glaciers in Karakoram generally increased their speed due to the positive mass balance, but the speed changes here are heavily influenced by the dynamic instabilities in this area.

Our study opens up for a range of other analyses based on regional or worldwide glacier velocity measurements as were demonstrated here. For instance, it seems possible to roughly estimate the response time of glaciers from inventory parameters (Haeberli and Hoelzle, 1995), and investigate their correlation with speed changes and mass balance measurements. Velocity measurements can be correlated against glacier inventory parameters such as length, area and hypsometry. Glacier velocities can also be used to estimate erosion rates or mechanisms (Scherler et al., 2011b) and transport times (Casey et al., 2011) and thus to contribute towards better understanding of glacial landscape development. On the more applied side, widespread decrease in glacier speed will increase the probability and speed of glacier lake development in areas prone to such lakes, because ice supply is one of the dominant factors in lake development and growth. Studies of speed change can help to point out areas where glacier lakes can develop or the growth of existing ones is expected (Kääb et al., 2005a; Bolch et al., 2008; Quincey et al., 2007).

Now that it is demonstrated to be feasible not just to focus velocity measurements on specific glaciers or smaller glacier regions, more effort should be put into deriving glacier velocities globally. This study shows that deriving glacier velocities for large regions or even on a global scale can give valuable insights to glaciers' dynamic climate change response and to glacier flow instabilities. It also shows that there is a potential to understand the importance of glacier sliding and deformation on regional scales better by investigating speed changes over time and the spatial structure of velocities.

Acknowledgements. Glacier outlines are downloaded from the GLIMS database http://glims.colorado.edu/glacierdata/. Landsat images are downloaded from http://glovis.usgs.gov/. The study is funded by The Research Council of Norway through the Precise analysis of mass movements trough correlation of repeat images (CORRIA) project (no. 185906/V30), the ESA Glaciers_CCI project, and the International Centre for Geohazards (SFF-ICG 146035/420). The study is also a contribution to the "Monitoring Earth surface changes from space" study by the Keck Institute for Space Studies at Caltech/JPL.

References

Bahr, D., Dyurgerov, M., and Meier, M.: Sea-level rise from glaciers and ice caps: a lower bound, Geophys. Res. Lett., 36, L03501, doi:10.1029/2008GL036309, 2009. 3028

Bernstein, R.: Image geometry and rectification, in: Manual of Remote Sensing, American Society of Photogrammetry, Falls Church, VA, 881–884, 1983. 3026

Berthier, E., Vadon, H., Baratoux, D., Arnaud, Y., Vincent, C., Feigl, K., Remy, F., and Legresy, B.: Surface motion of mountain glaciers derived from satellite optical imagery, Remote Sens. Environ., 95, 14–28, doi:10.1016/j.rse.2004.11.005, 2005. 3026

Berthier, E., Schiefer, E., Clarke, G. K. C., Menounos, B., and Remy, F.: Contribution of Alaskan glaciers to sea-level rise derived from satellite imagery, Nature Geosci., 3, 92–95, doi:10.1038/NGEO737, 2010. 3028

Bindschadler, R. and Scambos, T.: Satellite-image-derived veolocity field of an Antarctic ice stream, Science, 252, 242–246, 1991. 3026

Bishop, M., Olsenholler, J., Shroder, J., Barry, R., Raup, B., Bush, A., Copland, L., Dwyer, J., Fountain, A., Haeberli, W., Kääb, A., Paul, F., Hall, D. K., Molnia, J. K., Trabant, D., and Wessels, R.: Global land ice measurements from space (GLIMS): remote sensing and GIS investigations of the Earth's cryosphere, Geocarto International, 19, 57–85, 2004. 3029

Bolch, T., Buchroithner, M. F., Peters, J., Baessler, M., and Bajracharya, S.: Identification of glacier motion and potentially dangerous glacial lakes in the Mt. Everest region/Nepal using spaceborne imagery, Nat. Hazards Earth Syst. Sci., 8, 1329–1340, doi:10.5194/nhess-8-1329-2008, 2008. 3039

Casey, K. A., Kääb, A., and Benn, D. I.: Characterization of glacier debris cover via in situ and optical remote sensing methods: a case study in the Khumbu Himalaya, Nepal, The Cryosphere Discuss., 5, 499–564, doi:10.5194/tcd-5-499-2011, 2011. 3039

Copland, L., Pope, S., Bishop, M., Schroder Jr, J. F., Clendon, P., Bush, A., Kamp, U., Seong, Y. B., and Owen, L.: Glacier velocities across the Central Karakoram, Ann. Glaciol., 50, 41–49, 2009. 3026, 3027, 3034, 3038, 3051

Debella-Gilo, M. and Kääb, A.: Sub-pixel precision algorithms for normalized cross-correlation based image matching of mass movements, Remote Sens. Environ., 115, 130–142, 2011a. 3027

Debella-Gilo, M. and Kääb, A.: Monitoring slow-moving landslides using spatially adaptive least squares image matching, in: Proceedings of the Second World Landslide Forum, 3-9 Oct

2011, Rome, Italy, 2011b. 3027
Debella-Gilo, M. and Kääb, A.: Locally adaptive template sizes for matching repeat images of Earth surface mass movements, ISPRS J. Photogramm. Remote Sens., in review, 2011c. 3027, 3031
Fitch, A. J., Kadyrov, A., Christmas, W. J., and Kittler, J.: Orientation correlation, in: British Machine Vision Conference, Cardiff, UK, 2-5 September 2002, 133–142, 2002. 3030
Gardner, A., Moholdt, G., Wouters, B., Wolken, G., Burgess, D., Sharp, M., Cogley, J., Braun, C., and Labine, C.: Sharply increased mass loss from glaciers and ice caps in the Canadian Arctic Archipelago, Nature, 473, 357–360, doi:10.1038/nature10089, 2011. 3028
Haeberli, W. and Hoelzle, M.: Application of inventory data for estimating characteristics of and regional climate-change effects on mountain glaciers: a pilot study with the European Alps, Ann. Glaciol., 21, 206–212, 1995. 3039
Haefeli, R.: Changes in the behaviour of the Unteraargletscher in the last 125 years, J. Glaciol., 9, 195–212, 1970. 3028
Haug, T., Kääb, A., and Skvarca, P.: Monitoring ice shelf velocities from repeat MODIS and Landsat data – a method study on the Larsen C ice shelf, Antarctic Peninsula, and 10 other ice shelves around Antarctica, The Cryosphere, 4, 161–178, doi:10.5194/tc-4-161-2010, 2010. 3027
Heid, T. and Kääb, A.: Evaluation of different existing image matching methods for deriving glacier surface displacements globally from optical satellite imagery, Remote Sens. Environ., in review, 2011. 3027, 3030, 3032
Herman, F., Anderson, B., and Leprince, S.: Mountain glacier velocity variation during a retreat/advance cycle quantified using sub-pixel analysis of ASTER images, J. Glaciol., 57, 197–207, 2011. 3027
Hewitt, K.: Glacier surges in Karakoram Himalaya (Central Asia), Can. J. Earth Sci., 6, 1009–1018, 1969. 3034, 3038, 3051
Hewitt, K.: Tributary glacier surges: an exceptional concentration at Panmah Glacier, Karakoram Himalaya, J. Glaciol., 53, 181–188, doi:10.3189/172756507782202829, 2007. 3034, 3038, 3051
Johannesson, T., Raymond, C., and Waddington, E.: Time-scale for adjustment of glaciers to changes in mass balance, J. Glaciol., 35, 355–369, 1989. 3035
Kargel, J., Abrams, M., Bishop, M., Bush, A., Hamilton, G., Jiskoot, H., Kääb, A., Kieffer, H., Lee, E., Paul, F., Rau, F., Raup, B., Shroder, J., Soltesz, D., Stainforth, D., Stearns, L.,

and Wessels, R.: Multispectral imaging contributions to global land ice measurements from space, Remote Sens. Environ., 99, 187–219, doi:10.1016/j.rse.2005.07.004, 2005. 3029
Käser, G., Cogley, J. G., Dyurgerov, M. B., Meier, M. F., and Ohmura, A.: Mass balance of glaciers and ice caps: Consensus estimates for 1961–2004, Geophys. Res. Lett., 33, L19501, doi:10.1029/2006GL027511, 2006. 3028
Kaufmann, V. and Ladstädter, R.: Quantitative analysis of rock glacier creep by means of digital photogrammetry using multi-temporal aerial photographs: two case studies in the Austrian Alps, Permafrost, 1-2, 525–530, 2003. 3026
Kääb, A.: Monitoring high-mountain terrain deformation from repeated air- and spaceborne optical data: examples using digital aerial imagery and ASTER data, ISPRS J. Photogramm. Remote Sens., 57, 39–52, 2002. 3026
Kääb, A.: Combination of SRTM3 and repeat ASTER data for deriving alpine glacier flow velocities in the Bhutan Himalaya, Remote Sens. Environ., 94, 463–474, doi:10.1016/j.rse.2004.11.003, 2005. 3027
Kääb, A., Huggel, C., Fischer, L., Guex, S., Paul, F., Roer, I., Salzmann, N., Schlaefli, S., Schmutz, K., Schneider, D., Strozzi, T., and Weidmann, Y.: Remote sensing of glacier- and permafrost-related hazards in high mountains: an overview, Nat. Hazards Earth Syst. Sci., 5, 527–554, doi:10.5194/nhess-5-527-2005, 2005a. 3039
Kääb, A., Lefauconnier, B., and Melvold, K.: Flow field of Kronebreen, Svalbard, using repeated Landsat 7 and ASTER data, Ann. Glaciol., 42, 7–13, 2005b. 3029
Lee, D., Storey, J., Choate, M., and Hayes, R.: Four years of Landsat-7 on-orbit geometric calibration and performance, IEEE T. Geosci. Remote, 42, 2786–2795, doi:10.1109/TGRS.2004.836769, 2004. 3029, 3032
Lemke, P., Ren, J., Alley, R., Allison, I., Carrasco, J., Flato, G., Fujii, Y., Käser, G., Mote, P., Thomas, R., and Zhang, T.: Observations: changes in snow, ice and frozen ground, in: Climate Change 2007: The physical science basis. Contribution of Working Group I to the Fourth Assessment Report of the Intergovernmental Panel on Climate Change, edited by: Solomon, S., Qin, D., Manning, M., Chen, Z., Marquis, M., Averyt, K. B., Tignor, M., and Miller, H. L., Cambridge University Press, Cambridge, UK and New York, NY, USA, 2007. 3028
Leprince, S., Barbot, S., Ayoub, F., and Avouac, J.: Automatic and precise orthorectification, coregistration, and subpixel correlation of satellite images, application to ground deformation measurements, IEEE T. Geosci. Remote, 45, 1529–1558, doi:10.1109/TGRS.2006.888937,

2007. 3027
Lucchitta, B. and Ferguson, H.: Antarctica – measuring glacier velocity from satellite images, Science, 234, 1105–1108, 1986. 3026
Oerlemans, J.: Extracting a climate signal from 169 glacier records, Science, 308, 675–677, doi:10.1126/science.1107046, 2005. 3035
Paterson, W.: The Physics of Glaciers, 3rd edn., Elsevier, Oxford, 1994. 3028
Quincey, D. J. and Glasser, N. F.: Morphological and ice-dynamical changes on the Tasman Glacier, New Zealand, 1990–2007, Global Planet. Change, 68, 185–197, doi:10.1016/j.gloplacha.2009.05.003, 2009. 3027
Quincey, D. J., Richardson, S. D., Luckman, A., Lucas, R. M., Reynolds, J. M., Hambrey, M. J., and Glasser, N. F.: Early recognition of glacial lake hazards in the Himalaya using remote sensing datasets, Global Planet. Change, 56, 137–152, doi:10.1016/j.gloplacha.2006.07.013, 2007. 3039
Quincey, D. J., Copland, L., Mayer, C., Bishop, M., Luckman, A., and Belo, M.: Ice velocity and climate variations for Baltoro Glacier, Pakistan, J. Glaciol., 55, 1061–1071, 2009. 3027, 3028, 3034, 3037
Raup, B., Kääb, A., Kargel, J., Bishop, M., Hamilton, G., Lee, E., Paul, F., Rau, F., Soltesz, D., Khalsa, S., Beedle, M., and Helm, C.: Remote sensing and GIS technology in the global land ice measurements from space (GLIMS) project, Comput. Geosci., 33, 104–125, doi:10.1016/j.cageo.2006.05.015, 2007. 3029
Rignot, E., Rivera, A., and Casassa, G.: Contribution of the Patagonia Icefields of South America to sea level rise, Science, 302, 434–437, doi:10.1126/science.1087393, 2003. 3028
Rolstad, C., Amlien, J., Hagen, J. O., and Lundén, B.: Visible and near-infrared digital images for determination of ice velocities and surface elevation during a surge on Osbornebreen, a tidewater glacier in Svalbard, Ann. Glaciol., 24, 255–261, 1997. 3027
Rott, H.: Advances in interferometric synthetic aperture radar (InSAR) in earth system science, Prog. Phys. Geog., 33, 769–791, doi:10.1177/0309133309350263, 2009. 3027
Scambos, T. A., Dutkiewicz, M. J., Wilson, J. C., and Bindschadler, R. A.: Application of image cross-correlation to the measurement of glacier velocity using satellite image data, Remote Sens. Environ., 42, 177–186, 1992. 3026
Scherler, D., Leprince, S., and Strecker, M. R.: Glacier-surface velocities in alpine terrain from optical satellite imagery – accuracy improvement and quality assessment, Remote Sens. Environ., 112, 3806–3819, 2008. 3027

Scherler, D., Bookhagen, B., and Strecker, M. R.: Spatially variable response of Himalayan glaciers to climate change affected by debris cover, Nature Geosci., 4, 156–159, doi:10.1038/ngeo1068, 2011a. 3027
Scherler, D., Bookhagen, B., and Strecker, M. R.: Hillslope-glacier coupling: the interplay of topography and glacial dynamics in High Asia, J. Geophys. Res.-Earth, 116, F02019, doi:10.1029/2010JF001751, 2011b. 3027, 3039
Shahgedanova, M., Popovnin, V., Petrakov, D., and Stokes, C. R.: Long-term change, interannual and intra-seasonal variability in climate and glacier mass balance in the Central Greater Caucasus, Russia, Ann. Glaciol., 46, 355–361, doi:10.3189/172756407782871323, 2007. 3028, 3036
Skvarca, P., Raup, B., and De Angelis, H.: Recent behaviour of Glaciar Upsala, a fast-flowing calving glacier in Lago Argentino, Southern Patagonia, Ann. Glaciol., 36, 184–188, 2003. 3026
Span, N. and Kuhn, M.: Simulating annual glacier flow with a linear reservoir model, J. Geophys. Res., 108, 4313, doi:10.1029/2002JD002828, 2003. 3028
Storey, J. and Choate, M.: Landsat-5 bumper-mode geometric correction, IEEE T. Geosci. Remote, 42, 2695–2703, doi:10.1109/TGRS.2004.836390, 2004. 3029, 3032
Vincent, C., Vallon, M., Reynaud, L., and Le Meur, E.: Dynamic behaviour analysis of glacier de Saint Sorlin, France, from 40 years of observations, 1957–97, J. Glaciol., 46, 499–506, doi:10.3189/172756500781833052, 2000. 3028
Vincent, C., Soruco, A., Six, D., and Le Meur, E.: Glacier thickening and decay analysis from 50 years of glaciological observations performed on Glacier d'Argentiere, Mont Blanc area, France, Ann. Glaciol., 50, 73–79, 2009. 3028
WGMS: Glacier Mass Balance Bulletin No. 5 (1996–1997), edited by: Haeberli, W., Hoelzle, M., and Frauenfelder, R., IAHS (ICSI)/UNEP/UNESCO. World Glacier Monitoring Service, Zurich, Switzerland, 96 pp., 1999. 3028
WGMS: Global Glacier Change: Facts and Figures, edited by: Zemp, M., Roer, I., Kääb, A., Hoelzle, M., Paul, F., and Haeberli, W., UNEP, World Glacier Monitoring Service, Zurich, Switzerland, 88 pp., 2009. 3028
Williams, R. J. and Ferrigno, J., eds.: Glaciers of Asia, US Geological Survey Professional Paper 1386-F, United States Government Printing Office, Washington, 348 pp., 2010. 3037

Table 1. Overview of the image pairs used in this study.

Area	Sensor	Path/Row	Date image $t = 1$ period 1	Date image $t = 2$ period 1	Date image $t = 1$ period 2	Date image $t = 2$ period 2
Pamir	ETM+/TM	151/33	24 Aug 2000	26 Jul 2001	9 Aug 2009	27 Jul 2010
Caucasus	TM	171/30	6 Aug 1986	26 Sep 1987	8 Aug 2010	11 Aug 2011
Penny Ice Cap	TM	18/13	19 Aug 1985	24 Jul 1987	21 Aug 2009	7 Jul 2010
Alaska Range	TM	70/16	15 Jun 1986	21 Aug 1987	20 Aug 2010	6 Jul 2011
Patagonia	TM	231/94	26 Dec 1984	14 Jan 1986	20 Mar 2001	18 Jan 2002
Karakoram east	ETM+	148/35	16 Jun 2000	21 Jul 2001	28 Aug 2009	31 Aug 2010
Karakoram west	ETM+	149/35	29 Aug 2001	16 Aug 2002	20 Sep 2009	22 Aug 2010

Table 2. Matching window sizes and filtering thresholds in the different areas.

Area	Matching window m	Filtering threshold m
Pamir	240	± 105
Caucasus	120	–
Penny Ice Cap	240	± 90
Alaska Range	480	± 120
Patagonia	480	–
Karakoram	240	± 45

Table 3. Speed change for each area.

Area	Mean speed change $m\,a^{-1}$	Mean speed 1. period $m\,a^{-1}$	Percent speed change	Percent speed change per decade $decade^{-1}$	Number of points	Number of glaciers
Pamir	−17.0	45.8	−39 %	−43 %	3148	50
Caucasus	−4.9	25.7	−19 %	−8 %	1057	16
Penny	−12.6	21.3	−59 %	−25 %	471	12
Alaska Range	−15.9	61.2	−26 %	−11 %	1018	9
Patagonia	−85.3	248.6	−34 %	−20 %	85	10

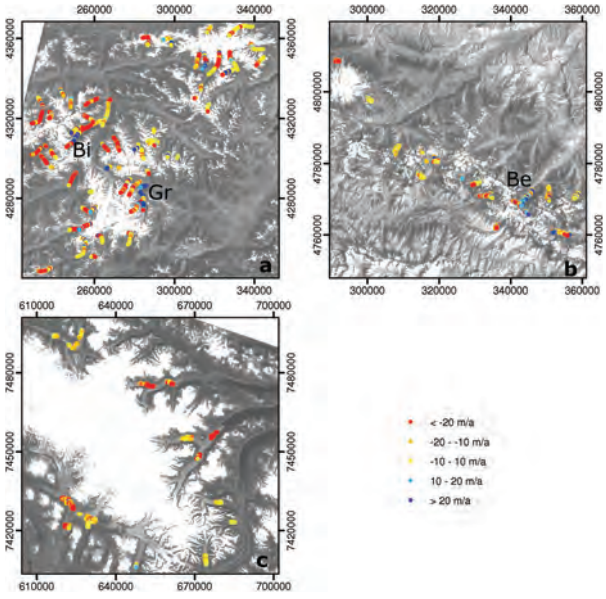

Fig. 1. Glacier speed changes between the two periods for **(a)** Pamir, **(b)** Caucasus and **(c)** Penny Ice Cap. Negative values indicate lower speeds in the second period. Changes between $-10\,m\,a^{-1}$ and $10\,m\,a^{-1}$ are insignificant. Bi indicates Bivachnyy, Gr indicates Grum-Grzhimailo and Be indicates Bezengi.

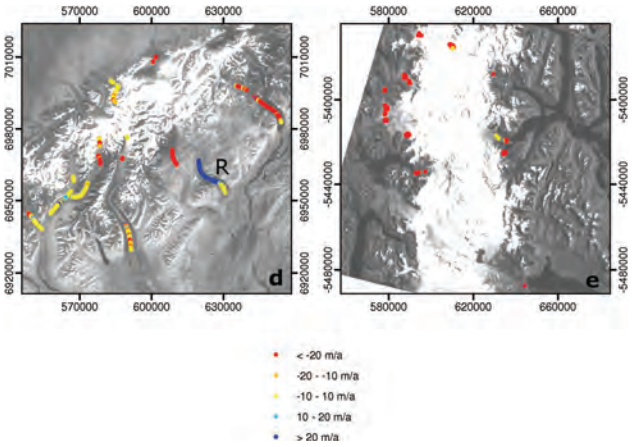

Fig. 1. Glacier speed changes between the two periods for **(d)** Alaska Range and **(e)** Patagonia. Negative values indicate lower speeds in the second period. Changes between $-10\,\mathrm{m\,a^{-1}}$ and $10\,\mathrm{m\,a^{-1}}$ are insignificant. R indicates Ruth Glacier.

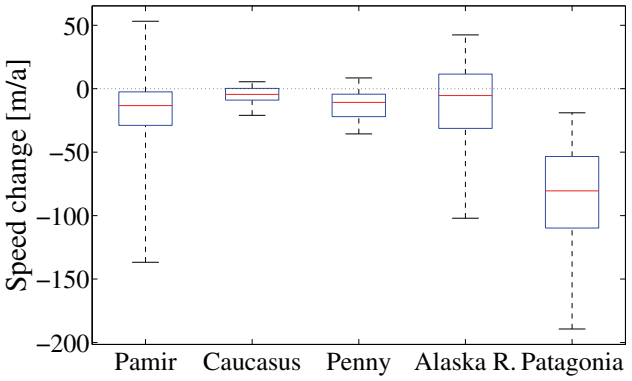

Fig. 2. Box plot showing the speed change of individual glaciers from the first to the second period for the five different regions. The box outline indicates the 25th percentile and the 75th percentile. The dotted bars indicate the range of the speed changes. Negative values indicate lower speeds in the second period.

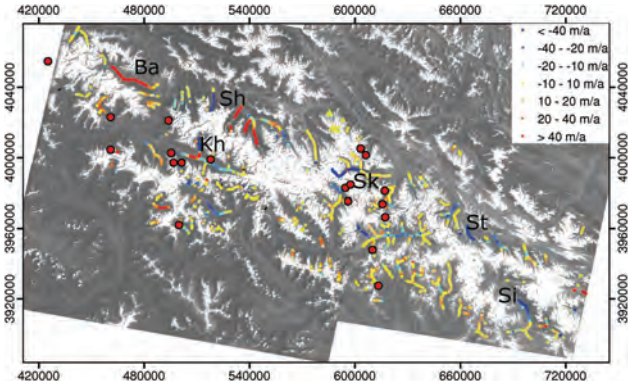

Fig. 3. Differences in centerline speed in Karakoram between the two periods 2001–2002 (east)/2000–2001 (west) and 2009–2010. Negative values indicate lower speeds in the last period. Changes between $-10\,\mathrm{m\,a^{-1}}$ and $10\,\mathrm{m\,a^{-1}}$ are insignificant. Note that the scale is different compared to Fig. 1. The large red circles indicate glaciers that are known to surge (Hewitt, 1969, 2007; Copland et al., 2009). Ba indicates Batura, Sh indicates Shimshal valley, Kh indicates Khiang, Sk indicates Skamri, St indicates Stanghan and Si indicates Siachen.